

# An implantable biosensor array for personalized therapy applications

THÈSE N° 5819 (2013)

PRÉSENTÉE LE 28 JUIN 2013

À LA FACULTÉ INFORMATIQUE ET COMMUNICATIONS

LABORATOIRE DES SYSTÈMES INTÉGRÉS (IC/STI)

PROGRAMME DOCTORAL EN MICROSYSTÈMES ET MICROÉLECTRONIQUE

ÉCOLE POLYTECHNIQUE FÉDÉRALE DE LAUSANNE

POUR L'OBTENTION DU GRADE DE DOCTEUR ÈS SCIENCES

PAR

**Andrea CAVALLINI**

acceptée sur proposition du jury:

Dr G. Boero, président du jury  
Prof. G. De Micheli, Dr S. Carrara, directeurs de thèse  
Dr T. Bachmann, rapporteur  
Prof. C. Guiducci, rapporteur  
Dr M. Op de Beeck, rapporteur



ÉCOLE POLYTECHNIQUE  
FÉDÉRALE DE LAUSANNE

Suisse  
2013



# Acknowledgements

My first acknowledgement goes to my supervisors, Giovanni de Micheli and Sandro Carrara, for the opportunity to work on a challenging, multi-disciplinary and innovative project, for their constant and encouraging support during the thesis, and for their efforts in creating a wonderful and relaxed atmosphere at the work place. For the same reasons I would like to thank Maaike Op de Beeck, who followed me during my internship in Imec. The development of a biocompatible packaging has been one of my favourite subjects during the PhD. Viktoria Shumiantseva is acknowledged for introducing me to the electrochemical measurements with the P450. Fabio Grassi and Tanja Rezzonico are acknowledged for the collaboration on the ATP biosensing and for the in-vivo test of the implantable device. John O'Callaghan, Karen Qian, Tomokasu Miyazaki, Mehmet Akif Erismis and Benjamin Gorissen are acknowledged for their help during the in-vitro biocompatibility test and for their help in the development of the implantable packaging. I am grateful to Davide Sacchetto for his precious advices on the microfabrication of the implantable platform. Thanks to Christina Govoni and Marie Halm for their help and patience with the EPFL bureaucracy: when it comes to official documents I am a disaster, but they always managed to fix everything.

The years of the PhD have been so far the best of my life: fun, full of new experiences and trips around the world in company of great people, my friends and colleagues. Thanks to Camilla, for all the experiences we are sharing together, her energy and enthusiasm, her flawless organization of everything, and for all the support in this work and in my life. Thanks to Michele, for his help in proofreading the thesis and in general for being a great flatmate with contagious curiosity and enthusiasm, always ready to engage in great intellectual discussions on the most different topics, and involve me in many outdoor adventures. Thanks to Cristina, with whom I have shared office, joy and pain of the PhD in these years, and to Irene, for all the useful advices on the most complicated electrochemistry matters. Thanks to Antonio, for his unique outlook on life, and for all the great hikes organized. Thanks to Fede for being a great companion in the trips around the world, for the countless number of times he drove me somewhere, and for all the nice discussions we had in these years. Thanks to Jacopo, Matteo, Ivan, Massimo, Anna, Vasilis, Ludo, Jaume, Michela, Ben, Shashi, Srini, Sommayeh, Sara, Wenqi, Alena, Pierre-Emmanuel, Gozen, Francesca, Joan, Sophie, Livo, Ariel, Larisa, Diana, Anna, Francesco, Pietro, Daniel, Kostantinos and Angela for all the experiences and the fun we have shared together.

Finally, thanks to my parents for their unconditioned support and love.

*Lausanne, April 2013*

D. K.



# Abstract

At present, most of the tests involved in personalized medicine are complex and must be conducted in specialized centers. The development of appropriate, fast and inexpensive diagnostic technologies can encourage medical personnel in performing preventive tests, providing the driving force to push users, industry and administrations to the adoption of personalized therapy policies. In this respect, the development of new biosensors for various healthcare applications needs may represent a concrete incentive.

The objective of this PhD project is the development of a fully implantable biosensor platform for personalized therapy applications. The thesis present innovative research on the electrochemical detection of common marketed drugs, drug cocktails, glucose and ATP with biosensors based on cytochromes P450 and different oxidases. The inclusion of carbon nanotubes provided increased sensitivity and detection limit, enabling the detection of several drugs in their therapeutic range in undiluted human serum.

A miniaturized, passive substrate capable to host 5 independent biosensor electrodes, a pH sensor, a temperature sensor as well as an interface for the signal processing electronics has been designed, microfabricated and tested. Different and reproducible nano-bio-functionalization for the single electrodes was obtained with high spatial resolution via selective electrodeposition of chitosan/carbon nanotubes/enzyme solutions at the various electrodes. The array, completely fabricated with biocompatible materials, was then integrated with a CMOS circuit and a remote powering coil for the realization of a fully implantable device.

The assembled system has been packaged with an inner moisture barrier in parylene C, to prevent circuit corrosion and toxic metals leaking, and an external biocompatible silicone shell to improve the host tolerance and reduce the local inflammation. The efficacy of the parylene barrier, as well as the toxicity of carbon nanotubes, has been assessed with in-vitro cytotoxicity tests conform to the ISO-109931 standards. The final packaged device was then implanted in mice to assess its short-term biocompatibility. Comparison between 7 and 30 days in in vivo implantations showed significant reduction of the inflammatory response in time, suggesting normal host recovery.

**Keywords:** biosensors, implantable, carbon nanotubes, cytochromes P450, ATP, packaging



# Sommario

Al giorno d'oggi, la maggior parte dei test di medicina personalizzata sono complessi e necessitano di infrastrutture dedicate. Lo sviluppo di un sistema di analisi semplice, rapido e poco costoso può incoraggiare il personale medico a prescrivere e ad effettuare test preventive, e quindi promuovere l'adozione di procedure di terapia personalizzata tra gli utenti, le amministrazioni e le aziende produttrici. In questo contesto, lo sviluppo di biosensori per applicazioni sanitarie può rappresentare un incentivo concreto.

L'obiettivo di questo progetto di dottorato è lo sviluppo di una piattaforma di biosensori completamente impiantabile, da utilizzare in applicazioni di terapia personalizzata. La tesi presenta ricerca innovativa sul rilevamento elettrochimico di farmaci, cocktail di farmaci, glucosio e ATP, con biosensori basati sul citocromo P450 e diverse ossidasi. L'integrazione di nanotubi al carbonio nei biosensori garantisce un aumento di sensibilità e di limite di rilevamento, permettendo la misura di diversi farmaci nel loro range terapeutico in campioni di siero umano non diluito.

Una piattaforma capace di ospitare fino a 5 diversi biosensori, un sensore di pH, uno di temperatura e un microchip elettronico è stata sviluppata, micro-fabbricata e testata. I singoli elettrodi sono stati funzionalizzati con alta precisione spaziale, in modo selettivo e riproducibile mediante elettrodeposizione di soluzioni contenenti chitosan, enzimi e nanotubi al carbonio. La piattaforma, completamente fabbricata con materiali biocompatibili, è stata poi integrata con un circuito CMOS e una spirale di alimentazione a induzione per la realizzazione di un dispositivo completamente impiantabile.

Il sistema assemblato è stato protetto con un microstrato di parylene C per prevenire corrosione dei circuiti e rilascio di metalli tossici, e un guscio esterno di silicone biocompatibile per migliorare la tolleranza del dispositivo nell'ospite e ridurre l'infiammazione locale. L'efficacia della barriera di parylene, così come la tossicità dei nanotubi al carbonio, sono state testate con esperimenti di citotossicità in-vitro conformi agli standard ISO 10993-1. Il dispositivo è stato poi impiantato in topi per misurarne la biocompatibilità a breve termine. Un confronto tra topi con dispositivi impiantati per 7 e 30 giorni ha dimostrato una significativa riduzione della risposta infiammatoria nel tempo, suggerendo una normale guarigione dell'ospite.

**Parole chiave:** biosensori, impiantabile, nanotubi al carbonio, citocromi P450, ATP, packaging





# Contents

<b>Acknowledgements</b>	<b>iii</b>
<b>Abstract (English/Italian)</b>	<b>v</b>
<b>1 Introduction</b>	<b>1</b>
1.1 Prospects for “personalized medicine”	1
1.2 Opportunities for biosensors in healthcare	3
1.3 State-of-the-art in personalized medicine: the –omics sciences	5
1.4 The current practice in personalized therapy: Therapeutic drug monitoring	7
1.4.1 Relevance of pharmacodynamics in TDM	8
1.4.2 Relevance of pharmacokinetics in TDM	10
1.5 Therapeutic drug monitoring practice and opportunities for biosensors technology	12
1.6 Thesis objective	15
1.7 Thesis organization	16
<b>2 Cytochromes P450: background</b>	<b>19</b>
2.1 Introduction	19
2.2 P450 nomenclature, classification and polymorphism	19
2.3 P450 catalytic cycle	21
2.4 P450 catalysis	25
2.5 Introduction to the enzyme kinetics	25
2.6 Atypical kinetic mechanisms in P450 enzymes	27
2.7 Design of a general kinetic model	28
2.8 Chapter Summary	30
<b>3 P450 biosensors: background and state-of-the-art</b>	<b>33</b>
3.1 Three electrode configuration and potential control	34
3.2 Background on voltammetry	35
3.3 P450 biosensors: state-of-the-art	38
3.3.1 Bare electrode immobilization	38
3.3.2 Layer-by-layer adsorption	39
3.3.3 Biomembrane-like films	39
3.3.4 Covalent linkage on self-assembled monolayers	40

## Contents

---

3.3.5	Immobilization on nanostructured surfaces . . . . .	40
3.3.6	Recombinant proteins and microsomes . . . . .	42
3.3.7	Summary and perspectives . . . . .	42
<b>4</b>	<b>P450 biosensors: assembly and results</b>	<b>45</b>
4.1	Cytochromes and drugs employed . . . . .	46
4.2	Characterization of the electrode bio/nano/structuration . . . . .	47
4.2.1	Methods . . . . .	47
4.2.2	Results . . . . .	48
4.3	Analysis of the reduction current and extrapolation of the microsomal contributes	51
4.4	Single drug detection . . . . .	54
4.4.1	Methods . . . . .	54
4.4.2	Results . . . . .	55
4.5	Multiple drug detection . . . . .	57
4.5.1	Methods . . . . .	58
4.5.2	Results . . . . .	58
4.6	Strategies to improve sensing accuracy . . . . .	60
4.7	Measurement of residual drug concentrations in mouse serum . . . . .	63
4.7.1	Methods . . . . .	63
4.7.2	Results . . . . .	63
4.8	Chapter summary . . . . .	65
<b>5</b>	<b>ATP biosensors</b>	<b>67</b>
5.1	Purinergic signaling during inflammation . . . . .	67
5.2	ATP detection: state-of-the-art . . . . .	69
5.2.1	H <sup>+</sup> ATPase . . . . .	69
5.2.2	Choline Kinase . . . . .	69
5.2.3	Apyrase . . . . .	70
5.2.4	Glycerol kinase / glycerol oxidase . . . . .	70
5.3	ATP detection with nanobiosensors: experimental results . . . . .	70
5.3.1	Detection principle . . . . .	70
5.3.2	Sensors fabrication . . . . .	71
5.3.3	ATP measurement and CNT nanostructuration . . . . .	72
5.3.4	Effects of multiple enzyme immobilization . . . . .	73
5.3.5	Biosensor response in physiological glucose concentrations . . . . .	73
5.4	Chapter summary . . . . .	75
<b>6</b>	<b>Design and test of an implantable sensor platform</b>	<b>77</b>
6.1	Platform design and microfabrication . . . . .	78
6.1.1	Material choices . . . . .	78
6.1.2	Process flow . . . . .	78
6.1.3	General design choices . . . . .	79
6.2	The biosensor array . . . . .	80

6.2.1 Design . . . . .	80
6.2.2 Characterization of bare electrodes . . . . .	81
6.2.3 Microelectrodes nanostructuration . . . . .	83
6.3 The pH sensor . . . . .	86
6.4 The temperature sensor . . . . .	87
6.5 Chapter summary . . . . .	89
<b>7 System packaging and biocompatibility</b>	<b>93</b>
7.1 Background and state of the art . . . . .	93
7.1.1 The foreign body reaction . . . . .	93
7.1.2 Biocompatibility: definition and test procedures . . . . .	94
7.1.3 Factors affecting implant biocompatibility and design solutions . . . . .	94
7.1.4 Biocompatibility of carbon nanotubes . . . . .	97
7.2 System packaging and biocompatibility: results . . . . .	98
7.2.1 Matrix corrosion test . . . . .	99
7.2.2 <i>In vitro</i> cytotoxicity test . . . . .	101
7.2.3 Assembly and packaging of the implantable device . . . . .	103
7.2.4 <i>In vivo</i> biocompatibility . . . . .	104
7.3 Chapter summary . . . . .	107
<b>8 Conclusions and future developments</b>	<b>109</b>
<b>A List of abbreviations</b>	<b>113</b>
<b>Bibliography</b>	<b>132</b>
<b>CurriculumVitae</b>	<b>133</b>



# 1 Introduction

*“All substances are poisons : there is none which is not a poison. The right dose differentiates a poison and a remedy”*

Paracelsus (1493-1541)

## 1.1 Prospects for “personalized medicine”

Medicine is the science or practice of the diagnosis, treatment, and prevention of disease based on the best information available about a person’s physical and mental state. The traditional approach to medicine relies on the *trial-and-error* model: make a diagnosis, prescribe a drug, evaluate patient response, and change medication or dosage if the outcome is not effective. The effect of trial-and-error medicine is huge in terms of both lives and money; as example, most of drugs prescribed in U.S. resulted effective in fewer than 60% of patients (Figure 1.1). The reason behind low efficacy is that drugs are developed and administered without considering the innate differences among individuals. The result is that for a same prescription, four different outcomes can be prospected:

- The drug is effective and well tolerated.
- The drug is effective but originates adverse drug reactions.
- The drug is not effective but well tolerated.
- The drug is not effective and poorly tolerated.

This approach costs the health care system millions of unnecessary dollars in wasted therapies and a consistent life toll, as patients with acute diseases often survive few months if not treated properly, and adverse drug reactions can be sometimes life threatening. In the last decades, advances in basic sciences have contributed numerous new diagnostic approaches which

## Chapter 1. Introduction

---

led to increased accuracy in diagnosis and remedies, allowing more focused, specific, and effective treatments.

These developments have vastly expanded doctors' power to customize therapy; however, the *trial-and-error* approach persists even when these technologies are available. The reason is that a full transition from *trial-and-error* medicine to *personalized* medicine is not only due to technological barriers but also to industrial and administrative reasons [11].

Due to the huge costs of research, the drug discovery process still focuses on the development of medications capable to target as many patients as possible (*blockbuster* model); there is therefore little interest in commercializing pharmaceuticals addressed to a particular sub-population. Incentives to develop diagnostics procedures together with specific drugs could push pharmaceutical companies towards a different policy, more oriented to the individual [175]. In addition, the reimbursement system rewards physicians more for procedures and prescriptions, and undercompensates them for the effort spent in making early diagnosis and prevention. Unless a diagnostic test can be performed in a doctor's office, the physician has no financial incentive to order it [11].

At present, most of the tests involved in personalized medicine are complex and must be conducted in specialized centers. The development of a quick and easy system for personalized analysis can therefore encourage medical personnel in performing preventive tests. The research of appropriate, fast and inexpensive diagnostic technologies can provide the driving force to push users, industry and administrations to the adoption of personalized therapy policies. In this respect, the development of new biosensors for various healthcare applications needs may represent a concrete incentive.

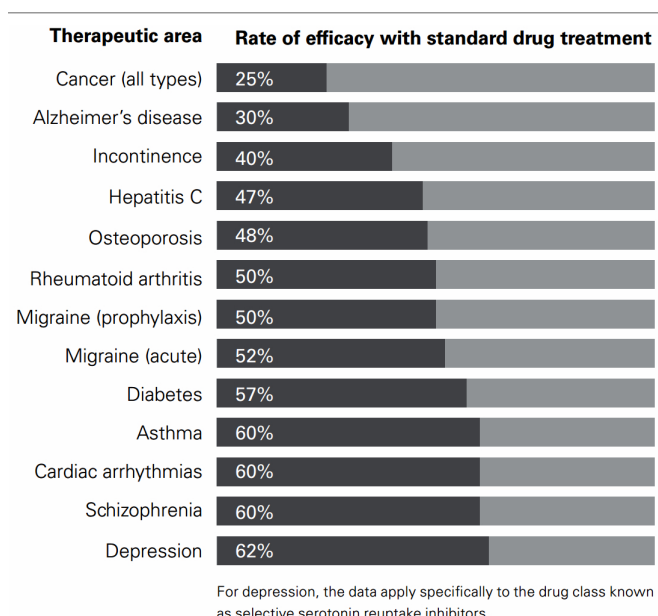


Figure 1.1: Rate of efficacy of standard drug treatments for some major pathologies [11].

## 1.2. Opportunities for biosensors in healthcare

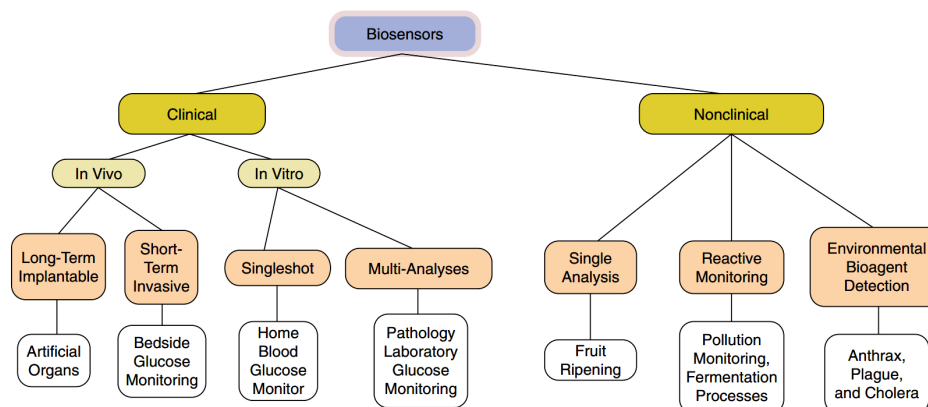


Figure 1.2: Potential biosensor applications [118].

## 1.2 Opportunities for biosensors in healthcare

A biosensor is a device for the detection of an analyte that combines a *bioelement*, capable to detect a chemical, physical or biological property of a specific analyte, and a *transducer*, that transforms the signal resulting from the interaction between analyte and bioelement into another signal that can be more easily measured and quantified. Basic concepts about biosensor classification and fabrication are well reviewed in literature [118]. Applications for biosensor technology are emerging in the fields of medicine, agriculture, biotechnology as well as the military and bioterrorism detection and prevention, as shown in Figure 1.2. This section reviews impact and perspectives of biosensors in healthcare applications.

The necessity and the possibility to find means to objectively assess the health of a patient, together with the increasing knowledge on biomarker<sup>1</sup> profiles of certain diseases, caused in recent years a major increase in the average number of diagnostic tests performed. According to the Molecular Diagnostics Survey Reports, diagnostics influence approximately the 70% of health care decisions [31]. Currently, testing for established biomarkers is typically performed at centralized laboratories using large automated clinical analyzers. This may force patients to wait a considerably long time, sometimes under enormous psychological stress, for the outcome of the test [109]. In contrast, biosensors have the potential to provide rapid, real-time, and accurate results at the physician's office, in accident and emergency departments, or even at the patient's bedside.

With respect to health care applications, the features that a biosensor should have are related to its specific employment. In this respect, it may be useful to classify biosensors according to their assay format, *labeled* or *label-free*; their analytical capability, *single-* or *multi-parameter*, and their reusability, *single-* or *multi-use*.

Labeled detection exploits the presence of an external agent that produces a measurable signal

<sup>1</sup>A Biomarker is a distinct biochemical, genetic, or molecular characteristic or substance that is an indicator of a particular biological condition or process

## Chapter 1. Introduction

---

in case of an event of biological recognition between the target analyte and the bioelement. Common labels include enzymes, radionuclides, nanoparticles and fluorescent probes. An example of labeled detection is the DNA microarray technology, in which the interaction between complementary DNA sequences is revealed by marking the target DNA with a fluorescent compound. At present, labeled test formats are widely exploited for their high-throughput screening capability, and their higher sensitivity to lower concentrations. For example, DNA, RNA, protein, cells and tissue microarrays relying on labeled detection are extensively used in the fields of predictive medicine and pharmacological research [81, 177]. An example is the Amplichip microarray, a commercial assay for the detection of P450 2D6 and 2C19 genetic variability [46].

Label-free detection reduces sample preparation and assay costs. Test formats exploit electrochemical, optical, acoustic and thermal transduction mechanisms and are capable to give an immediate response. Due to their low cost of realization, easiness to use, and immediacy, electrochemical label-free biosensors are particularly interesting for the realization of point-of-care devices and self-testing applications. Widely known examples are the commercial devices for glucose self-monitoring in diabetic patients (<http://goo.gl/x9dG6>), and recently, commercial kits for blood clotting monitoring during warfarin therapy (<http://goo.gl/XzTxn>).

Available commercial self-test biosensors are designed to determine a single analyte only; this restricts their market to few utilizations. There is still demand for advanced and more complex biosensor devices, particularly in the field of multi-parameter diagnostics (RAPP2010). Promising applications for multi-parameter biosensors could be found in the metabolic profiling of a patient or in the therapeutic drug monitoring, both described in the next sections.

Patients' compliance represents another driving force in the future biosensors direction. While some applications may require sporadic self-testing, for example an allergy test, or a pregnancy test, in other cases there is a daily need for measurement, as in case of glucose monitoring in diabetes, or in the follow up of hospitalized patients in life-threatening conditions. While in the first case the development of single-use biosensors is more indicated, in the second the realization of fully implantable systems would represent a major breakthrough, since periodic measurements, as well the communication of anomalous parameters to the patient or the physician can be completely automatic. Up to date, no commercial fully implantable biosensors are being commercialized, although a promising prototype for glucose was successfully implanted in pigs and maintained its functionality for one year [64].

In conclusion, biosensors can provide quick, inexpensive and accessible diagnostic technology which can contribute to the diffusion of various personalized medicine practices. The next sections will describe state-of-the-art and current practice in the personalized-medicine approach.



## 1.3 State-of-the-art in personalized medicine: the –omics sciences

The so-called –omics sciences, *pharmacogenomics*, *transcriptomics*, *proteomics* and *pharmacometabonomics* represent the state-of-the-art in our ability to predict the reaction of a patient to a specific therapy [121].

- **Pharmacogenomics:** 20 to 25% of all drug therapies lead to different therapeutic outcomes because of genetic differences [80]. Pharmacogenomics is a branch of pharmacology which correlates gene expression or single nucleotide polymorphisms (SNP)<sup>2</sup> with efficacy or toxicity of drugs. The goal of pharmacogenomics is to optimize a therapy according to the unique genetic profile of patients<sup>3</sup>, ensuring maximum efficiency with minimal adverse effects. Pharmacogenomics represents the whole genome application of *pharmacogenetics*, which examines single gene interactions with drugs. In cancer therapy, pharmacogenomic assessment of drug metabolizing enzymes can improve the ability to optimally dose patients treated with agents such as 6-mercaptopurine, irinotecan, tamoxifen, and flurouracil. Two of these agents (6-mercaptopurine and irinotecan) already have mention of pharmacogenomic testing in their FDA-approved package insert [164]. However, the predictive power of this discipline has limitations due to the complexity of genetic variability and expression, and to non-genetic alterations of metabolism. The cytochrome P450 2D6 (CYP2D6), which presents over 75 polymorphisms, is a valid example of genetic variability. Unless every variant site in the genome is tested is therefore difficult to ascertain a univocal correspondence between genetic profile and metabolism. CYP1A2 is another example of complexity of genetic expression. 33 different allelic variants have been reported, with different levels of activity or inducibility. A study reported by [82] on CYP1A2 concluded that genotyping cannot unequivocally be used to predict the metabolic phenotype in any individual patient. The bottom line is that pharmacogenomics alone cannot provide absolute certainty in predicting drug responses for individual patients.
- **Transcriptomics.** The process of protein formation is complex. The DNA from one gene must be *transcribed*<sup>4</sup> into mRNA before being *translated*<sup>5</sup> into a protein sequence. The transcription is not straightforward: only some parts of a gene called exons contain

---

<sup>2</sup>A SNP is a genetic variation in a DNA sequence that occurs when a single nucleotide – A, T, G or C - in a genome is altered; SNPs are usually considered to be point mutations that have been evolutionarily successful enough to recur in a significant proportion of the population of a species

<sup>3</sup>When speaking of unique characteristics of an individual two terms are extensively used: the *genotype*, is the genetic makeup of an organism with reference to a single, a set, or an entire complex of traits; the *phenotype* is the expression of a specific trait, such as a stature or blood type, based on genetic and environmental influences.

<sup>4</sup>*Transcription* is the process of copying genetic information from DNA to RNA. The term is used because the chemical structure of RNA as well as the chemical “code” employed is practically identical to the one of DNA. By analogy it is like copying something from paper to the computer. Different supports - nucleic acids, same rules – triplets of nucleotides.

<sup>5</sup>*Translation* is the process of transferring genetic information from RNA to protein. Chemical code and support conveying the information in this case are different; hence the term translation is used. By analogy, translation is the same of reading a blueprint (RNA) and realizing the project described (protein).

the structural information needed for the protein assembly. In simple words, like a Lego, different exons from the same gene combined together produce different mRNA that will be used to assemble different proteins<sup>6</sup>. *How* the exons are assembled together and *how much* mRNA is produced greatly affects the phenotype. Transcriptomics is the discipline that studies the gene transcripts, and with respect to personalized therapy has led to several breakthroughs. For example, transcriptome analysis of some tumors has successfully correlated gene expression with patient prognosis and therapy responsiveness. [168]. The drawback of Transcriptomics is due to difficulty of reparability of sources for transcript analysis (typically from biopsies). In healthy individuals it is both unreasonable and unethical to attempt to predict drug responses from tissues slices coming – for example – from brain and liver [121].

- **Proteomics.** Proteomics is the large-scale study of proteins, particularly their structure and functions. After genomics and transcriptomics, proteomics is the next step in the study of biological systems. Quantification of gene transcription gives only a rough estimate of its level of expression as a protein: first, a mRNA produced in abundance may be degraded rapidly or translated inefficiently, resulting in a small amount of protein; second, after translation many biomolecules undergo *post-translational modifications*, typically chemical modifications like phosphorylation, glycosylation, acetylation, or enzymatic cleavage which strongly affect their activity. Proteomics also accounts for protein degradation and protein interactions, which cannot be evaluated with using the former two disciplines. At present, proteomics suffers the same limitation of assay sources as Transcriptomics; moreover reproducibility is low. For example, [129] and [170] both compared the proteome of yeast finding only 57-59% of homology between results. In future proteomics might enable investigators to identify protein profiles correlated with either efficacy or adverse drug reactions, however at present, knowledge in this field and experimental methodologies are not sufficiently mature for mass application of this approach.
- **Pharmaco-metabonomics<sup>7</sup>.** The big picture emerging from genomics, transcriptomics and proteomics is that living systems, at every level of organization (genes, transcripts, proteins, cells, organs, body, and environment) are affected by factors that alter the metabolism (mutations, expressions, age, weight, lifestyle etc. . .). As consequence, every discipline focusing on a specific level of organization to forecast the body response respect to a specific stimulus (*i.e.* an administered drug), leads to approximate predictions, as it does not take in account *how* next level will affect the outcome. Metabolites are the end products of cellular regulatory process, and their levels can be regarded as the ultimate response of biological systems to genetic or environmental changes. The

---

<sup>6</sup>The DNA, including non-coding sequences is initially transcribed into an mRNA called *primary transcript*. Before translation, the primary transcript is subjected to *RNA splicing*, a process which “cuts and paste” together the exons. After the splicing and other chemical modifications aimed to increase the stability, the mRNA is called *mature* and is ready to be translated into protein.

<sup>7</sup>Parallel to trascriptome, or proteome, the set of metabolites synthetized by a biological system is known as metabolome.

#### 1.4. The current practice in personalized therapy: Therapeutic drug monitoring

---

metabonome represent an integrated analysis, of all endogenous and exogenous stimuli such as drugs, environmental exposures, lifestyle, age, sex, menstrual and diurnal rhythms, seasonal effects, diet, virus, bacteria and parasites [121]. The potential to follow a patient phenotype as function of age, nutrition, course of disease and drug therapy from samples of urine, blood, or other excreta holds great promise in personalization of drug therapy and also great opportunities for the realization of multi-parameter biosensors. The work of [41] provides the first proof-of-principle of the metabonomic approach for a personalized drug treatment: by using NMR spectroscopy, the group compared the metabonomic profile obtained from urine samples of rat collected before and after the administration of paracetamol, and correlated the results obtained with histopathologic analysis of liver tissue. The study found a statistically significant relationship between pre-dose data and post-dose variation in histopathology and in the urinary level of a drug metabolite relative to its parent, demonstrating that drug induced responses in individuals are potentially predictable their pre-dose metabolite profiles. Unfortunately, with respect to cheap biosensor opportunities, pharmaco-metabonomics is, for the moment, too advanced. High sensitivity techniques and profiling of hundreds of different metabolites at once are necessary for a correct metabonomic profiling.

Genomics, Transcriptomics, proteomics and metabonomics investigate on different levels the causes that lead to a specific therapeutic outcome, and the combination of these disciplines will grant in future a high degree of therapy personalization; however for some applications a simple prediction of drug response is not enough to ensure safe drug administration, as for several medications the difference between a harmless dose and a toxic one is very narrow. Drug dosage and its concentration in the body have a direct effect on strength, time and reversibility of a drug, so the development of dose-response models is central to determining safe and hazardous levels and dosages for a compound. The *therapeutic drug monitoring* (TDM) is a multi-disciplinary clinical specialty aimed at improving patient care by individually adjusting the dose of drugs for which clinical experience or clinical trials have shown it improved outcome in the general or special populations. As it will be explained in the next chapter, the TDM practice is a field which can greatly benefit from the development of innovative biosensors.

#### 1.4 The current practice in personalized therapy: Therapeutic drug monitoring

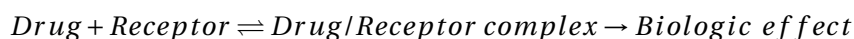
The philosophy of TDM can be summarized with a simple statement:

*Only a narrow drug concentration can grant a beneficial effect and absence of adverse reactions, therefore the more we control the drug concentration in the body, the more we improve efficacy and safety of a given therapy.*

Although the above statement looks simple, concepts like *narrow* drug concentration, *efficacy*, and *concentration control* are not straightforward. Exhaustive understanding of what TDM is, when it should be used, and how biosensors can improve its practice, implies the introduction of some pharmacology concepts. The first thing which is necessary to know is the relationship between drug concentration, therapeutic effect and side effects; a concept explained by *pharmacodynamics*; the second, is which factors affect drug concentration during time, a concept explained by *pharmacokinetics*.

### 1.4.1 Relevance of pharmacodynamics in TDM

Pharmacodynamics describes the actions of a drug on the body and the influence of drug concentrations on the magnitude of the response. Most drugs exert their effects, both beneficial and harmful, by interacting with cellular receptors. Drugs act as signals, and their receptors act as signal detectors. Receptors initiate a series of reactions, the *transduction cascade*, that ultimately result in a specific response. The magnitude of the response is proportional to the number of drug–receptor complexes according to the following relationship



Connections between biological effect and drug concentration are clearly visualized with *concentration-response curves*, which enable the calculation of two fundamental drug properties: *potency* and *efficacy*.

- **Potency** is a measure of the amount of drug needed to produce a response of given intensity. It is expressed as the *Median Effective Concentration (EC50)* or the amount of the drug that produces the 50% of the maximal response. The smaller is the EC50, the more potent is the drug.
- **Efficacy** is the ability of a compound to elicit a response when interacting with a receptor. It is dependent by the total number of drug/receptor complexes and by the receptor efficiency in initiating the transduction signal (receptor coupling).

Figure 1.3 illustrates the concentration-response curve of three drugs showing different potencies or efficacies. Another application of concentration-response curves is the visualization of drug interactions. Pharmaceuticals may either activate or inhibit a receptor transduction. Molecules of the first type are called *agonists*; while compounds of the second group are called *antagonists*. The way a second compound bounds to the receptor, as well as its concentration, affect potency and efficacy of a specific drug and can lead to unwanted effects. This explains why drug monitoring is important when assuming drug cocktails.

Pharmaceuticals safety is evaluated *in-vivo* using *quantal dose-response relationships*, which relate the amount of drug administered (dose) to the percentage of individuals achieving a particular biological effect, such as therapeutic action or side effect. Figure 1.4 shows a

#### 1.4. The current practice in personalized therapy: Therapeutic drug monitoring

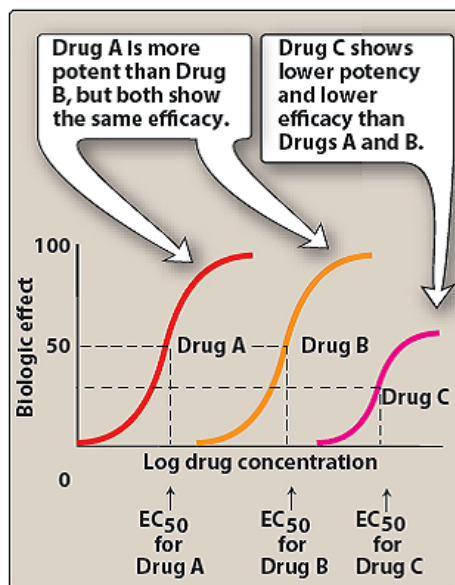


Figure 1.3: Examples of concentration-response curves [114]

quantal dose-response curve for the therapeutic (blue) and side effect (red) of a generic drug, and introduces some points widely used in the pharmacodynamic characterization of a compound:

- **NOEL and NOAEL** - No Observable (Adverse) Effect level, correspond to the lowest experimental dose where no measurable effect is known.
- **LOEL and LOAEL** – Lowest Observable (Adverse) Effect Level, is the point at which a drug response is observed for the first time.
- **ED50** - Median Effective Dose, is the dosage inducing the wanted effect on the 50% of the population.
- **TD50** – Median toxic Dose, is the drug amount causing a particular side effect on the 50% of the population.

Drug safety is evaluated with the *therapeutic index (TI)*, the ratio between TD50 and ED50; a second method, is the calculation the *margin of safety (MOS)*, the ratio between the drug dosage which is lethal to the 1% of animals (LD01) and the dosage effective to the 99% of subjects (ED99). The most important concept of dose-response plots is that the more the two curves are close the more a drug is likely to generate side effects if incorrectly administered, as even slight variations in concentration may be sufficient to generate side effects (Figure 1.5). A common feature of compounds subjected to therapeutic drug monitoring is their low therapeutic index.

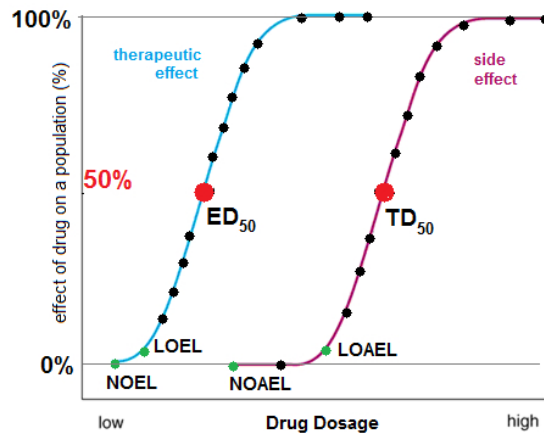


Figure 1.4: Example of Dose-response relationship for the therapeutic and the side effect of a generic drug.

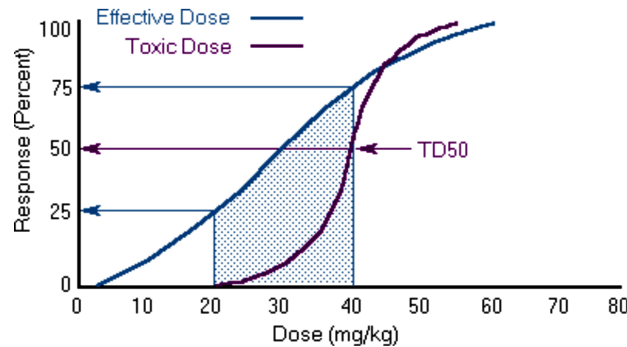


Figure 1.5: Example of dose-response curves for a generic high risk drug. The toxic effect appears at low dosages.

### 1.4.2 Relevance of pharmacokinetics in TDM

Once administered through one of the several available routes (*i.e.* from a pill or injected), the body interacts with the medication, affecting the speed of onset of drug action, the intensity of the effect, and the duration of drug action [114]. Monitoring what the body does to a medicine is therefore critical in the optimization of the therapeutic regime.

The ensemble of body “actions” on a drug is called *pharmacokinetics (PK)* and it is divided in 4 phases known under the acronym *ADME: Adsorption, Distribution, Metabolism, Excretion*<sup>8</sup>.

Most medicines in intensive care are given intravascularly, but when they are delivered by other routes, for example in form of a pill, *Absorption* has to happen across several physiological barriers, like the gastrointestinal tract. In this respect, the *bioavailability* is the drug proportion that actually reaches systemic circulation. *Distribution* occurs when the formulation leaves

<sup>8</sup>Although not treated here, an additional initial phase, the drug *Liberation* from its form, is object of specific pharmacokinetic studies

#### 1.4. The current practice in personalized therapy: Therapeutic drug monitoring

the vascular system to different compartments, either tissues or organs. Drug *metabolism* converts the medicines into molecules easier to eliminate; while *excretion* is the irreversible elimination of a compound from the body. Drug formulation, delivery route and frequency of administration, inter-individual differences, as well as patient compliance affect all the stages of pharmacokinetics. The therapeutic drug monitoring focus on drugs subjected to high pharmacokinetic variability.

Figure 1.6: Time variation of plasma concentration of a generic drug administered shows the time variation in plasma concentration of a generic drug administered orally. Since the medicine is not directly injected in the bloodstream, there is an initial adsorption phase in which plasma concentration builds up to a maximum value,  $C_{max}$ . After this peak, plasma concentration gradually decreases due to distribution, metabolism and excretion. The figure also present two important parameters: the *therapeutic range* is the plasma concentration comprised between the *minimal effective concentration (MEC)* and the *minimal toxic concentration (MTC)*, while the *duration of action* corresponds to the time in which plasmatic drug levels are in the therapeutic range.

The purpose of multiple doses is to maintain the therapeutic range for all the duration of therapy. After several administrations, the drug begins to accumulate in the body. At a certain point in therapy, the amount delivered during a dosing interval replaces the drug excreted; when this equilibrium occurs, peaks and trough drug concentrations are the same for each additional dose given and a *steady state* condition is reached (Figure 1.7).

As shown by Figures 1.6 and 1.7, in a dosing study it is important to consider peaks (highest concentration) and troughs (lowest concentration) of drug levels following dose administration. Blood samples are drawn at a prescribed time after the dose is administered to capture the peak concentration, another sample must be drawn prior to the next dose to capture the trough level; sample timing depends by the drug type and route of administration and adsorption. Accurately timing drug administration and sample collection is therefore critical to fine-tune the patient's dosage, and to ensure an accurate measurement of plasmatic concentrations [65]. A continuous and automated monitoring of drug levels can therefore help

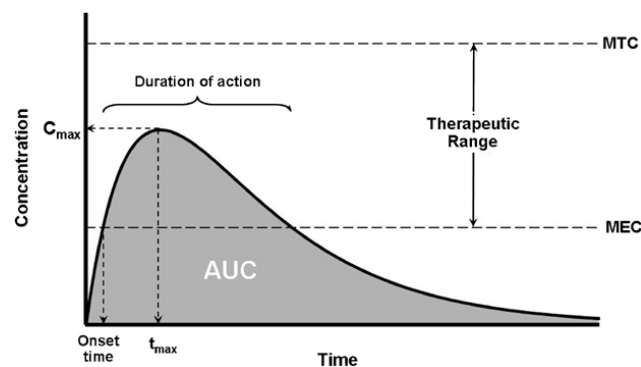


Figure 1.6: Time variation of plasma concentration of a generic drug administered orally.

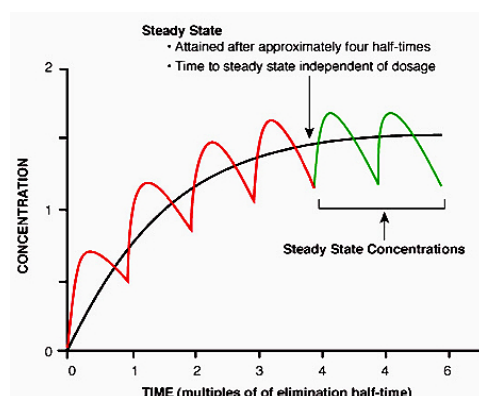


Figure 1.7: Effect of multiple doses and drug steady state.

achieving maximum precision in TDM practice.

### 1.5 Therapeutic drug monitoring practice and opportunities for biosensors technology

The previous sections explained why narrow therapeutic index and pharmacokinetic variability are potential sources of adverse drug reactions. This section will provide a brief description of TDM practice and explain how the implementation of biosensors can provide benefits to this discipline.

TDM is requested as aid for the manipulation of the current medication regimen for patients that are unresponsive to a given therapy; in case of suspected toxicity; to assess the compliance with the medication regimen, or when the clinical status of the patient is changed [65]. This last point is of particular interest, as many drugs that are monitored therapeutically are taken for a lifetime and must be maintained at steady concentrations year after year while the patient ages and goes through life events such as pregnancies, temporary illnesses, infections, emotional and physical stresses, accidents, and surgeries. Over time, patients may become addicted to the drug, and need a higher dosage to achieve a therapeutic effect, as in case beta-blockers or benzodiazepines, or may acquire other chronic conditions that also require lifetime medications which may affect the processing of their monitored drugs. Examples of these conditions include cancer, cardiovascular disease, kidney disease, thyroid disease, liver disease, and HIV/AIDS.

At present, routine therapeutic drug monitoring procedures have been established for compounds with narrow therapeutic index and high inter-patient pharmacokinetic variability [65, 75]. These include antifungal, antiretroviral, anticonvulsant and immunosuppressant drugs, theophylline, aminoglycosides, and psychotropic drugs [123]. After the request is assessed, sampling, analysis and interpretation of results should be ideally reported within a single working day in order to ensure a quick and safe regimen optimization. Drug concentra-



## 1.5. Therapeutic drug monitoring practice and opportunities for biosensors technology

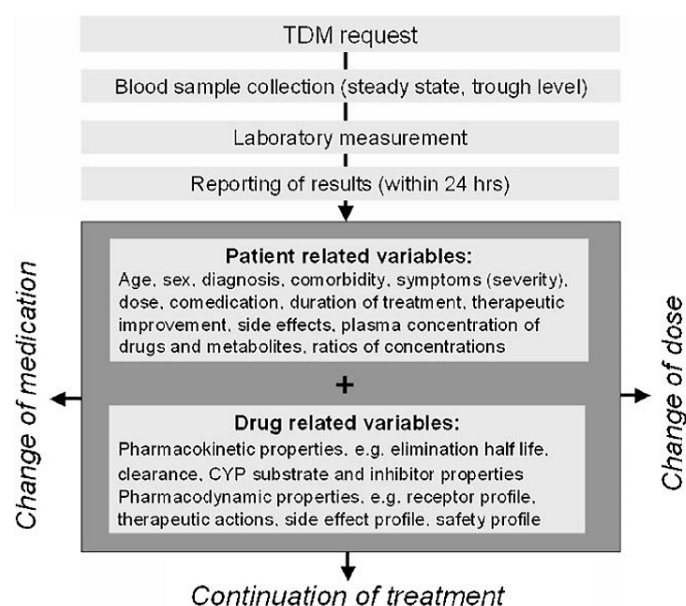


Figure 1.8: Example of therapeutic drug monitoring procedure. Blood analysis is interpreted on the basis of patient and drug related variables.

tion results are interpreted by a team of experts on the basis of patient-related and drug-related variables and then finally sent to the physician who can decide eventual modifications of the therapeutic regime. The whole TDM procedure is summarized in Figure 1.8.

Despite the advantages of TDM, its use has been limited to few patients and only to a few indications [75]. This is due to the following reasons:

- **Technology:** Current analytical techniques which grant drug sensing with sufficient accuracy, specificity, selectivity and reproducibility require highly trained personnel and specific equipment. Analysis is therefore carried out by few laboratories, at high costs and at the expense of a longer time lag between the TDM request and the reporting of results. Examples of analytical techniques include various forms of chromatography, mass spectroscopy and immunoassays. Although high throughput technologies become available in the last years enabling faster reporting of results, sampling and analysis is still carried out in specific centers.
- **Knowledge:** A reason for the lack of TDM is the absence of sufficient information regarding a drug pharmacokinetic/pharmacodynamic data and its therapeutic ranges. Implementation of TDM procedures in preclinical and clinical drug development as well as in pharmacovigilance, can give earlier insight about drug-related and patient-related variables enabling the development of more specific compounds, and higher degree of therapy personalization [65]. Examples of information relevant to pharmacological research obtained from TDM include the discovery of CYP2D6 poor and ultrafast metabolizers as well as the discovery of accidental drug interactions [75].

- **Human error:** It has been estimated that about 20% of therapeutic adjustments following TDM of antidepressants were incorrect [75]. Most of the reasons are due to human errors. Drugs must be sampled at steady state; time of dose administration, dosage regimen as well as time and frequency of blood sampling must be carefully planned and recorded in order to reconstruct the correct pharmacokinetic profile [65, 123]. Errors are proportional to the number of samplings performed; additionally, repetitive manual data handling represent an additional source of errors in diagnosis as omissions and confusion can happen.

According to these considerations, the introduction of biosensors can benefit the TDM practice by improving practice diffusion; subjects' compliance, and pharmaceutical research:

- **Diffusion.** Biosensors can be designed to be small, inexpensive, and easy to use. Moreover electrochemical biosensors provide an immediate reading of the substance of interest. Cost reduction and simplicity of employ may allow the diffusion of TDM test from a small number of specialized laboratories to a bigger number of medical centers or even the patient's houses.
- **Compliance.** The introduction of biosensors can improve the compliance of both patients and operators. Home testing can both simplify the life of patients and reduce the cost of hospitalization. The development of automatic sampling procedures and remote data transmission can reduce the human error during analysis and data manipulation. An electronic device can automatically collect relevant information regarding patient status, testing procedure and analyses results, and send this data directly to a specialized center for clinical interpretation. Ideally a patient can self-test at home and receive new therapeutic indications online. Additionally, the diffusion of long-term implantable biosensors can benefit patients with chronic pathologies for which frequent control of drug pharmacokinetics may be essential. In this respect, elderly people, more subjected to aging effects and to the insurgence of chronic pathologies represent a potential target.
- **Research.** The diffusion of cheap TDM procedures and the automatic data collection can help discovering unknown drug interactions; pharmacokinetics and pharmacodynamics data obtained from TDM can be classified and used to predict therapeutic outcomes in new patients with similar clinical history or in the design of new compounds. Finally, the introduction of implantable biosensors may result useful in preclinical research on animals. Constant monitoring of pharmacokinetics during toxicology and efficacy investigations could provide better information during the preclinical development of a drug. Additionally an implanted sensor is expected to reduce human intervention on the test subjects, improving their conditions.

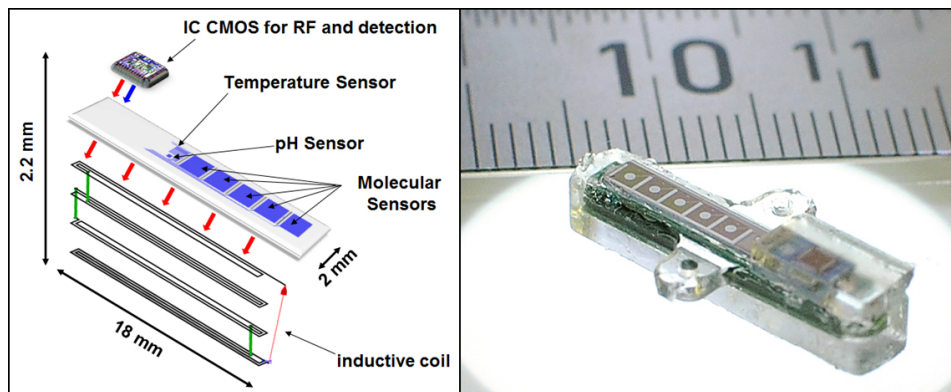


Figure 1.9: Schematics and (specular) picture of the assembled and packaged implantable device.

## 1.6 Thesis objective

Developing operational stand-alone biosensor components is a task commonly performed within the scientific community, and it is suitable for proof-of-principle evaluation or preliminary sensor characterization. However, a mature diagnostic device is an *integrated system* which has to take in account constraints from different disciplines:

- **Efficacy.** Effective biosensors systems for self-care must be capable to: 1) detect the target analytes in biologic concentrations 2) perform the detection without any additional processing of the target biological fluid 3) be capable to operate with small volumes.
- **Design.** The biosensor platform must be designed according to the application: the realization of a biosensor array is often necessary in personalized therapy, where multiple parameters must be controlled at the same time. Additional challenges are arising in the case of implantable sensors, since the dimensions must be kept at minimum, and materials should be biocompatible.
- **System integration.** Mature analytical devices must also face the challenges of signal processing, data transmission, powering and end-user interface. Electronics and biosensor components must be integrated together. The need for system integration forces the interaction and the application of design constraints from every actor involved in the device realization. As an example, the sensor platform must be capable to host the electronic equipment, while the sensing techniques employed must be simple enough to be coordinated with a low-power consumption circuitry, and grant at the same time sufficient precision to allow reliable measurements.
- **System packaging.** A mature biosensor device must be protected from external influences and ensure both electrical and biological integrity. If implanted, the final device as well its single components must be tested for in-vitro and in-vivo biocompatibility according international standards.

The objective of this PhD project is the development of a fully implantable biosensor system for personalized therapy applications. The thesis presents innovative research on:

- **Nanobiosensors for drugs and metabolites detection.** Electrochemical detection of common marketed drugs and drug cocktails with biosensors, as well as detection of glucose and ATP has been achieved with biosensors based on P450 enzymes, glucose oxidase and hexokinase. Carbon nanotubes have been employed as support for the immobilization of the biosensor proteins. The realized nanobiosensors provided increased sensitivity and detection limit, allowing the detection of drugs in their therapeutic range in undiluted human serum. References [36] and [37]; [29], [30] and [33] describe in detail the results obtained in this field during the PhD.
- **System design, fabrication, and integration.** A miniaturized passive substrate capable to host 5 independent biosensor electrodes, a pH sensor, a temperature sensor as well as the electronic interface for the signal acquisition has been designed, microfabricated and tested. Different and reproducible nano-bio-functionalization for the single biosensors was obtained with high precision via selective electrodeposition of chitosan/carbon nanotubes/enzyme solutions at the various electrodes. The array, completely microfabricated with biocompatible materials, was then integrated with a CMOS circuit and a remote powering coil for the realization of a fully implantable device<sup>9</sup>. The original research contribution has been described in [35].
- **System packaging and biocompatibility assessment.** The assembled system has been packaged with an inner moisture barrier in parylene C, to prevent circuit corrosion and toxic metals leaking, and an external biocompatible silicone shell to improve the host tolerance and reduce the local inflammation. The efficacy of the parylene barrier, as well as the toxicity of carbon nanotubes, has been assessed with *in-vitro* cytotoxicity tests conform to the ISO-109931 standards. The final packaged device, in Figure 1.9 was then implanted in mice to assess its biocompatibility. Comparison between 7 and 30 days in *in-vivo* implantations showed significant reduction of the inflammatory response in time, suggesting normal host recovery. Original research in this topic is presented in [4], submitted for peer review.

### 1.7 Thesis organization

P450 biosensors are treated in Chapters 2, 3 and 4: Chapter 2 introduces the cytochrome P450 proteins and provides information about their unique catalytic mechanism; Chapter 3 describes the working principle of electrochemical P450 biosensors and reviews the state-of-the-art; finally, in the Chapter 4, the original research on the P450 biosensors developed during this doctorate is presented.

---

<sup>9</sup>CMOS circuit and inductive coil have been realized by other collaborators.

ATP biosensors are treated in Chapter 5. The first part explains the importance of ATP in the modulation of inflammatory response and reviews the state-of-the art in the electrochemical ATP biosensors; the last part presents the data from the ATP biosensors developed in this doctorate.

Chapter 6 covers the implantable sensor platform developed during this PhD, presenting data on design, microfabrication, functionalization and test of the sensor array.

Chapter 7 focus on the system packaging and biocompatibility: the first part reviews the immune response to an implant, the strategies to solve specific biocompatibility and biostability issues and the controversies about the biocompatibility of carbon nanotubes; The last part describes the packaging developed in this project, and present data about the short term *in-vitro* and *in-vivo* biocompatibility of the implantable sensor platform.



## 2 Cytochromes P450: background

### 2.1 Introduction

Cytochromes P450 (abbreviated as P450s or CYPs) are a large group of enzymes involved in the metabolism of over 1'000'000 different xenobiotic<sup>1</sup> and endogenous compounds [47]. Depending on the organism, they contribute to vital processes including carbon source assimilation, biosynthesis of hormones and or structural component of cells, and also carcinogenesis and degradation of xenobiotics [171]. More importantly, CYPs are the major enzymes involved in human drug metabolism and bioactivation, accounting for about 75% of the total number of different metabolic reactions [68].

In humans, only 5 P450 isoforms are responsible for the metabolisms of the 95% of known pharmacological compounds [67]; this makes the CYPs promising candidates for the construction of biosensors for therapeutic drug monitoring. In principle, a sensor bearing the 5 cytochromes altogether, can be used to follow the drug response of individuals in almost every kind of pharmacological treatment 2.1. The following internet site <http://medicine.iupui.edu/clinpharm/ddis/table.aspx> contains an updated list of common drugs that are CYP substrates.

### 2.2 P450 nomenclature, classification and polymorphism

Cytochromes P450s belong to the hemoproteins superfamily. The letter *P* in P450 represents the word pigment, while the number *450* reflects the wavelength of maximum adsorption in spectroscopy. In simple words, concentrated quantities of protein appear red at sight due to the iron atom present in their active site. CYP enzymes have been identified in all domains of life. At present, more than 11500 distinct proteins are known, but only 57 of them are present in humans [67].

Cytochromes P450 are classified in families, subfamilies, isoforms and polymorphisms accord-

---

<sup>1</sup>A xenobiotic is a chemical which is found in an organism but which is not normally produced or expected to be present in it, for example a drug.

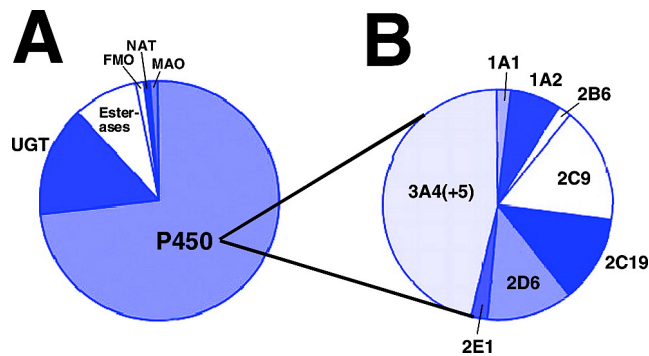


Figure 2.1: Contributions of Enzymes to the metabolism of marketed drugs. (A) Fraction of human enzymes involved in drug metabolism: FMO, flavin containing monooxygenase, NAT, n-acetyltransferase, MAO, monoamine oxidase. (B) P450 isoforms contribution to drug metabolism. Reprinted from [68].

ing to their amino acid sequence homology:

- A *family* groups all the genes with at least 40% of sequence homology. At present more than 780 families have been discovered in nature; 18 of them shared by humans.
- A *subfamily* encloses genes of the same family sharing at least 55% of sequence homology.
- An *isoform* identifies the different proteins coded by an individual gene within the subfamily
- A *polymorphism* can be described as a slightly different protein isoform, usually occurring with 1% frequency in a population.

This classification is summarized in the nomenclature of P450 proteins: the acronym CYP, followed by a number (family), a letter (subfamily), a second number (isoform) and \*number (polymorphism). CYP2B6\*4 for example identifies a P450, family 2, subfamily B, isoform 6, polymorphism 4. Cytochromes polymorphism is one of the major causes in drugs metabolism differences among individuals. It has been estimated that 20 to 25% of all drug therapies lead to different therapeutic outcomes because of genetic differences [80]. According to the differences in P450s expression, a population can be classified in 4 major phenotypes:

- *Ultrarapid metabolizers* (UM), presenting 3 or more genes encoding a specific P450, and therefore showing an increased enzymatic activity.
- *Extensive metabolizers* (EM), carrying 2 functional genes and presenting standard enzymatic activity.
- *Intermediate metabolizers* (IM), being deficient of one allele, and showing reduced activity.



- *Poor metabolizers* (PM), lacking the functional enzyme due to defective or deleted genes.

Genetic analysis of the cytochrome polymorphisms represents the actual state-of-the-art in personalized therapy. The work of Ingelman-Sundberg, provides an extensive review describing the major polymorphic CYP alleles and their effect on major therapies [80].

## 2.3 P450 catalytic cycle

The most common reaction catalyzed by the P450s is the insertion of an oxygen atom into a substrate (RH). The biological significance of this reaction, called *monooxygenation*, is to transform liposoluble compounds in hydrosoluble, in order to be easily excreted with the urine. While some P450s do not require additional protein and cofactor components to achieve the monooxygenation reaction, the vast majority performs the catalysis after interaction with redox partners in an electron transfer (ET) chain: the *P450 systems*. At present, ten different classes of P450 systems have been discovered. Table 2.1, from Hannemann et al., provides a summary of each class [70].

Class/source	Electron transport chain	Localization/remarks
<i>Class I</i>		
Bacterial	NAD(P)H ► [FdR] ► [Fdx] ► [P450]	Cytosolic, soluble
Mitochondrial	NADPH ► [FdR] ► [Fdx] ► [P450]	P450: inner mitochondrial membrane, FdR: membrane associated, Fdx: mitochondrial matrix, soluble
<i>Class II</i>		
Bacterial	NADH ► [CPR] ► [P450]	Cytosolic, soluble; <i>Streptomyces carbophilus</i>
Microsomal A	NADPH ► [CPR] ► [P450]	Membrane anchored, ER
Microsomal B	NADPH ► [CPR] ► [cytb5] ► [P450]	Membrane anchored, ER
Microsomal C	NADH ► [cytb5Red] ► [cytb5] ► [P450]	Membrane anchored, ER
<i>Class III</i>		
Bacterial	NAD(P)H ► [FdR] ► [Fdx] ► [P450]	Cytosolic, soluble, <i>Citrobacter braakii</i>
<i>Class IV</i>		
Bacterial	Pyruvat, CoA ► [OFOR] ► [Fdx] ► [P450]	Cytosolic, soluble, <i>Sulfolobus tokadaii</i>
<i>Class V</i>		
Bacterial	NADH ► [FdR] ► [Fdx-P450]	Cytosolic, soluble, <i>Methylococcus capsulatus</i>
<i>Class VI</i>		
Bacterial	NAD(P)H ► [FdR] ► [Fdx-P450]	Cytosolic, soluble, <i>Rhodococcus rhodochrous</i> strain 11Y
<i>Class VII</i>		
Bacterial	NADH ► [PFOR-P450]	Cytosolic, soluble, <i>Rhodococcus sp</i> strain NCIMB 9784, <i>Burkholderia sp.</i> , <i>Ralstonia metallidurans</i>
<i>Class VIII</i>		
Bacteria, fungi	NADPH ► [CPR-P450]	Cytosolic, soluble, <i>Bacillus megaterium</i> , <i>Fusarium oxysporum</i>
<i>Class IX</i>		
Only NADH dependent, fungi	NADH ► [P450]	Cytosolic, soluble, <i>Fusarium oxysporum</i>
<i>Class X</i>		
Independent in plants/mammals	[P450]	Membrane bound, ER

Table 2.1: Classes of P450 systems classified depending on the topology of the protein components involved in the electron transfer to the P450 enzyme. Reprinted from [70]

## Chapter 2. Cytochromes P450: background

---

The biosensors described in this thesis employ human microsomal P450s, which rely on a class 2 electron transfer system. In this system the *cytochrome P450 reductase* (CPR) and the *cytochrome b5 reductase*, provide the CYP with the two electrodes needed for the catalysis. The global reaction of P450 with a substrate RH can be summarized by the equation below:

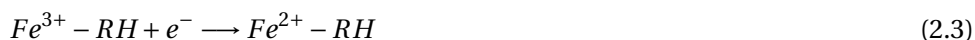


In a class 2 electron transfer system, this reaction can be described with the following steps:

1. **Substrate binding:** the substrate docks to the active site in close proximity of the heme group, displacing a water molecule coordinated to the heme Iron.



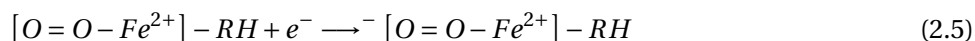
2. **First electron transfer.** The first electron is transferred to the active site via the interaction of the P450 with the Cytochrome P450 reductase. The ferric heme is reduced.



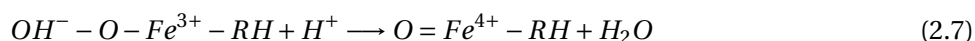
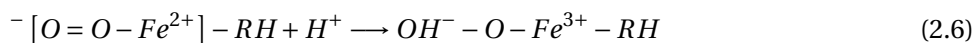
3. **Binding of molecular oxygen.** An oxygen molecule bounds the heme and induces a slow rearrangement of the complex creating an intermediate called *oxy-P450 complex*.



4. **Second electron transfer.** This stage represents the rate limiting step of the cycle. A second electrode supplied by the CPR or from the faster cytochrome b5 reductase feeds into the complex and forms a *peroxy-ferric intermediate*



5. **Protonation of the peroxy-ferric intermediate.** The peroxy group ( $O^{2-}$ ) formed in the previous step is protonated by surrounding amino acids. As result the O-O bonding undergoes heterolysis, a molecule of water is released and a highly reactive Iron (IV)-oxo species is formed. At this stage the P450 is ready transform the substrate.



6. **Insertion of the oxygen into substrate and product release.** Depending on substrates

and enzyme involved, the P450s can catalyze a wide variety of reactions. A complete list of monooxygenations is reported in Figure 2.3.

7. **Product dissociation.** The different chemical structure of the product induces its release from the active site. The cytochrome returns to its resting state with a water molecule coordinated to the heme group.



Exceptions can occur in the cycle. Some instable intermediates can lead to substrate dissociation, regeneration of the active site and production of intermediary products. The 3 major abortive reactions (shunts) are the:

- **Autoxidation shunt (point 3 of the cycle).** Causes the release of a superoxide ( $O_2^-$ ) radical.
- **Peroxide shunt (point 5a of the cycle).** The hydroperoxide group ( $HO-O^-$ ) dissociates from the enzyme. An additional protonation leads to the production of Hydrogen peroxide.
- **Oxidase shunt (point 6 of the cycle).** Causes the decoupling of oxygen in the Iron (IV) oxo species and the production of an additional molecule of water.

In electrochemical P450 biosensors, the electrons needed for the monooxygenation reaction can be directly provided to the cytochrome by the electrode. The demand of electrons depends on the activity of the enzyme and can be directly correlated to the substrate concentration at the electrode interface. Ideally, higher concentrations of substrate will increase the electrons demand and therefore will generate higher currents.

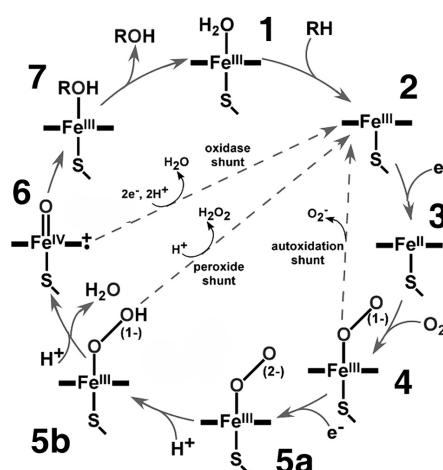
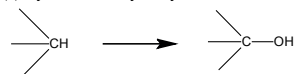


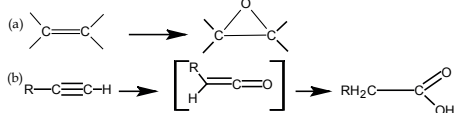
Figure 2.2: The P450 catalytic cycle. Copyright 2005 American Chemical Society.

## Chapter 2. Cytochromes P450: background

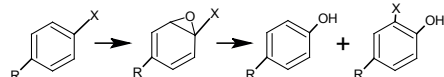
### (1) Hydrocarbon hydroxylation



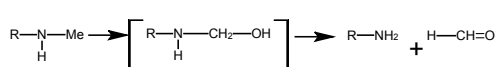
### (2) Alkene epoxidation/ Alkyne oxygenation



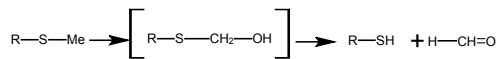
### (3) Arene epoxidation, aromatic hydroxylation, NIH shift



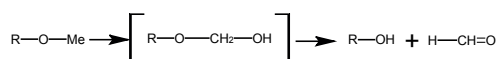
### (4) N-Dealkylation



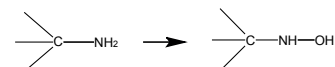
### (5) S-Dealkylation



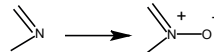
### (6) O-Dealkylation



### (7) N-Hydroxylation



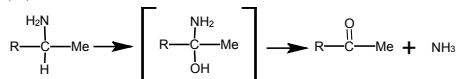
### (8) N-Oxidation



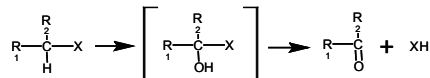
### (9) S-Oxidation



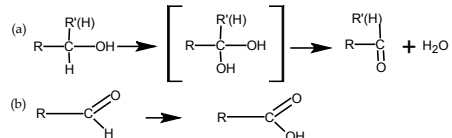
### (10) Oxidative deamination



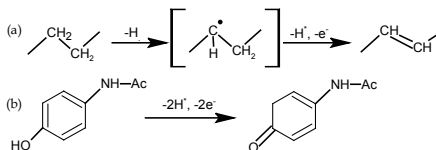
### (11) Oxidative dehalogenation



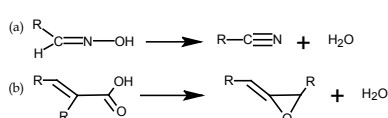
### (12) Alcohol and Aldehyde oxidations



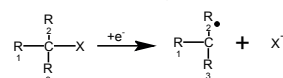
### (13) Dehydrogenation



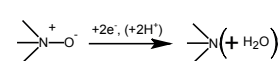
### (14) Dehydrations



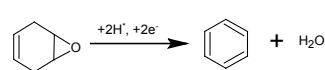
### (15) Reductive dehalogenation



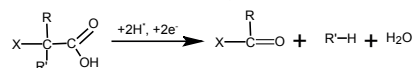
### (16) N-Oxide reduction



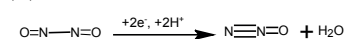
### (17) Epoxide reduction



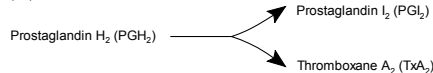
### (18) Reductive $\beta$ -scission of alkyl peroxides



### (19) NO reduction



### (20) Isomerizations



### (21) Oxidative C-C bond cleavage

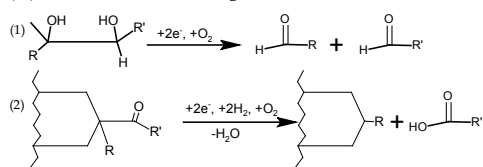


Figure 2.3: List of reactions catalyzed by cytochromes P450. Reprinted from [17].

## 2.4 P450 catalysis

One of the most important features of CYPs is their broad substrate range. As said before, only 5 cytochrome isoforms are responsible for the 95% of metabolism of all known drugs. The reasons for this wide substrate range are due to the p450 active site features, described in this section.

The structural core of P450 is formed by 4 highly conserved alpha helices (named D, L, I, E) holding in place the heme group. As seen before, the heme is exploited to catalyze substrate oxidations or reductions thanks to the reversible oxidation and reduction of its Fe atom. The active site dimension is diverse among cytochromes: CYP3A4, CYP2C8 and CYP2C9 for example possess very large active sites, whilst that of CYP2A6 is quite small. However, the active site area is surrounded by flexible domains capable to adapt to molecules of different sizes. For example, the CYP3A4 active site can expand up to 80% of its original dimensions to accommodate erythromycin [17]. Substrate binding in P450 is not well definite: at the simplest structural level, P450 active sites present multiple docking points called *substrate recognition sites* (SRS) [72]. The way compounds bind to the SRS, depends by the substrates involved, their relative concentration and their affinity for the enzyme. Substrates can induce a *ligand-dependent conformational change*, where each combination of ligands induces alternative enzyme conformations with unique kinetic properties; a second type of alteration is due to the interaction between different ligands: a molecule can influence the affinity of the binding site for a second molecule, even if no significant protein conformational change takes place.

Multiple docking of different molecules on diverse SRS is greatly affecting the catalytic activity of cytochromes P450, giving rise to atypical kinetic profiles. Up to 8 different kinetic behaviors can manifest in the cytochromes. Among these, *homotropic* kinetic profiles are originated by the interaction of the enzyme with a single substrate; while *heterotropic* kinetic responses appear when a compound affects the interaction of the enzyme with a second compound. Enzyme kinetics is an important aspect to consider in the design and in the calibration of biosensors. Before proceeding to the description of the complex behaviors of P450, some basic kinetic notions will be introduced in the following paragraphs.

## 2.5 Introduction to the enzyme kinetics

The kinetic profiles are equations describing the velocity of product formation given specific amounts of enzymes and substrates. Any enzymatic reaction can be described with the following diagram:



Where  $E$  is the enzyme concentration,  $S$  the substrate concentration, and  $P$  the product formed.  $k_1$ ,  $k_2$  and  $k_d$ , and are constants: the first indicates the rate of formation of the

## Chapter 2. Cytochromes P450: background

---

complex enzyme-substrate (ES), the second the rate of dissociation of the complex ES, while  $k_d$  describes the rate of product formation. This general enzymatic reaction can be divided in two parts:

- A *fast stage*  $E + S \rightleftharpoons ES$  where the complex ES is rapidly formed. Assuming the enzyme concentration is constant, the rate of formation  $V$  of the complex is proportional to the substrate concentration according the equation  $V=k[S]$
- A *slow stage*  $ES \longrightarrow E + P$  where the enzyme needs to overtake the activation energy in order to form the product. The rate of product formation  $E+P$  is proportional to the concentration of the ES complex and is described by the equation  $V=k[ES]$  the complex ES is therefore the rate limiting step in determining the overall speed of the enzyme.

The concentration of ES depends by the initial amount of enzyme. When all the enzymes are saturated, increasing substrate concentrations do not affect the speed of catalysis. In this situation, called steady state, the reaction speed is proximal to the maximum possible value. The simplest kinetic equation and the most common among enzymes is the *Michaelis Menten equation*, which describes a hyperbolic kinetic profile.

$$V = \frac{V_{max} [S]}{k_m + [S]} \quad (2.10)$$

Where  $V_{max} = k_p [E]$  is the enzyme reaction rate at the steady state, and  $k_m$ , the constant of Michaelis Menten is defined as  $\frac{k_2+k_d}{k_1}$ . As basic assumption in this equation S, ES and E are in equilibrium [122].

Substrate concentration, enzyme concentration and  $k_m$  change the profile of the hyperbolic kinetic and are important parameters to consider in the design of biosensors: more concentrated enzymes increase the maximum amount of substrate that can be processed, and therefore affect the  $V_{max}$  of the enzyme. The substrate concentration is the most important factor in determining the speed of reaction: when  $[S] \gg [E]$ ,  $k_m$  at the denominator is negligible. The reaction speed is therefore equal to  $V_{max}$  and is independent by the substrate amount. Conversely, when  $[S] \ll [E]$ , the equation is simplified, and  $V_{max}$  is proportional to  $[S]$  according to the relationship  $V_0 = \frac{V_{max}[S]}{k_m}$ . Biologically,  $k_m$  represents a measure of the affinity of the enzyme for its substrate. Low values of  $k_m$  indicate that the enzyme binds tightly to the substrate and saturates at relatively low concentrations; conversely, large  $k_m$  indicate low affinity for the enzyme and saturation at high concentrations. The knowledge of kinetic parameters is an important aspect to understand how a CYP electrochemical biosensor works. P450-based detection is a measure of the electron transfer rate between the electrode and the enzyme given a certain substrate. According to this, the electron transfer rate can be compared to the enzymatic speed. Therefore, given the same amount of enzyme immobilized, a higher current indicates increasing substrate concentrations.

## 2.6 Atypical kinetic mechanisms in P450 enzymes

As previously stated, multiple docking of different molecules on diverse SRS is greatly affecting the catalytic activity of cytochromes P450, giving rise to atypical kinetic profiles. As general effect, the presence of a particular mixture of compounds, or of a critical amount of substrate(s) induces contextual responses in the activity of P450 [13]. This means that biosensor calibration, sensitivity and operative window for a specific substrate are greatly influenced by the composition of the sample analyzed. The knowledge of atypical kinetic behaviors and of the conditions that trigger a determinate response in the cytochromes, are therefore important for the construction of models that allow to adapt and to correct the data coming from the biosensor. While the development of such models is outside the objective of this thesis, it may be interesting giving a glimpse of the complexity of P450 catalysis and a starting point for their design. This section will present an overview of the atypical kinetic profiles, and examples of drugs that trigger a specific response.

Atypical profiles fall into five categories: *auto-activation*, *hetero-activation*, *auto-inhibition*, *hetero-inhibition*, and *biphasic* kinetic [78], (Figure 2.4). Profiles originated by the interaction of the enzyme with a single substrate are called *homotropic*, while profiles due to the interaction of different compounds with the protein are called *heterotropic*. As additional complexity, heterotropic effects for a given ligand combination are CYP isoform dependent [13].

- *Auto activation* (Positive homotropic cooperativity) occurs when the binding of the substrate at one site improves the binding affinity of other sites. The increased affinity causes a rapid and coordinated increment of the reaction speed at higher [S], until  $V_{max}$  is achieved. Plotting  $V_0$  vs[S], a sigmoidal shape is observed, with low activity at low substrate concentration and a rapid and immediate increase in enzyme activity to  $V_{max}$  as [S] increases. Positive cooperativity makes enzymes much more sensitive to [S] and their activities can show large changes over a narrow range of substrate concentration.
- In *hetero activation* (positive Heterotropic cooperativity), the substrate "A" improves the catalysis of the substrate "B" inducing structural or electronic changes in the P450 structure. In most cases both compounds are substrates of the enzyme, but only the metabolism of one is increased.
- In *auto inhibition* (negative homotropic cooperativity), the binding of the substrate at one site decrease the binding affinity of other sites. As result higher [S] are catalyzed at lower speeds. The  $V_0$  vs[S] plot present a convex profile, as the  $V_{max}$  expected from the standard hyperbolic kinetics is never reached.
- In *hetero inhibition* (negative heterotropic cooperativity), the substrate A hinders the catalysis of the substrate B. Hetero inhibition is defined partial when despite the presence of saturating concentrations of the compound "B" the catalysis of "A" is not completely blocked. When the compound "A" blocks the catalysis of "B" but not of the substrate "C", the Hetero inhibition is defined substrate-dependent.

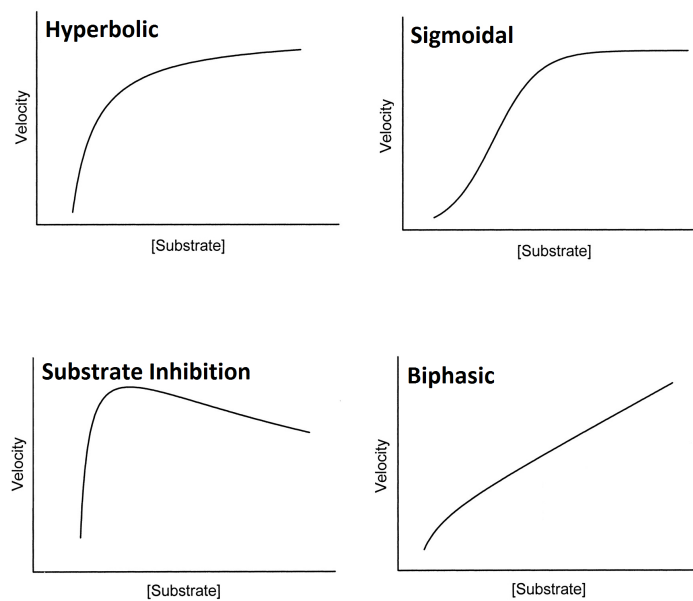


Figure 2.4: Possible kinetic profiles with homotropic effects.

- *Biphasic kinetics* occurs when the protein present two binding sites for the same compound with different catalytic efficiency. The kinetics is characterized by an initial hyperbolic behavior with increasing substrate concentrations, however the profile never become asymptotic but tends to linearity at high concentrations, leading to the inability to predict  $V_{max}$  and  $k_m$ .

### 2.7 Design of a general kinetic model

Several steady state kinetic models have been developed to describe homotropic and heterotropic kinetics. Figure 2.5 describes a general scheme of enzymatic reaction for a cytochrome with 2 binding sites, and two active compounds: a substrate (S) and an effector (E).

The model accounts for homotropic and Heterotropic binding of the compounds, but for simplicity, only the substrate S is converted into product (P). In this model,  $k_S$ ,  $k_E$ , and  $k_{cat}$  values for substrate and effector change according to the occupational state of the active site. When allosteric binding takes place,  $k_E$ , and  $k_{cat}$  values for substrate and effector are multiplied for a sub-constant that accounts for the effect of compound already present in the active site:

- The sub-constant  $\varepsilon$ , acting on  $k_E$ , accounts for the homotropic binding of the effector to the active site.
- $\sigma$ , acting on  $k_S$ , accounts for the homotropic binding of the substrate to the active site.



## 2.7. Design of a general kinetic model

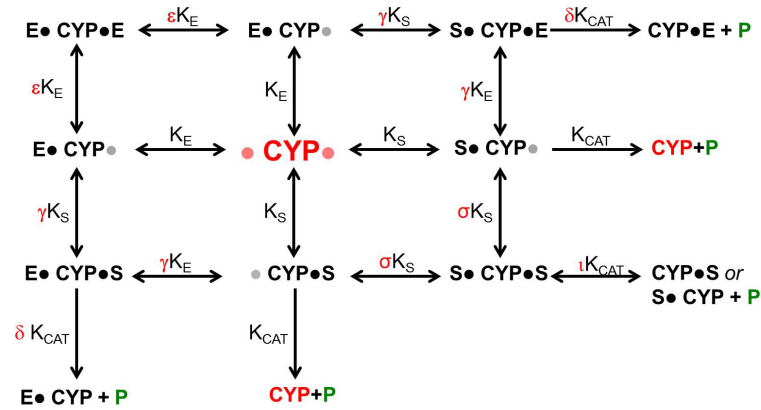


Figure 2.5: Substrate and effector binding combinations for a Cytochrome with 2 binding sites (•). Adapted from [13].

- $\gamma$  describes an heterotropic binding in the active site, and affects both  $k_S$  and  $k_E$ . For simplicity, in this model  $\gamma$  is identical for different compounds arrangement in the active site.
- $\delta$  affects the  $k_{cat}$  of substrate when different ligands are present in the active site.
- $\iota$  affects the  $k_{cat}$  of the substrate when identical compounds are present in the active site.

Values of  $\epsilon$ ,  $\gamma$  and  $\sigma$  bigger than 1 will lead to positive cooperativity between substrates, while values lower than 1 will generate substrate inhibition effects. Variation in  $\delta$  and  $\iota$  affect the rate of product formation and modulate the  $V_{max}$  of the enzyme. The following equation, obtained from Figure 2.5, can be used to calculate the reaction speed [13], and it was successfully employed to examine context dependent heterotropic effects in CYP3A4 [58, 89, 147].

$$V_0 = \frac{\frac{[S]}{k_S} + \frac{\iota[S]^2}{\sigma k_S^2} + \frac{\delta[S][E]}{\gamma k_S k_E}}{1 + \frac{2[S]}{k_S} + \frac{[S]^2}{k_S^2} + \frac{2[S][E]}{\gamma k_S k_E} + \frac{2[E]}{k_E} + \frac{[E]^2}{\epsilon k_E^2}} \quad (2.11)$$

Variations in substrate and effector concentration yield a series of different contextual kinetic profiles that can be plotted as a surface. Figure 2.6, from [92] shows the effect of the substrate quinidine on the diclofenac hydroxylation.

Some works suggest that the effect of specific compound on the P450 catalysis can be guessed *a priori*. For example, crystallographic structures and kinetic experiments have identified for CYP3A4 three model compounds that show distinctive kinetic properties and preferential binding domains in the active site: midazolam gives hyperbolic kinetic profiles; testosterone yields sigmoidal kinetics, while nifedipine induce substrate inhibition curves [58]. Compounds presenting similar features such as, steric bulk, charge, flexibility and others, can be classified

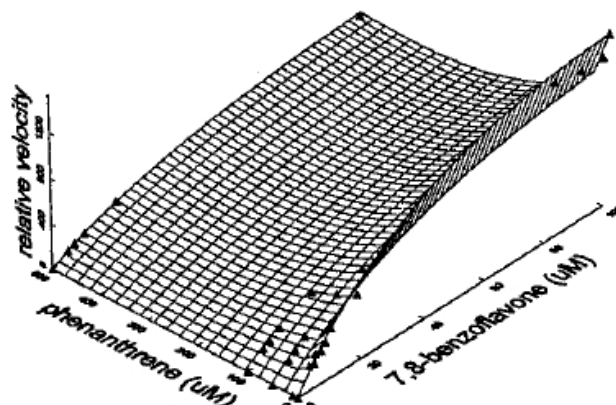


Figure 2.6: Interactions between phenanthrene and benzoflavone. The surface represents predicted results to experimental data. Reprinted from [92].

into a specific subgroup and are therefore expected to induce behaviors similar to one of the three model compounds [59, 165].

The knowledge of these parameters *a priori* could be useful in the configuration of the P450 biosensor in presence of different drug combinations.

## 2.8 Chapter Summary

This chapter presented an overview about cytochromes P450 and enzyme kinetics. Cytochromes P450 possess a broad substrate range, and only 5 isoforms are responsible for the 95% of metabolism of all known drugs. The most common reaction catalyzed by the P450s is the monooxygenation, which transforms liposoluble compounds in hydrosoluble. Cytochromes possess large active sites and are capable to host and transform multiple molecules at the same time. The multiple docking of different molecules on the P450 active site affects the catalytic activity and gives rise to atypical kinetic profiles. With respect to the biosensor development, the knowledge of the kinetic parameters can help in fitting the data, optimizing the sensitivity, calibrate the biosensor, define appropriate concentration ranges for the analytes and predict the response in presence of different drug combinations. For example:

- Sensitivity is usually calculated for linear behaviors. As consequence, biosensor detection is significant only with good approximations of first order kinetics.
- Increasing enzyme concentrations produce higher currents and therefore increase the overall sensitivity of the sensor.
- Substrates with high  $k_m$  give significant current variations only with big increase in the substrate concentration. Sensitivity for these compounds will be therefore low, and detection is appropriate only in broad concentration ranges.

- Substrates with low  $k_m$  give significant current variations with small increase in the substrate concentration; higher amounts of substrate will lead to saturating currents. Detection will be appropriate only in narrow concentration ranges.
- Due to the competition for the active site, compounds present a higher  $k_m$  when other substrates are present in solution. The increase in their  $k_m$  depends by the affinity of the competitors and their relative concentrations.

The broad substrate range of cytochromes, their atypical kinetic profiles and the contextual catalytic behavior of cytochromes represent a challenge in the development of P450 biosensors, as they make the response subject to many variables. Despite this, the development of electrochemical P450 biosensors remains an appealing objective for two reasons. First, P450-biosensors represent the sole way to detect non-electroactive compounds electrochemically: the biosensor measures the electron transfer between protein and electrode, an index of the enzyme activity and a direct effect of the substrate concentration. Second, few cytochromes isoforms account for almost the totality of the xenobiotics metabolism, therefore the development of a method capable to distinguish and quantify the contribution of different compounds, prospects the realization of a versatile device suitable to follow many different therapeutic schemes. In this respect P450 biosensors represent the ideal choice in the realization of long-term implantable devices for personalized therapy.



### 3 P450 biosensors: background and state-of-the-art

P450 biosensors measure the electron transfer between protein and electrode. Proteins are immobilized on the electrode surface, and the electrons needed for the monooxygenation reaction are supplied by the electrode (Figure 3.1). Electron demand depends on the activity of the enzyme and is correlated to the substrate concentration at the electrode interface. Ideally, higher concentrations of substrate will increase the electrons needed, and therefore will generate higher currents. The different nature of substrates bound to the cytochrome will change the energy required for activating the electron transfer, and therefore the potential at which this reaction will take place [83]. The need to query the cytochrome response at different potentials makes the voltammetric techniques the ideal choice for P450-based detection.

In order to perform a voltammetric analysis, current and potential must be accurately measured and controlled; for this reason, electrochemical biosensors rely on a 3-electrode cell configuration, described in the next section.

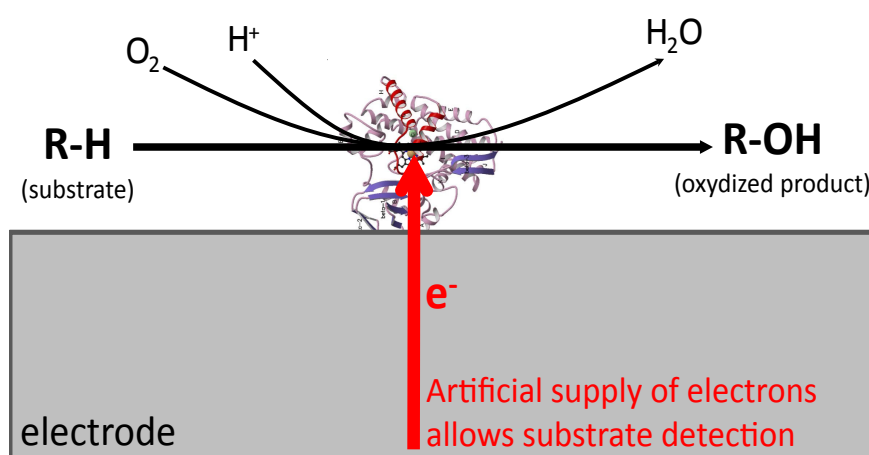


Figure 3.1: Simplified principle of the P450 biosensor: the electrons needed for the catalysis are supplied by the electrode, allowing substrate detection.

### 3.1 Three electrode configuration and potential control

An electrolytic cell is an electrochemical system that undergoes a redox reaction when electrical energy is applied. The cell has three component parts: an electrolyte and two electrodes. The electrode/electrolyte couple is called *half cell*. The electrolyte is usually a solution of water or other solvents in which ions are dissolved. When an external voltage of correct polarity and sufficient magnitude is applied to the electrodes, the electrolyte can exchange electrons with the electrode and become oxidized or reduced generating a current flow across the cell. In general, the minimum requirement for voltammetric analysis is a *two-electrode* configuration. In this setup, the *working electrode* (WE), where the enzyme is immobilized, must apply the desired potential in a controlled way and facilitate the transfer of charge to or from the enzyme. The second electrode must assume a known potential with which to gauge the potential of the WE; furthermore, it must balance the charge added or removed by the working electrode. Unfortunately, with this arrangement it is extremely difficult to maintain a constant potential while passing current to counter redox events at the working electrode. To solve this problem, the role of supplying electrons and referencing potential has been split in two separate electrodes: the *reference electrode* (RE) is a half cell with a known potential; it acts as reference in measuring and controlling the WE potential and it does not enable any current flow; the *counter electrode* (CE) pumps (or collects) all the current needed to balance the current required (or observed) at the working electrode. Current and potential in the 3-electrode cell are controlled by a potentiostat, which functions by maintaining the potential difference between RE and WE at a constant level, by adjusting the current at the CE. Fig. 3.2 shows a schematic of the three electrode configuration and the potentiostat-principle. A fully implantable sensor based on voltammetric techniques will therefore require a miniaturized 3-electrode cell, a potentiostat circuit, and a power source.

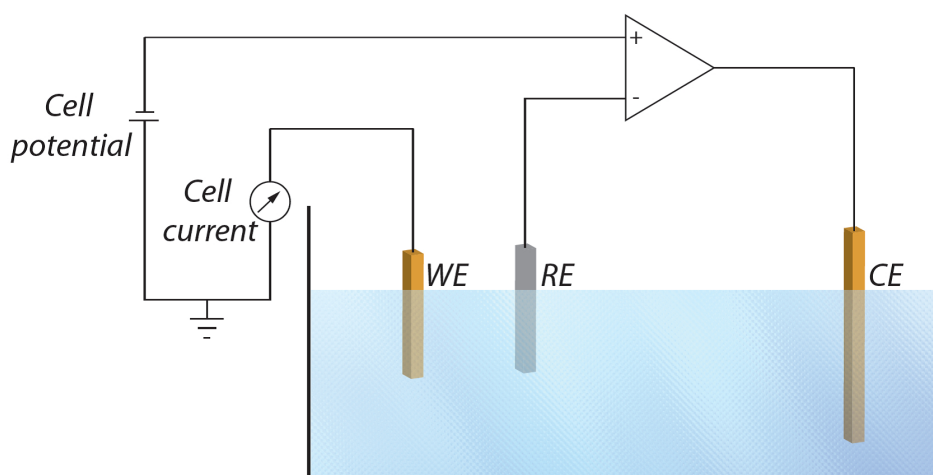


Figure 3.2: Diagram of a three-electrode cell.

## 3.2 Background on voltammetry

Voltammetry is the study of current as function of applied potential. In cyclic voltammetry, the potential is swept back and forth at a constant rate between two extreme values, and the actual current value is measured as the dependent variable. The total current in the cell is the difference between the *oxidative current*, generated by the potential sweep towards more positive values, and of the *reductive current*, produced when the potential is swept back more negative values. The behavior of the current as a function of the applied potential is described by the *Butler-Volmer equation*:

$$I = I_{ox} - I_{red} = nFAk_0 \left\{ [O]_{0,t} e^{\frac{-\alpha F(E-E_{eq})}{RT}} - [R]_{0,t} e^{\frac{-\alpha F(E-E_{eq})}{RT}} \right\} \quad (3.1)$$

where,  $I$  is the net current of the cell,  $I_{ox}$  and  $I_{red}$  are respectively the oxidation and the reduction current in their absolute values,  $E$  is the applied potential,  $E_{eq}$  the equilibrium potential,  $F$  the Faraday constant,  $R$  the universal gas constant,  $T$  the absolute temperature,  $n$  the electrons exchanged in the redox and  $A$  the electroactive area. The constant  $k_0$  is a measure of the redox efficiency: small values of  $k_0$  indicate very slow redox processes. The parameter  $\alpha$  is the charge transfer coefficient.

The current generated during the potential scan is the sum of two components: capacitive and Faradic. The capacitive current originates when solution electrolytes become polarized and migrate to the electrode bearing opposite charge. The accumulation of charged ions at the interface generates an electrical double layer that behaves like a capacitor with area equivalent to the electroactive surface. The capacitive current  $i_c$  is defined as:

$$i_c = C \frac{dE}{dt} = Cv \quad (3.2)$$

where  $C$  is the capacitance of the electrical double layer,  $E$  the applied potential,  $t$  the time and  $v$  the scan rate. In voltammetric analysis, the capacitive current is considered non-specific background interference and must be subtracted from the total current to obtain the Faradic contribution. In cases where the concentration of the electroactive compound is too low, or when the scan rate is too high, the Faradic current can be masked by the capacitive current causing problems in the detection.

The *Faradic current* is due to the electron transfer at the electrode interface, and represents the current of interest for the electrochemical detection. In steady state conditions, the Faradic current assumes a peak shape with the current maximum centered on the formal potential of the analyte (Fig. 3.3). In a backward potential sweep of a soluble electroactive species, when the electrode potential approaches the specimen's formal redox potential, the reduction of the analyte begins, and current starts to flow (A). As the potential continues to grow more negative, the surface concentration of the species drops; hence, the flux to the surface (and the current) increases (B). At the formal redox potential (C), the current intensity is defined by

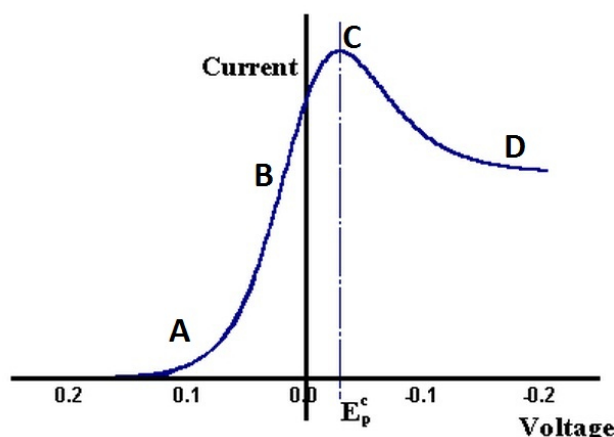


Figure 3.3: Voltammetric sweep of an electroactive species in solution.

the *Randles-Sevcik equation*:

$$i_p = 0.4463nFAC \left( \frac{nFvD}{RT} \right)^{\frac{1}{2}} \quad (3.3)$$

where  $i_p$  is the peak current,  $C$  the analyte concentration, and  $D$  the diffusion coefficient of the analyte. As the potential crosses the reduction potential peak, surface concentration drops nearly to zero, mass transfer reaches a maximum rate at the surface, and then it declines as the depletion effect sets in. This is the case where the current is limited by the diffusion of the reagents to the electrode surface (D). When the potential is swept in the opposite direction, symmetric mechanisms take place and the reduced species are oxidized again.

The P450 biosensors presented in this thesis rely on a technique called *catalytic protein film cyclic voltammetry* [8]. In the absence of substrate and at sufficiently high coverage, a redox enzyme immobilized onto an electrode gives peak-like signals resulting from the reversible transformation of its redox centers. The potential sweeping in cyclic voltammetry is used to artificially turn “on” and “off” the redox center of the enzyme (Figure 3.4): in the previous chapter, it was shown how the P450 active site needs 2 electrons to perform the monooxygenation reaction. In a P450 biosensor, those electrons are artificially provided by the electrode when sufficient energy for the electron transfer is furnished. In absence of substrate, this current flow will continue until all the proteins immobilized will have their substrate reduced (enzyme “on”). As result a peak-shape Faradic current is generated. Ideally, a potential sweep in the opposite direction will regenerate the active site producing a symmetrical peak (enzyme “off”).

During the catalysis, the electrons of the active site are further transferred to the substrate, allowing the heme to accept new electrons from the electrode and producing a Faradic contribution known as *catalytic current*. The catalytic protein film cyclic voltammetry establishes a relationship between current, enzyme concentration and substrate concentration:



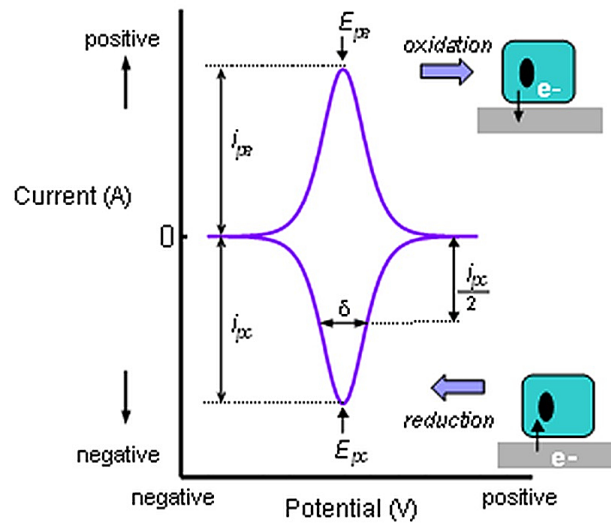


Figure 3.4: Cyclic voltammetry response from a film of adsorbed protein containing a single redox active centre undergoing reversible electron transfer.

- The detected Faradic current is associated only with the electron transfer between enzyme and electrode. The substrate is not electroactive.
- Higher amounts of enzyme immobilized (electroactive coverage) allow the conversion of a bigger number of substrates in a given period of time, leading to higher catalytic currents.
- The demand of electrons in presence of substrate is directly related to the speed of the enzymatic catalysis and is therefore dependent on the enzyme kinetics: when the substrate concentration at the interface is much lower than the enzyme concentration, the reaction speed (and therefore the generated current) is proportional to the substrate concentration. Conversely, if the concentration of substrate at the interface is bigger than the enzyme concentration, the enzymatic speed (and therefore the current generated) reaches a maximum, making it impossible to establish a relationship with the substrate concentration.
- The electron demand also depends on the substrate diffusion to the electrode. When a fixed substrate concentration is supplied at a constant rate and products do not accumulate at the electrode interface, the catalytic current takes the shape of a wave. The wave shape is achievable controlling diffusion at the interface with rotating disk electrodes or with microelectrodes. The absence of diffusion control, will lead to peak-shaped catalytic currents.

The reliable measure of the Faradic current represents one of the core aspects of biosensor research, while the understanding of its variation upon different experimental conditions is a part of the sensor characterization. Both aspects will be described later in this chapter.

### 3.3 P450 biosensors: state-of-the-art

Besides personalized therapy, P450 reactions are of extreme interest to the pharmaceutical industry. Knowing how drugs affect the P450s, enables the prediction of dangerous interactions and is fundamental in the isolation of new substances in the early stages of drug discovery. Although the high speed of drug screening over the past several years, there is still a difference of orders of magnitude in throughput methods for the lead compound identification, such as combinatorial libraries, and screening rate/capacity for CYP activity [5]. Chromatography and mass spectroscopy of CYP metabolites remain the standard in industry but the throughput is limited to the number of samples processed in parallel and by the analysis time of an individual sample. This results in a bottleneck in the drug development process. Existing high throughput methods for CYP metabolism screening are based on indirect detection: in one case, substrates yielding fluorescent products once metabolized, are used to probe the ability of an unknown drug to inhibit or compete with the fluorogenic compound in the P450 reaction [120, 161]. A second type of assay measures the CYP activity indirectly, by detecting oxygen and NADPH consumption via fluorescence [160]. A drawback of this approach is the need for multiple reagents and enzymes, which makes this strategy expensive and time-consuming.

The immobilization of CYPs onto an electrode surface can open the way to a fast, inexpensive and direct monitoring of P450 metabolism, and therefore is a promising strategy for high throughput sensing techniques and personalized therapy applications. Two of the main issues in P450 biosensors concern the improvement of the electric coupling between protein and electrode, and the protein stability. It is therefore not surprising that many reviews on P450 biosensors focus on the enzyme immobilization [22, 138, 143, 148]. This section will present the most common strategies employed in the realization of P450 biosensors.

#### 3.3.1 Bare electrode immobilization

Direct electron transfer was found to be very difficult to achieve when unmodified metal electrodes are used: the bare metal lacks proper functional groups that improve protein orientation and electric contact between the metal and the active site of the protein [56], so the enzymes tend to denature and to passivate the electrode. A general requirement for good interactions is that the electrode surface must be electrostatically compatible with the protein. The role of surface selectivity in the direct electrochemistry of redox proteins is exemplified by their behavior at pyrolytic graphite electrodes. According to the way pyrolytic graphite is cut, the surface exposed can present hydrophobic character, if parallel to the single graphene sheets (basal plane), or hydrophilic behavior, if obtained by cutting the graphite across the aromatic rings (transversal plane). Initial studies on cytochrome C showed that the electrochemical behavior of proteins immobilized on the hydrophilic side is significantly higher compared to the basal plane and that improved electrochemical response is lost when the functional groups of the transversal plane are blocked with hydrophobic functionalities [9]. From these pioneering experiments, it became clear that modification of the electrode

with an appropriate medium helps in attaining the native structure of the protein, appropriate orientation of the enzyme, and better electron transfer.

Common immobilization strategies include layer-by-layer adsorption (LbL), biomembrane-like films, covalent attachment to self-assembled monolayers (SAM) and use of nanoparticles (NP).

#### 3.3.2 Layer-by-layer adsorption

In this method, multiple layers of oppositely charged films and/or CYPs are built up on the electrode: a solid substrate with a negatively charged surface is immersed in a solution containing cationic polyelectrolytes, and a layer of polycation is adsorbed via electrostatic attraction. Since adsorption is carried out at relatively high concentrations of polyelectrolyte, a number of cationic groups remain exposed to the solution, thus the surface charge is effectively reversed. After being rinsed in water, the substrate is immersed in a solution containing anionic polyelectrolyte. A new polymer layer is adsorbed, but at this stage the original surface charge is restored. By repeating these steps, alternating multilayer assembly is obtained [104]. Materials commonly employed for layer-by-layer adsorption include poly(styrenesulfonate) (PSS), used by Estavillo *et al.* to sense styrene with a CYP1A2 biosensor [54], and poly(diallyldimethylammonium chloride) (PDDA), successfully employed by Joseph *et al.* in a CYP3A4 biosensor capable to respond to verapamil, midazolam, quinidine and progesterone [84].

#### 3.3.3 Biomembrane-like films

Cytochromes P450 are membrane proteins. Mimicking a biomembrane environment on the electrode surface can provide the enzymes a natural environment, and improve their activity. The most common materials used in the preparation of biomembranes are surfactant molecules: organic compounds containing groups of opposite polarity at their extremities. Best stable films are obtained from compounds that do not form micelles in solution, usually characterized by a hydrophilic head with ionic properties and 2 or more hydrophobic tails of 12 carbons or more [176]. Drop cast and drying of the surfactant solution onto the electrode surface leads to the formation of stacked bilayer films. Proteins can be premixed to the surfactant solution before the drop cast, or uptaken afterwards, by placing the coated electrode in an electrochemical cell containing a solution of the protein [176].

Didecyltrimethylammonium bromide (DDAB) is one of the most common surfactant employed in P450 biosensors. Johnson *et al.*, successfully employed a DDAB film to adsorb CYP2C9 onto a pyrolytic graphite electrode, succeeding in detecting torsemide, diclofenac, warfarin, tolbutamide and sulaphenazole, and showing how in presence of oxygen, different substrates induce a characteristic potential shift of the P450 electrochemical peak [83]. A drawback of employing DDAB is that the polymer induces the formation of P420, a cytochrome

isoform which retains a visible electrochemical peak but is not able to catalyze substrates [162].

### 3.3.4 Covalent linkage on self-assembled monolayers

A third strategy of immobilization relies on covalent linkage of proteins to self-assembled monolayers (SAM). Molecules employed in the SAM formation are characterized by the structure X-spacer-Y, where X is the chemical group interacting with the electrode, the spacer is usually a carbon chain and Y is the chemical group interacting with the protein and the solution. Variations of X enable functionalization of different surfaces (i.e., thiol groups are for example indicated for immobilization on gold); different spacer lengths allow controlling the distance between the protein and the electrode, while different type of Y groups (i.e. -COOH, -NH<sub>2</sub> acetylene) can be employed to bind specific aminoacids on the protein, allowing more regular protein orientations, and also to prevent electrode fouling [30]. As an example, Yang *et al.* [179] successfully immobilized CYP2C9 via its N-terminal lysine to a SAM of 11-mercaptoundecanoic acid and octanethiol on gold. Their sensor was responsive to increasing concentrations of warfarin, and kinetic activity very similar to data obtained from microsomes in solution.

### 3.3.5 Immobilization on nanostructured surfaces

Owing to their small size (normally in the range of 1 – 100 nm), nanoparticles exhibit unique chemical, physical and electronic properties that are different from those of bulk materials, and that can be exploited to construct novel and improved sensing devices. Due to their large surface area and high surface free energy, nanoparticles can strongly adsorb molecules [72]. Many kinds of nanoparticles, including metal, oxide and semiconductor ones, have been widely used in electrochemical biosensors as effectors for immobilization of biomolecules; catalysis of electrochemical reactions; enhancement of electron transfer and labeling of biomolecules [103]. Clay and gold nanoparticles were commonly employed on P450 biosensors. Clay colloid has been reported to facilitate heterogeneous electron-transfer processes to proteins and enzymes [99]. In this respect, Shumyantseva *et al.* successfully employed nanoparticles of sodium montorillonite combination with the surfactant Tween 80 to achieve direct electrochemistry of CYP2B4. Catalytic currents were observed upon addition of substrates such as aminopyrine and benzphetamine and successful suppression of the current was recorded upon the addition of the CPY2B4 inhibitor methyrapone [149].

Another promising nanomaterial is the carbon nanotube (CNT). Conceptually, CNTs can be thought as graphene sheets rolled up to form a hollow tube. The tubes can be capped at their extremities and range from tens of nanometers to several microns in length. CNT are classified according to the number of walls they possess: a single graphene roll up produces *single walled carbon nanotubes* (SWCNT), while multiple concentric rolls originate *multi walled carbon nanotubes* (MWCNT). Single- or multi-walled nature, chirality, presence of

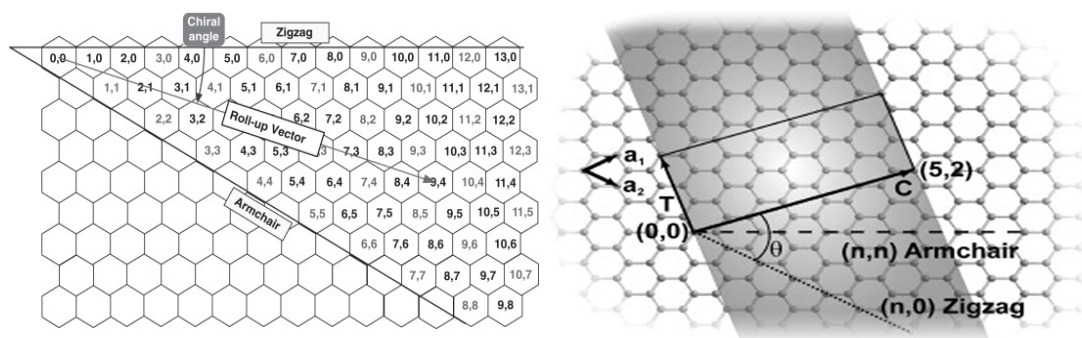


Figure 3.5: Principles of SWCNT folding. Left - Graphene sheet map illustrating possible single-walled nanotube structures. The resulting nanotube is labeled by the pair of integers in the cell that becomes overlapped with the origin cell [150]. Right - Diagram of the parameters defining a graphene sheet and CNTs constructed from it. By wrapping C onto itself a CNT is formed, as highlighted in grey, with axis parallel to T. The angle  $\theta$  defines the CNT chirality. The vector families individuating non-chiral kinds of CNTs, i.e. armchair and zigzag CNTs, are represented as dashed and dotted lines, respectively [115]. The red dots indicate the two possible zigzag configurations.

imperfections in their structure, length, diameter and chemical functionalization greatly affect the ensemble of CNT properties.

SWCNT can assume metallic or semiconductor behavior according to the alignment of the  $\pi$  orbitals in the tube, which depends on the way graphene is folded (Fig. 3.5.). Graphene sheets are made of a honeycomb-like lattice of carbon atoms: considering for simplicity of explanation a carbon hexagon as the graphene unit cell, given an origin, it is possible to find the position of every other exagon with two numbers describing the vertical and horizontal distance in unit cells from the origin  $(m, n)$ . A *roll up vector* connects the origin to another unit cell in the graphene sheet and describes the way in which the carbon nanotube can be folded. When  $(m=0)$  – *zigzag* configuration) or when  $(m=n)$  – *armchair* configuration) the graphene wrapping exhibits metallic behavior. In any other folding configuration described by the chiral angle  $\theta$ , the CNT is called *chiral*, and has semiconductor properties. Statistically, 1/3 of produced SWCNT will therefore possess metallic properties, while the other 2/3 will show semiconductor behavior. The different conductivities of SWCNT could complicate their application in electrochemistry [2].

Multi-walled carbon nanotubes consist of multiple layers of graphene. Their structure can be arranged in concentric cylinders of SWCNT of various diameters (Russian Doll model), or in a single graphene sheet is rolled in around itself multiple times (Parchment model). The interlayer distance in MWCNT is approximately 0.34 nm, a value close to the distance between graphene layers in graphite. Because of statistical probability, one of the shells, and thus the whole MWCNT, is usually a metal conductor.

The biosensors described in this thesis are based on MWCNT. With respect to P450 biosensors, Carrara *et al.* demonstrated how the electron transfer attained by the use of CNT in P450-based

cholesterol biosensors increased up to 2.4 times with respect to using gold nanoparticles and up to 17.8 times with respect to immobilization on bare electrodes [32].

### 3.3.6 Recombinant proteins and microsomes

Besides engineering of the electrode surface, a better electron transfer can be achieved by acting directly on the protein. This can be done in two ways:

- By engineering the protein and conferring improved functionality,
- By including the other proteins involved in the P450 cycle.

The first approach, firstly described by Ashton *et al.* [10] as *Molecular Lego*, is based on the construction of recombinant enzymes using domains taken from different proteins. Domains are conserved amino acid arrangements that function and exist independently of the rest of the protein chain. Since each domain can be independently stable and folded, it can be used as a “brick” in the construction of artificial proteins with improved functionality. Examples of domains can be the amino acids anchoring the protein to the plasmatic membrane or parts responsible with the interaction with other proteins. With respect to P450, the approach of Molecular Lego was employed by Dodhia *et al.* [49] to improve the coupling efficiency of CYP3A4. The protein was fused to the reductase domain of bacteric cytochromes possessing high homology with the human CPR. The reductase domain improved the efficiency of the electron transfer between the electrode and the heme group, decreasing the frequency of the shunts in the catalytic cycle and therefore improving the products formation.

Analog results can be achieved using microsomes. A microsome is a construct obtained during the artificial disruption of cells. The endoplasmic reticulum with the associated proteins (P450, CPR, cytochrome b5) is fragmented and recombined in vesicles that can be isolated towards centrifugation. The cast of microsomes onto an electrode surface provides both a physiological environment for the P450 and their natural redox partners. CYP3A4 microsomes were successfully immobilized on gold electrodes coated with hydrophobic material and successfully detected testosterone catalysis and CYP3A4 inhibition in presence of ketoconazole [115]. The group also concluded that the amount of product in the microsomes containing the reductase was almost double respect to what obtained with P450 alone. The result suggested that the presence of reductase is necessary to improve the efficiency of the cytochromes.

### 3.3.7 Summary and perspectives

The big picture emerging from the state of the art is that:

- Electrode modifications create more favorable conditions for the adhesion of proteins and increase the stability of the enzyme.

- Proper electrode functionalization can improve the communication between proteins and electrodes, and generate better electrochemical signals.
- P450 efficiency increases when supported by the other natural redox partners.

The current state-of-the-art on P450 biosensors provides an ever increasing characterization of the electrochemistry of these proteins. However, there is little research concentrating on P450 biosensors as diagnostic instruments. With the idea of realizing a device for personalized therapy, equally important questions which need to be addressed are:

- For which medical treatments is a biosensor for drug monitoring indicated? Which compounds should be given priority for characterization?
- Is the biosensor responsive to therapeutic drug concentrations?
- Is the biosensor capable to operate in complex environments like plasma?
- Is it possible to distinguish different substrates of different nature? When more than one substrate is present is still possible to do discrimination?
- In which way different environments affect the biosensor performance?

The research on P450 presented in this thesis aims to address these questions and to tackle the issues concerning the application of these devices in realistic scenarios.





## 4 P450 biosensors: assembly and results

This chapter will describe the effect of carbon nanotubes addition on the electrode morphology and electrochemistry, propose a method to insulate and extract the information related to the drug detection from a cyclic voltammogram, present results on the single and multiple drug detection with P450 biosensors and strategies to improve the accuracy of the measurement; finally it will be shown the results of first attempt of detection of unknown drug concentrations in mouse serum.

The P450 biosensors described in this thesis are made of three separate elements: a commercial screen printed 3-electrode cell (SPE); multi-walled carbon nanotubes (MWCNT) nanostructuration, and commercial P450 human microsomes. The working electrode is first functionalized with a solution of CNT dispersed in chloroform and then with the P450 microsomes. Nanoparticles and enzymes are immobilized onto the electrode by electrostatic interactions.

Screen printed electrodes were chosen for two reasons: low fabrication and market costs and possibility to work with few microliters of sample. These features make the SPE not only suitable for preliminary investigations on the P450 electrochemistry, but also ideal candidates for the realization of single-use biosensors in point-of-care applications.

Carbon nanotubes are attractive due their unique structural, mechanical and electronic properties: CNT can display metallic, semiconducting and superconducting electron transport, and have the largest elastic modulus of any known material [134].

Finally, microsomes were employed because, as already written in the state-of-the-art, the presence of the other proteins of the P450 cycle improves the coupling efficiency of the enzyme, while cellular membrane fragments contribute in creating a suitable environment for the proteins. Besides that, P450 microsomes are already used as standard in many pharmaceutical assays, are commercially available and do not require specific treatments before being used.

### 4.1 Cytochromes and drugs employed

As described in the introduction, the goal of this thesis is to design and test the P450 biosensors in practical applications. Instead of common CYP probes like testosterone or warfarin [182] we wanted to test the sensor response against compounds widely used in common medications or widespread pathologies, which may be easily assumed together with other prescriptions. While some of the drugs selected are administered under strict medical control, others are widely distributed and can be obtained *over-the-counter* (OTC), which means that a medical prescription is not necessary, and a misuse is more likely to happen. A common feature of all these medications is that they interact with a big number of other compounds, and that they can potentially lead to severe adverse effects in subjects at risk. The drugs considered are:

- *Cyclophosphamide (CP)*<sup>1</sup>. Used to treat various types of cancer and some autoimmune disorders, CP interferes with the cell cycle of cancer cells slowing their growth and their diffusion in the body. This drug presents severe and life threatening adverse effects, including acute myeloid leukemia, bladder cancer and permanent infertility, especially at higher doses. At the present day, CP is known to interact with 257 other drugs. Among these, 32 interactions provide highly clinically significant effects (major interactions). It is sensed with CYP3A4 biosensors.
- *Dextrometorphane (DX)*<sup>2</sup> is a cough suppressant drug. It is one of the active ingredients in many prescription-free medicines against cold and cough; therefore is widely available to patients. In combination with quinidine, a cyp2b6 inhibitor, it is employed to alleviate symptoms of easy laughing and crying, in patients affected by multiple sclerosis. Other uses include treatment of neuropathic pain and fibromyalgia pain. Up to date, 56 drugs interact with DX; 28 lead to major interactions. DX is sensed with CYP3A4 biosensors.
- *Erythromycin (EM)*<sup>3</sup> is a macrolide antibiotic. It acts slowing or sometimes killing sensitive bacteria by reducing the production of proteins essential for survival. Common employs include treatment of respiratory tract infections, acne, otitis and syphilis. 528 drugs interact with this compound; 119 lead to major interactions. EM is sensed with CYP3A4 biosensors.
- *Benzphetamine (BZ)*<sup>4</sup> is an appetite suppressant drug that targets the central nervous system. It is used together with diet and exercises to treat obesity. Structurally is very similar to amphetamines. BZ interacts with 404 other drugs, 87 causing severe effects. It is sensed with CYP2B4 biosensors.
- *Naproxen (NAP)*<sup>5</sup> is a non-steroidal anti-inflammatory drug (NSAID) mainly used to treat pain and inflammation caused by conditions such as arthritis, tendinitis, bursitis, gout,

---

<sup>1</sup> <http://www.drugs.com/pro/cyclophosphamide.html>

<sup>2</sup> <http://www.drugs.com/dextromethorphan.html>

<sup>3</sup> <http://www.drugs.com/monograph/erythromycin.html>

<sup>4</sup> <http://www.drugs.com/mtm/benzphetamine.html>

<sup>5</sup> <http://www.drugs.com/naproxen.html>

## 4.2. Characterization of the electrode bio/nano/structuration

---

or menstrual cramps. It works reducing hormones that cause pain and inflammation in the body. The drug is sold over-the-counter. Naproxen may cause life-threatening heart or circulation problems such as heart attack or stroke, especially if used long term. Other serious effects can be bleeding or perforation of stomach or intestines, as the drug also aspecifically acts on the cellular receptors responsible for the protection of the stomach lumen. The drug interacts with 416 other compounds, 45 of them lading to severe effects. It is sensed with CYP2C9 biosensors.

- *Ibuprofen (IBU)*<sup>6</sup> is another NSAID OTC drug. It is used to reduce fever, and treat pain or inflammation caused by many conditions such as headache, toothache, back pain, arthritis, menstrual cramps, or minor injury. The drug compares in the List of World Health Organization Essential Medicines as one of the minimum medical needs for a basic healthcare system. Side effects are similar to the ones caused by naproxen. 372 drugs interact with ibuprofen, 80 leading to major health complications. Ibuprofen is sensed with CYP2C9 biosensors.
- *Flurbiprofen (FLU)*<sup>7</sup> is a NSAID OTC drug. It is especially used in the treatment of arthritis. Side effects are common to the other NSAID drugs. Flurbiprofen interacts with 357 drugs, 43 leading to major interactions. It is sensed with CYP2C9 biosensors.

In some cases the same compound is metabolized, and therefore can be detected, by different cytochrome isoforms. The data on drug detection presented in this chapter is obtained with biosensors based on P450 -2B4, -3A4, and -2C9. CYP2B4 is one of the best studied mammalian xenobiotic metabolizing P450 [144]; CYP3A4 is responsible of the metabolism of almost 50% of known drugs [68], while CYP2C9 has a central role in the catalysis of anti-inflammatory compounds [62].

## 4.2 Characterization of the electrode bio/nano/structuration

### 4.2.1 Methods

Screen printed electrodes were purchased from Dropsens. The electrode cell was composed by Ag/AgCl reference electrode, a graphite counter electrode and a graphite working electrode (diameter 4 mm). The total area of the cell was 22mm<sup>2</sup>.

MWCNT (diameter 10nm – length 1-2 $\mu$ m, -COOH content 5%, purity 95% - Dropsens) were suspended in chloroform at the concentration of 1mg/ml and sonicated until a homogeneous suspension was obtained. Working electrodes were then nanostructured by gradual drop cast of 30 $\mu$ l of MWCNT solution.

CYP3A4 microsomes were bought from Sigma. 9 $\mu$ l of microsomal suspension were drop cast

---

<sup>6</sup> <http://www.drugs.com/ibuprofen.html>

<sup>7</sup> <http://www.drugs.com/mtm/flurbiprofen.html>

## Chapter 4. P450 biosensors: assembly and results

onto the MWCNT nanostructured electrode and incubated at 4°C overnight. The excess of cytochrome was then removed washing with milliQ water.

Morphological analysis of the functionalized electrodes was done using a Zeiss SUPRA 40 scanning electron microscope (SEM). Images were acquired in the 5-20kV range.

The electrochemical response of the CNT nanostructuring was investigated by cyclic voltammetry using a Versastat 3 potentiostat under aerobic conditions (potential window -600, +300 mV, scan rate 20mV/s).

### 4.2.2 Results

After MWCNT deposition the working electrode surface becomes highly corrugated, as shown in Figure 4.1. The nanotubes appear randomly organized in a *tridimensional conductive net* that greatly increases the electrode surface [36, 79]. Measured fibers diameter resulted  $11.14 \pm 2.59$  nm, as we reported in [29], and correspond well to the CNT size declared by the producer (10 nm).

The enlarged electrode surface was also confirmed by cyclic voltammetry experiments. Figure 4.2 shows a comparison between a bare graphite electrode and a MWCNT nanostructured electrode. As can be seen, CNT dramatically increase the capacitive current, up to one order of magnitude. This effect is due to the solution penetration in the nanostructure, and to the buildup of the electrical double layer around every single CNT. The MWCNT voltammetry also shows the presence of a big reduction peak at -350 mV, and a broad oxidation peak at -150 mV. These peaks, attributed to the redox active oxides present at the CNT tips and to some imperfections along the tube, are generated during the formation process, and are already known and discussed in literature [101].

Washing the electrode with water didn't reduced the capacitive current. Since the capacitive current is directly correlated to the electro-active surface, this finding shows that the bulk CNT nanostructure remain adsorbed on the electrode surface.

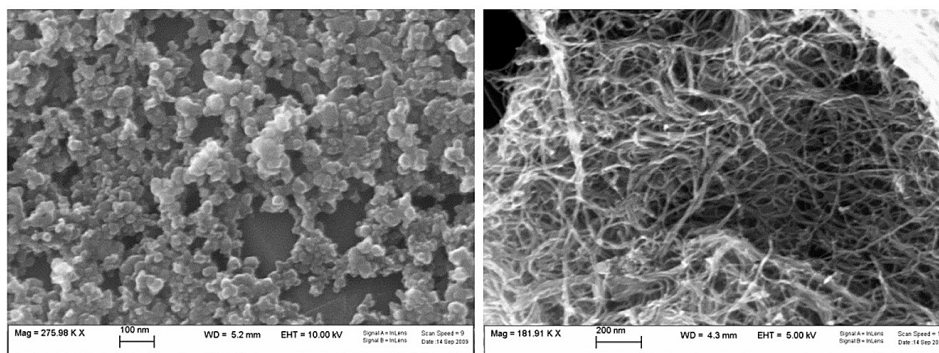


Figure 4.1: SEM images of the screen printed electrode before (left) and after (right) drop cast of 30  $\mu$ g of MWCNT.

## 4.2. Characterization of the electrode bio/nano/structuration

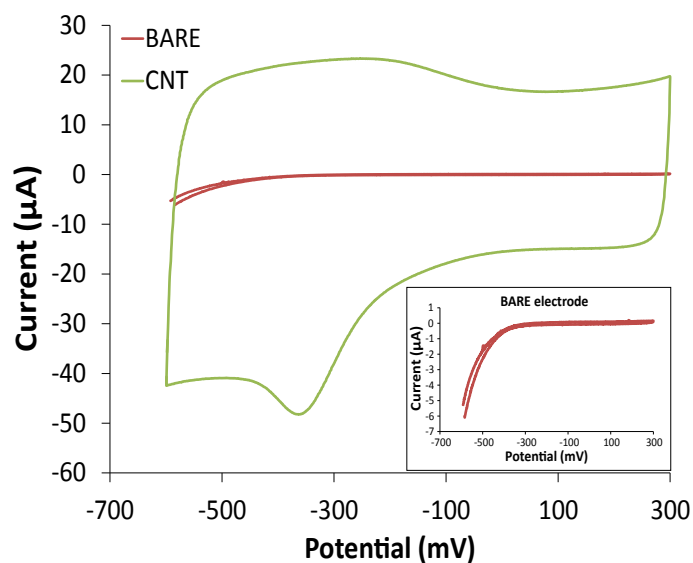


Figure 4.2: Cyclic voltammetry comparison between MWCNT nanostructuration (green) and bare electrode (red). The nanostructured electrode presents 1 order of magnitude higher capacitance and characteristic peaks at -350 and -150mV. The inset shows the CV for the bare electrode only.

From this initial characterization it can be concluded that the CNT nanostructuration adds the third spatial dimension to the electrodes. Therefore, given the same surface area, a CNT-functionalized electrode can generate more current from the electron transfer, and host a bigger number of enzymes.

Figure 4.3 shows the MWCNT nanostructure before and after the drop cast of P450 microsomes. The carbon nanotube net is still visible, but fibers are thickened, presenting an average value of  $19.51 \pm 5.72$  nm, in average 8 nm thicker than the bare MWCNT. Considering that the average diameter of microsomes varies between 50-150 nm [153], the slight thickness increase suggested rupture of the microsomes and the formation of a lipid/protein monolayer around the nanotube. This hypothesis was confirmed with Monte Carlo simulations [69]. We first calculated the average diameter of P450 proteins from the CYP3A4 crystal structure on the RCSB protein data bank [180], and we estimated an average diameter of 4-5 nm. SEM images of non-functionalized MWCNT were then used to select a pool of different carbon nanotube diameters. 10,000 depositions of proteins in random orientations were then simulated to estimate the final average diameter reached by the fibers. We obtained a value of  $21.71 \pm 2.78$  nm, a number which statistically confirms the experimental results obtained with the SEM. It is therefore possible to conclude that the microsomes establish strong hydrophobic interactions with the CNT, leading to the formation of a lipid/protein monolayer which can assure an intimate electrical contact between the enzymes and the electrode.

Figure 4.4 shows the cyclic voltammogram of a P450 / MWCNT electrode. The most visible feature is the masking of the reduction peak at -300 mV. Since the peak on bare CNT is due to the exposed redox active oxides present at the tips and at the wall imperfections, we concluded

## Chapter 4. P450 biosensors: assembly and results

that the microsome rupture covered these functions decreasing the peak. The comparison of a small peak in the region comprised between -300 and -600mV resulted to be the empirical confirm of the presence of a working biosensor. Absence of the peak resulted in reduced Faradic currents upon drug additions or totally absence of signal. Multiple microsomal drop cast increased the enzyme quantity, and produced more pronounced peaks. We found that 3 depositions constitute the optimal number respect to the sensor performance.

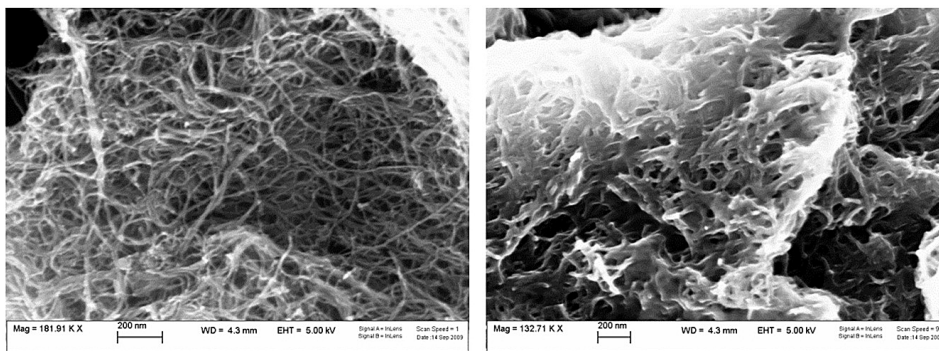


Figure 4.3: SEM images of the working electrode nanostructured with MWCNT (left) and with MWCNT and P450 microsomes (right).

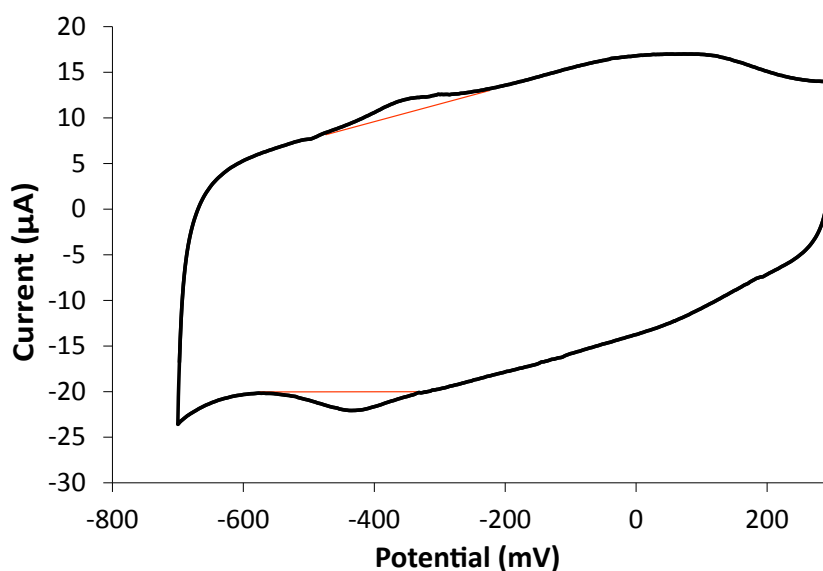


Figure 4.4: Cyclic voltammogram of a MWCNT/CYP3A4 electrode. The comparison of a redox peak between -300 and -600 mV, here highlighted with the red lines, is the most indicative presence of an active P450 complex.

### 4.3 Analysis of the reduction current and extrapolation of the microsomal contributes

Microsomes contain not only the P450 but also the cytochrome reductase (CPR) and the cytochrome B5; moreover, a contribution from MWCNT oxides can still be present. This suggests that the voltammogram shape is the result of multiple Faradic contributions. An important question to answer is which part conveys the information relative to the drug detection.

Figure 4.5 shows the same voltammetry presented in Figure 4.4 processed with an automatic peak recognition software. As can be seen, the reduction current between -600 and +200mV shows a profile with broad peaks halfway between capacitive background and Faradic current. While MWCNT oxides peak position is well documented [101], the peak potential of the P450 or of the other microsomal components is still not clear from literature: for example, CYP3A4 peaks were detected at -380mV [115, 150]; -200mV [84]; or -735mV [79]. These positions are also likely to be subjected to different factors, like the presence of oxygen, the nanostructuration employed or the solution pH.

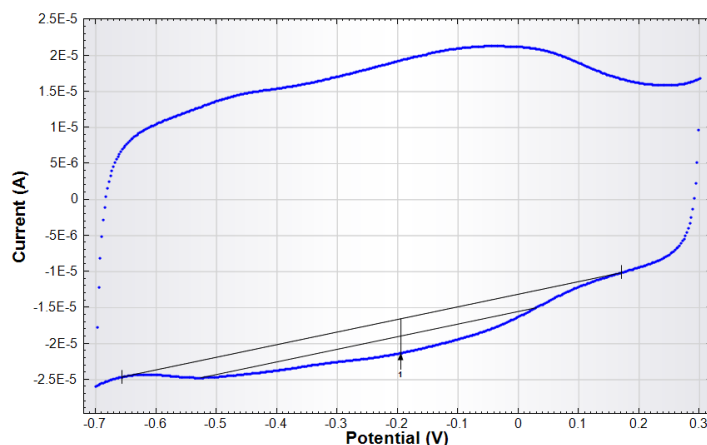


Figure 4.5: MWCNT/CYP3A4 biosensor processed with the peak recognition algorithm of the Nova software (Metrohm).

We attempted to deduce the position of microsomal proteins by running a peak search in voltammeteries obtained from different MWCNT electrodes functionalized with microsomes deprived of CPR, Cytochrome B5 and P450. The microsomes employed and the peaks found are listed in Table 4.1.

From the table, it can be deduced that the most probable peak position for the P450 peak is located at -380mV; the peak at -460mV seems to be due to the CPR, while the cytochrome b5 could be responsible of peaks at -180 and 0mV. The P450 and the CPR peak potentials we found reflect the ones calculated by Mie et al. by using CYP3A4 microsomes [115]. From this data, position of cytochrome b5 cannot be established with certainty.

## Chapter 4. P450 biosensors: assembly and results

Table 4.1: Voltammetric reduction peaks obtained microsomes deprived of specific P450-cycle proteins.

	-460mV	-380mV	-180mV	0mV
CPR + B5	X		X	X
P450 + B5		X	X	X
P450		X		

The presence of multiple contributions creates the problem of how the current generated during the P450 catalysis can be extrapolated from the voltammogram. The resolution of peak overlapping with mathematical functions, is a procedure well known in literature [26, 157], and can be used to visualize the Faradic current generated by the various biosensor components. The basic functions used for decomposition are the *Gaussian*, the *Hyperbolic cosine* and the *Cauchy* [134]. More complex functions are usually based on modifications or combinations of these three. In order to visualize the individual contributes of CNT, P450, CPR and cytochrome B5, We normalized the reductive current between +200 and -600mV to the baseline obtained with the automatic peak recognition software, and we used four Gaussian functions centered at -460mV, -380mV, -180mV and 0mV to describe the different Faradic contributes. The Y values of each Gaussian where then summed together, while height and amplitude where fit to reply the current profile obtained from the raw data.

The fitting procedure is summarized by the following equation

$$i(V) = i_C(V) + \sum_{\forall k} A_k e^{-\frac{(V-V_k)^2}{\sigma_k^2}} \quad (4.1)$$

Where  $i_C$  accounts for the capacitive current, and the following sum of Gaussian curves (where  $A$  describes the gaussian amplitude, or the putative peak current,  $V$  the potential at which the peak is centered and  $\sigma$  the peak width) accounts for all the Faradic contributes generated by the microsomal proteins. The result presented in Figure 4.6 shows the best fitting obtained.

In presence of increasing drug concentrations, the reduction current increase as shown in Figure 4.7. From the data, it is interesting to note that:

- Increasing drug concentrations seem to affect the reduction current only in the region comprised between +100 and -400 mV
- In absence of drugs, the region between +100 and -400mV can be approximated as a straight line.



### 4.3. Analysis of the reduction current and extrapolation of the microsomal contributes

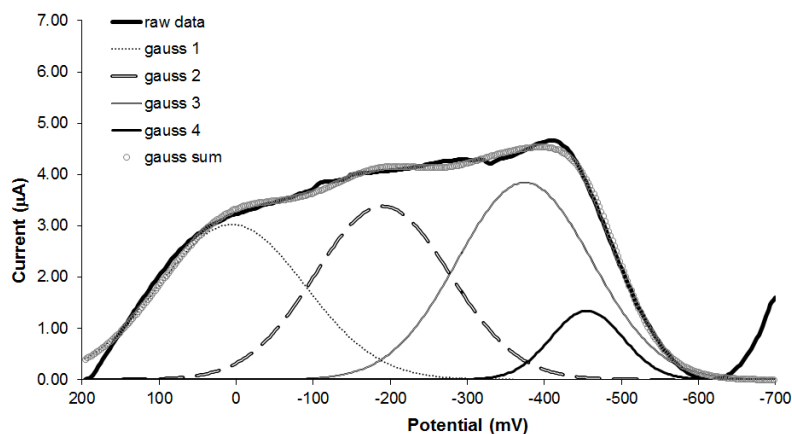


Figure 4.6: Gaussian decomposition of the peak highlighted in Figure 4.5. The the gauss functions describe the Faradic contribution of the various microsomal proteins.

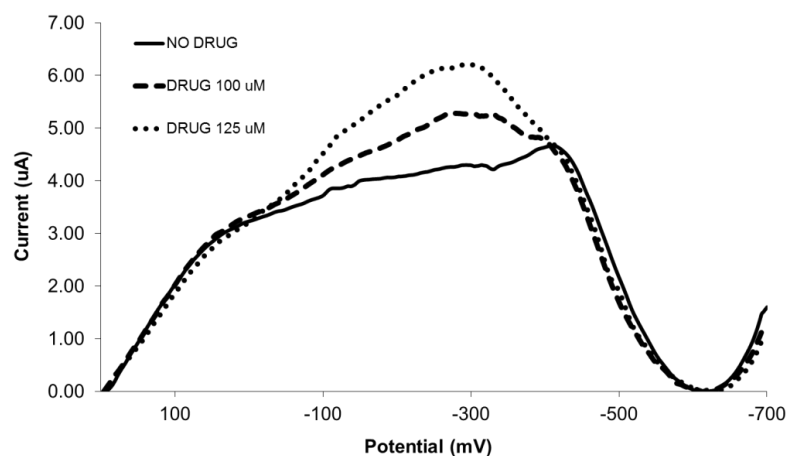


Figure 4.7: Effect of increasing drug concentrations on the reduction peak highlighted in Figure 4.5 and Figure 4.6.

In conclusion, in presence of drugs the current variation is recorded in a narrower region. This seems to exclude the contribution of the external Gaussians, and therefore of some microsomal components, in the electron transfer chain between enzyme and electrode.

A way to unequivocally highlight the drug contributions to the Faradic current is to normalize the voltammogram data with a baseline which excludes all the current generated in absence of substrate. In the example presented, this means to normalize current between 0 and -400mV. Voltammogram profiles slightly differ from sensor to sensor: in some cases a small peak is visible even in absence of substrate (residual current). In order to discern the current variation following the injection of drugs, in these situations the residual peak current must be subtracted to the catalytic peak current as shown in Figure 4.8.

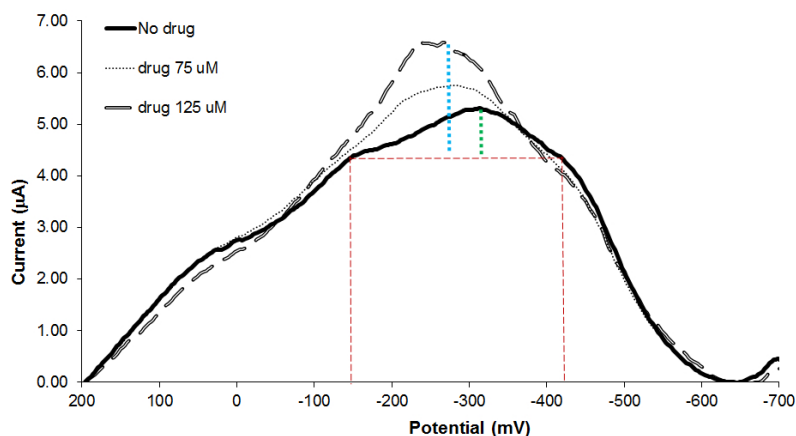


Figure 4.8: Highlighting of drug contributions in conditions of non-flat background current. The peak current in absence of substrate (residual current) needs to be subtracted from the catalytic current. The potentials of current flexes defining the the residual current peak are used to draw a baseline (red lines). Residual peak current (green) and catalytic peak current (cyan) are calculated respect to the baseline. The final catalytic current is then obtained subtracting the value of the residual peak current to the catalytic peak current.

## 4.4 Single drug detection

The employ of electrodes modified with carbon nanotubes improves sensitivity and detection limit of the P450 biosensors, allowing detection of compounds in the therapeutic range and in complex solutions. This paragraph focus on relevant results obtained with CYP3A4 and Cyclophosphamide detection, published in [29].

### 4.4.1 Methods

Screen printed electrodes were purchased from Dropsens. The electrode cell consists of an Ag/AgCl reference electrode; a graphite counter electrode, and a graphite working electrode (diameter 4mm). The total area of the cell was 22mm<sup>2</sup>. MWCNT (diameter 10nm – length 1-2µm, -COOH content 5%, purity 95% - Dropsens) were suspended in chloroform at the concentration of 1mg/ml and sonicated until a homogeneous suspension was obtained. Working electrodes were then nanostructured by gradual drop cast of 30µl of MWCNT solution. CYP3A4 and CYP2C9 microsomes were bought from Sigma. P450 2B4 was isolated and purified from the microsomal fraction of rabbit [149] and was obtained as a courtesy from the Institute of Biomedical Chemistry of the Russian Academy of Science. 9µl of microsomal suspension were drop cast onto the MWCNT nanostructured electrode and incubated at least 6 hours at 4°C to promote the enzymes adhesion, then dried at 37°C 45% humidity to concentrate the proteins. The procedure was repeated two more times in order to increase the amount of enzyme immobilized. The biosensors were washed with milliQ water before the measurement, in order to remove material weakly adsorbed. Drugs were bought from Sigma and diluted to the working concentrations in ethanol, DMSO or water according to

their solubility.

The electrochemical response of the biosensor was investigated by cyclic voltammetry under aerobic conditions. Voltammograms were acquired using a Versastat 3 potentiostat (Princeton Applied Technologies). The electrode was covered with 100  $\mu$ l of PBS 10x pH 7.4 or undiluted human serum (Lonza). Drugs samples were added in drops of 1  $\mu$ l. Cyclic voltammograms were acquired by sweeping the potential between -600 and +300mV at a scan rate of 20mV/sec. Reduction peak currents values were extracted on stabilized voltammograms in the according to the procedure described in the previous chapter. The currents obtained in presence of drugs were subtracted to the background current and plotted against the respective concentration values in order to obtain a calibration curve.

Biosensor sensitivity was calculated dividing the slope of the calibration curve for the working electrode area; biosensor detection limit was calculated considering the IUPAC definition [112]:

$$LOD = \frac{k\delta i}{S} \quad (4.2)$$

Where  $LOD$  is the limit of detection,  $\delta i$  the standard deviation of the blank measures,  $S$  the sensor sensitivity and  $k$  is a parameter accounting for the confidence level ( $k=1,2$  or  $3$ , corresponding to the 68.2, 95.4 or 99.6% of statistical confidence). The results presented here consider a 68.2% of statistical confidence.

#### 4.4.2 Results

The behavior of CYP3A4 peak current upon increasing concentrations of CP is shown in Figure 4.9. When P450 is immobilized onto bare electrodes, significant current responses were obtained only at high drug concentrations. The best detection limit achieved with bare electrodes resulted to be 256.0  $\mu$ M. Such behavior is unacceptable for practical applications, since Cyclophosphamide concentration range in conventional therapies, the so-called *therapeutic range*, has been calculated to vary from 2.6  $\mu$ M to 76.6  $\mu$ M [85]. On the other hand, when electrodes are nanostructured with CNT, we achieved in the best case a 2.4-fold sensitivity increase and a detection limit of 7.5  $\mu$ M, which allows drug detection in the therapeutic range. Sensitivity increase due to MWCNT nanostructuring has been reported for identical concentration ranges, and it has been shown for benzphetamine detection with CYP2B4 biosensors [30], naproxen detection with CYP2C9 biosensors [29], and for glucose and lactate detection with the respective oxidases [24]. In a second experiment (Figure 4.10) we tested the response to therapeutic concentrations of Cyclophosphamide in undiluted human serum. In this case the detection limit resulted to be higher, 53.1  $\mu$ M, but still close to the therapeutic range. The lower sensitivity achieved in serum, 0.17 nA/ $\mu$ Mmm<sup>2</sup>, is attributed to the plasma components, which can produce electrode fouling and can retain drug molecules. It is known that 56% of cyclophosphamide circulates bound to plasma metabolites [16]; therefore, especially at low concentrations, the amount of free cyclophosphamide can be lower than the nominal quantity

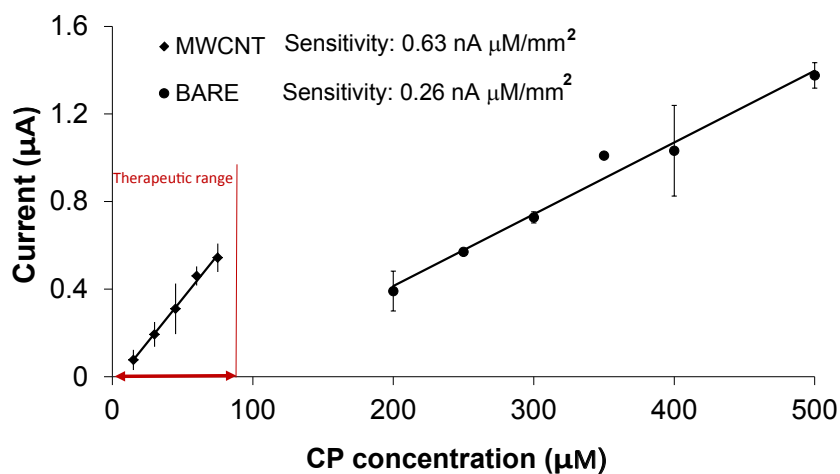


Figure 4.9: Cyclophosphamide calibration curves obtained from bare and MWCNT-nanostructured electrodes. Values reported are normalized to the P450 residual current. Error bars: average of 3 measurements. Image adapted from [29].

injected.

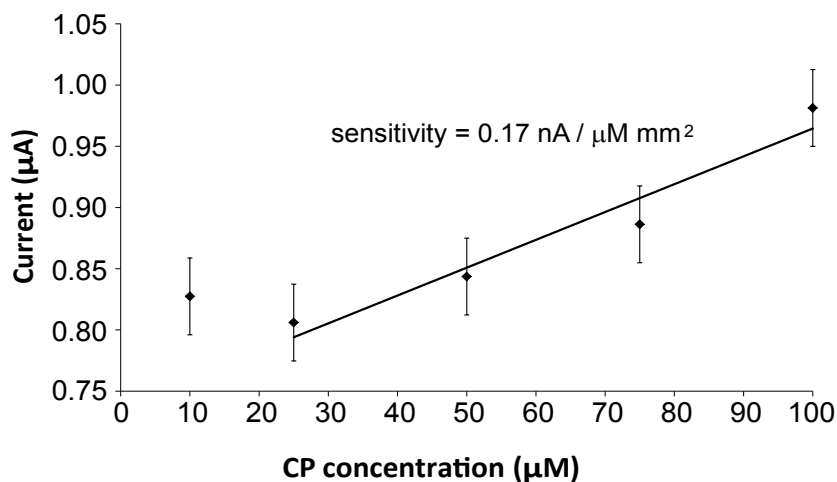


Figure 4.10: Current response of MWCNT/CYP3A4 biosensor versus therapeutic concentrations of CP in undiluted human serum. Error bars: instrument noise. Image from [29].

The possibility to detect drugs in plasma in their therapeutic range represent an important step towards the realization of biosensors for real life applications such as the therapeutic drug monitoring. One of the biggest obstacles to overcome drug detection is the capability to sense compounds in complex media, with concentrations typically in the order of -micro or -nano moles. At best of our knowledge, most of the literature demonstrates detection windows in the mM scale and only in PBS. For example P450 detection of Verapamil is shown between 0.5 and 3mM [84], while the therapeutic range is typically below 55nM [52]. Table 4.2 summarizes the

best results obtained in the detection of the drugs mentioned before.

Table 4.2: Drugs detected with the realized P450 biosensors.

CYP	Drug	Therap. Range ( $\mu\text{M}$ )	Ref.	Meas. Range ( $\mu\text{M}$ )	Best Sensitivity ( $\text{nA}/\mu\text{M} \cdot \text{mm}^2$ )	LOD ( $\mu\text{M}$ )	Ref.
2B4	BZ	0-0.074	[142]	500-5000	2.14	2.23	[30]
3A4	CP	2.6-76.6	[85]	10-100	0.17 (serum)	53.14	[29]
	DX	0-0.3	[50]	100-500	0.12 (pbs)	39.87	Unpub.
	ER	0-68	[15]	10-75	0.26 (pbs)	18.40	Unpub.
2C9	NAP	21-215	[136]	100-500	0.05 (serum)	95.69	[36]
	IBU	0.48-291	[107]	100-500	0.03 (pbs)	159.48	Unpub.
	FLU	0.04-41	[98]	100-500	0.08 (pbs)	59.80	Unpub.

An interesting question is answering why carbon nanotubes enhance biosensor sensitivity and detection limit. The reasons are both structural and electronic:

- Carbon nanotubes and P450 have similar dimensions. Enzyme adsorption can occur without significant loss of enzyme shape or catalytic activity [12].
- The CNT nanostructuring provides a third dimension available for the enzyme immobilization. The increased electroactive coverage allows the conversion of a bigger number of substrates in a given period of time, leading to higher catalytic currents. Moreover, the porous nature of the nanostructuring allows deeper penetration of the electrolytes solution and a larger surface available for the redox reaction.
- Physical adsorption of the enzymes onto CNT enables direct electron transfer between the electrode and the active site, minimizing the electron tunneling distance [105]
- Sidewall and tips functionalization with carboxylic groups provides reactive sites that improve the electron transfer rate between active site and electrode [40].

## 4.5 Multiple drug detection

A crucial aspect in P450 biosensor development is the sensor specificity. Every cytochrome isoform has a broad substrate range, and the same protein can metabolize hundreds of different compounds. However, different molecules can induce different active site conformations, and may need slightly different energies to be mono oxygenated. As result, cyclic voltammograms acquired in presence of different substrates show catalytic current peaks at specific potentials referred as *electrochemical signatures*. An example is the work reported by Johnson et al., which shows different reduction peak potentials for CYP2C9 in presence of Torsemide, Tolbutamide and S-Warfarin [83].

In therapies like cancer or HIV treatment, as well as in common diseases like flu or bronchitis, patients are obliged to assume drug cocktails which may likely contain substrates metabolized

by the same P450 isoform. A method to recognize and quantify the contribution of different drugs to P450 catalytic current is therefore necessary, and so far it has never been attempted. In this section, it will be shown an approach to discriminate different drug contributions from mixtures containing both Cyclophosphamide (CP) and Dextromethorphan (DX) or Naproxen (NAP) and Flurbiprofen (FLU).

### 4.5.1 Methods

CYP3A4 and CYP2C9 biosensors and drug substrates were prepared and measured as described in section 4.4.1.

### 4.5.2 Results

Previously it has been shown how individual Faradic contributes in a cyclic voltammogram can be approximated by a Gaussian curve, and how the proximity of different peaks can change the aspect of the plot, giving rise to broad peaks. According to the electrochemical signature principle, different drugs produce peaks at slightly different potentials. We can assume that enzymes in contact with a mixture of two drugs can metabolize either the compound A, the compound B or the two compounds at the same time. This effect can cause the comparison of two peaks in the catalytic current at a specific potential, each one reflecting a fraction of the enzymes bound to one of the two substrates. The contribution of the single drugs to the total catalytic current can therefore be described by multiple gaussian curves.

Figure 4.11 shows the Gaussian decomposition of the catalytic current of a CYP3A4 biosensor in presence of two different concentrations of CP and DX. As can be seen, the peak profile is asymmetric and presents a shoulder at -390mV, suggesting the presence of multiple contributors. The fitting proposed was obtained placing the two Gaussians in correspondence of the peak current potential and of the shoulder potential, and assuming a higher contribute from the cyclophosphamide, present in higher concentrations. The effect of increasing concentrations of DX upon a fixed amount of CP is shown in Figure 4.12: higher DX concentrations seem to produce an inhibitory effect on the cyclophosphamide catalysis as the peak potential, detected at -296mV, gradually decreases. A possible description of this effect could be a negative heterotropic cooperativity of the two substrates [159], where the presence of a second substrate inhibits the catalysis of the first in a concentration dependent fashion. However, it is important to say that at best of our knowledge, there are no works in the literature that support or deny that the couple CP/DX produces this particular effect. In a second experiment we tested the interaction of naproxene and flurbiprofene with CYP2C9 biosensors (Figure 4.13). In this case, increasing amounts of NAP produce a distinct peak at -10mV but also seem to enhance the catalysis of FLU, detected at +50mV, as the current at that potential increase even if the concentration of the drug is maintained constant. A possible description of this effect could be a positive heterotropic cooperativity, where the presence of a second substrate enhances the catalysis of the first one. Again, we didn't find other works in the literature that

confirm or negate this particular enzyme kinetics for the couple NAP/FLU.

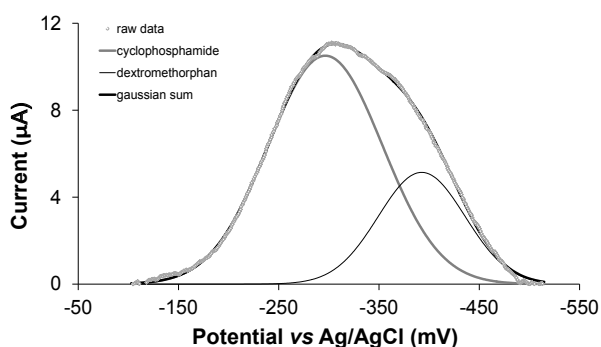


Figure 4.11: Catalytic peak current of a CYP3A4 biosensor in presence of different concentrations of cyclophosphamide and dextromethorphan. Each drug contribute has been modeled with a Gaussian function.

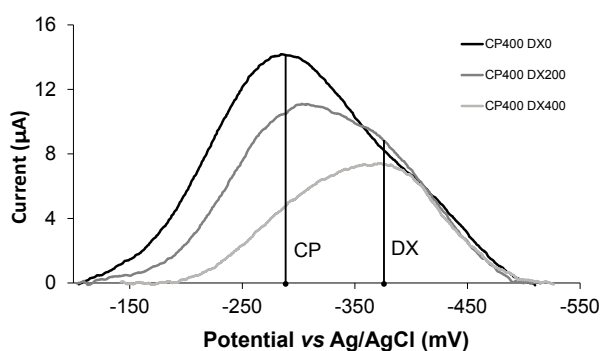


Figure 4.12: Catalytic peak current of CYP3A4 in presence of different ratios of CP and DX. The dotted lines show the respective compounds' electrochemical signatures. CP peak seems to decrease in presence of increasing DX concentrations. Image adapted from [29]

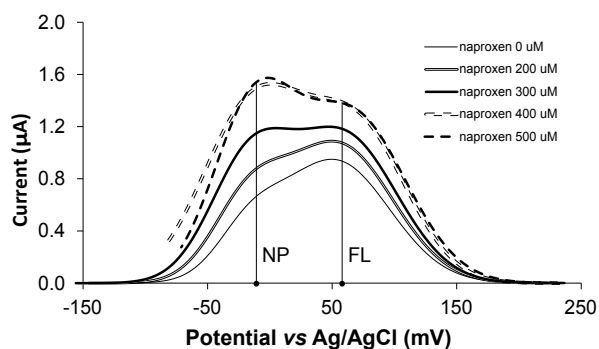


Figure 4.13: Catalytic peak current of CYP2C9 in presence of different ratios of NAP and FLU. The dotted lines show the respective compounds' electrochemical signatures. FLU peak seems to increase in presence of increasing NAP concentrations. Image adapted from [29].

## 4.6 Strategies to improve sensing accuracy

According to the electrochemical theory, pH and temperature variations change the peak position and, if not properly considered, can twist the results obtained with the peak analysis leading to false-positives in case of a solution with unknown substrates. pH and temperature monitoring ensures strict and precise control over the electrochemical detection when multiple drugs are present in the sample, extends the applicability of the sensor to biological fluids with different pH and temperature levels like blood, urine and interstitial liquid and, from an implantable perspective, is important to account for temporary variations in the host environment, like fever. In order to test pH and temperature effect on the biosensor response, we acquired cyclic voltammograms of a CYP3A4 biosensor in PBS at different temperature or pH values. The microsome Faradic peak at -420 mV was then extracted, and the peak current plotted in function of different pH and temperature values.

Figure 4.14 shows the effect of different solution pH on the microsome peak potential. The shift resulted to be reproducible and linear. We obtained a variation of 65.3mV/pH unit from the regression equation. Such linear behavior is well explained by the *Nernst equation*

$$E = E_0 - \frac{RT}{nF} \ln \left( \frac{C_r}{C_0} \right) - \frac{RT}{F} pH \quad (4.3)$$

In the equation,  $E$  represent the peak potential,  $E_0$  is the standard potential,  $R$  is the gas constant,  $F$  is the Faraday constant,  $n$  is the number of electrons involved in the redox,  $C_r$  and  $C_0$  are the concentrations of the reduced and oxidized species at the interface. Although the equation also shows that the peak potential depends on temperature, from our measurements we didn't noticed a clear correlation between temperature and potential.

The biggest effect on temperature is however on the peak current, as shown in Figure 4.15: current is decreasing regularly when the sample is heated, showing a direct relationship between the two parameters. From the regression equation, we obtained a variation of -16.7nA/°C. The link between current and temperature is well explained by the *Randles-Sevcik* equation [19].

$$i \propto nFAD \left( \frac{nFvD}{RT} \right)^{\frac{1}{2}} C_r \quad (4.4)$$

Introducing the scanning velocity ( $v$ ), the working electrode area ( $A$ ) and the diffusion coefficient ( $D$ ), the equation shows an inverse relationship with the square of temperature, which is approximated by a linear curve for small windows in temperature.

As demonstrated by these experiments, the monitoring of pH and temperature is necessary to precisely correlate the peak potential with the drug detected and the peak current with the drug concentration. In a practical application, the biosensor response should be ideally calibrated at controlled pH and temperature, and then all the measurements should be normalized in current and potential according to calibrations similar to the ones presented.



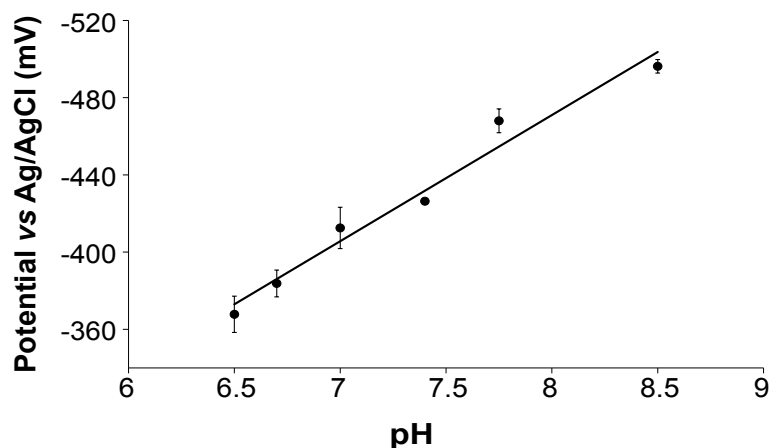


Figure 4.14: Microsome peak potential shift upon different pH. Error bars: inter-electrode variation. Image adapted from [29].

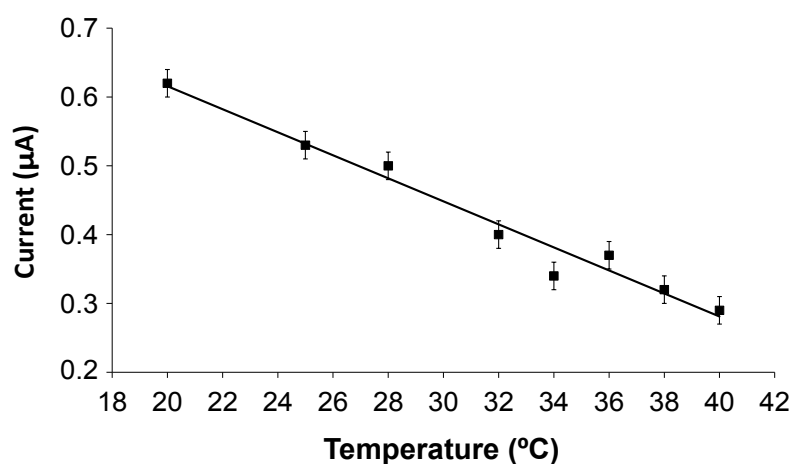


Figure 4.15: Microsome peak current variation respect to different temperatures. Error bars represent the inter-electrode variation. Image adapted from [29].

A second issue in the accuracy of the P450 biosensor is the univocal identification of a single drug using enzymes possessing a broad substrate range. Although the electrochemical signature can help in identifying a drug candidate, some compounds can induce the same potential shift, as shown for Diclofenac and Sulphenazole [83]. A method to increase the identification accuracy of a P450 biosensor relies in sensing a drug mixture with an array of cytochromes capable to selectively respond to only a fraction of the compounds. An interpolation of the answers can then help in identifying the analyte.

An approach for an appropriate array construction and compound identification can be achieved by solving a covering problem, and it has been described in [30]. Figure 4.16 shows an example of irredundant cover approach for the construction of P450 biosensor arrays:

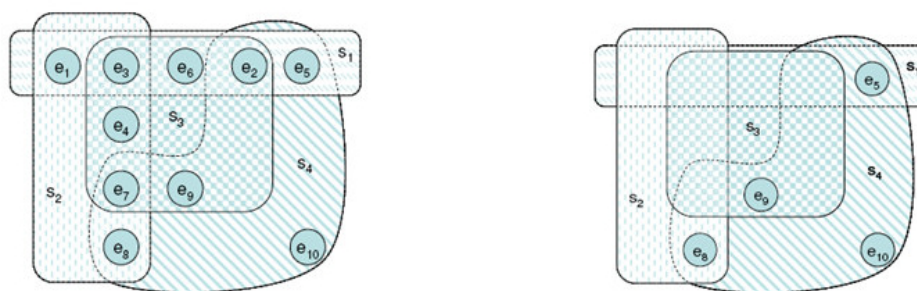


Figure 4.16: Irredundant cover approach for the design of a P450 biosensor array. Given a pool of enzymes specific for different substrates (left) it is possible to eliminate the redundant signals and reduce the number of the enzymes present on the array (right). Image adapted from [30].

given a pool of ten different enzymes ( $e_1 \dots 10$ ) with different substrates in common ( $S_1 \dots 4$ ), a univocal identification and quantification of the four compounds can be achieved querying only 4 enzymes, eliminating the need for useless additional biosensor arrays, while the use of the combined response of the array allows avoiding errors in the signal interpretation. In the example reported, in case of a solution presenting a single compound,  $S_1$  will produce a signal only on  $e_5$ ;  $S_2$  on  $e_8$ ,  $S_3$  on  $e_9$ , while  $S_4$  must generate a signal on all the four enzymes altogether, each one with an electrochemical signature characteristic of the enzyme and the compounds. The combination of the electrochemical signatures of all the enzymes of the array can be used as a “code” which will identify the drugs in a univocal manner. *A priori* knowledge of the drugs present in the sample will be anyway necessary to execute Gaussian decomposition on the enzymes specific for multiple substrates. For example, from the administration of  $S_2$  and  $S_4$ , the biosensor signal will be decomposed only for  $e_8$ , while the concentration information on  $S_4$  coming from the other enzymes will help improving the accuracy of the decomposition on  $e_8$  to calculate the value of  $S_2$ . The table 4.3 summarizes the codes obtained querying the array of Figure 4.16 against a single substrate or a combination of two substrates.

	e5	e8	e9	e10
s1	s1e5			
s2		s2e8		
s3			s3e9	
s4	s4e5	s4e8	s4e9	s4e10
s1s2	s1e5	s2e8		
s1s3	s1e5		s3e9	
s1s4	s1e5 / s4e5	s4e8	s4e9	s4e10
s2s3			s3e9	
s2s4	s4e5	s2e8 / s4e8	s4e9	s4e10
s3s4	s4e5	s4e8	s3e9 / s4e9	s4e10

Table 4.3: Identification codes for different substrate combinations in the example reported in Figure 4.16. For each investigation all the four enzymes of the array are queried. Red boxes show absence of signal, green boxes show enzyme/substrates interactions, while the code  $S(x)e(y)$  correspond to the electrochemical signature of the substrate  $x$  on the enzyme  $y$ . The combined response of all the enzymes of the array help in eliminating false positives, in better estimation of a drug contribute in Gaussian decompositions and in providing a unique identification code for each drug.

### 4.7 Measurement of residual drug concentrations in mouse serum

In order to test the applicability of the biosensor in a situation as close as possible to the reality, we administered known drug amounts to mice, and collected samples of serum to sense the residual drug concentration with a point-of-care approach.

#### 4.7.1 Methods

Drug administration to mice, and samples collection were courtesy of the Institute for Research in Biomedicine (IRB) of the Università della Svizzera Italiana. Briefly, 3880 $\mu\text{g}$  of cyclophosphamide, 2225 $\mu\text{g}$  of naproxen, or 275 $\mu\text{g}$  of flurbiprofen were injected in mouse. After 3 hours, 200 $\mu\text{l}$  of blood serum from the mice treated with the drugs and from mice not subjected to drug administration (negative controls) were collected and stored at -80°C until used. CYP3A4, CYP2A1, and CYP2C9 biosensors and were prepared and measured as described in section 4.4.1.

Sensor calibration was done covering the electrodes with 100 $\mu\text{l}$  of serum from the negative controls, and injecting physiological concentrations of naproxen or cyclophosphamide. After the calibration the sensor was washed by immersion in PBS and then tested versus samples bearing unknown drug concentrations. PBS washing was performed before measuring a new sample.

#### 4.7.2 Results

Figure 4.17, Figure 4.18 and Figure 4.19 respectively show P450 peak current and calibration curves for CYP1A2, CYP3A4, and CYP2C9 biosensors. Unknown drug concentrations were obtained by interpolation with the calibration curve. Sensitivities, detection limits and unknown drug concentration estimations are summarized in the table below.

CYP	Drug	Calibration Range( $\mu\text{M}$ )	Sensitivity ( $\text{nA}/\mu\text{M}\cdot\text{mm}^2$ )	Detection Limit ( $\mu\text{M}$ )	Estimated Conc. Mouse 1( $\mu\text{M}$ )	Estimated Conc. Mouse 2( $\mu\text{M}$ )
1A2	Naproxen	50-200	0.63	15.15	135	160
3A4	Cyclophosphamide	25-100	1.18	8.09	45	70
2C9	Flurbiprofen	50-300	0.68	164.07	163	168

All the considered sensors responded well to the drug calibration showing a linear increase in the considered range, with the exception of CYP2C9, which resulted insensitive to the lower amounts of flurbiprofene. Unknown drug concentrations seem to fit well into the calibration curve; different individual metabolisms can be a possible explanation for the differences in concentration found between the two samples. It is important to say that even if promising and coherent with the calibration curve, the results shown have to be considered an estimation, since cross validation of the concentrations found by interpolation with an independent method like mass spectroscopy is needed to fully validate the detection

## Chapter 4. P450 biosensors: assembly and results

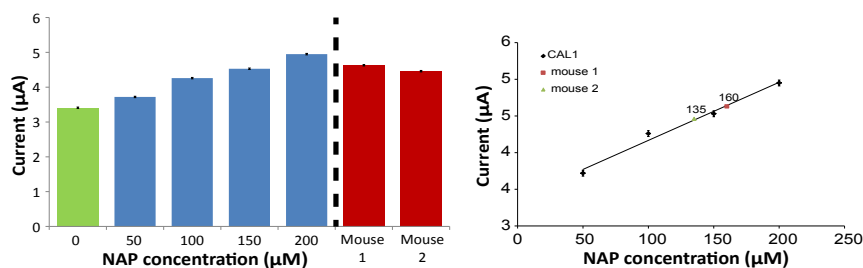


Figure 4.17: CYP1A2 current response to naproxen (NAP) in mouse serum. Left: P450 peak current (green – negative control; blue - current increase due to controlled drug addition to the negative control; red – measurement of unknown drug concentrations from two different animals) Right drug calibration curve and extraction of the unknown drug concentrations by interpolation.

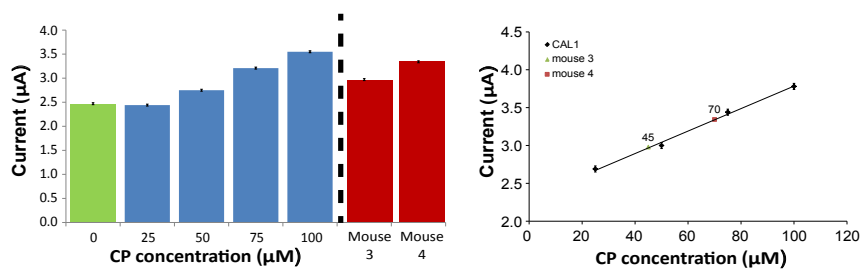


Figure 4.18: CYP3A4 current response to cyclophosphamide (CP) in mouse serum. Left: P450 peak current (green – negative control; blue - current increase due to controlled drug addition to the negative control; red – measurement of unknown drug concentrations from two different animals) Right drug calibration curve and extraction of the unknown drug concentrations by interpolation.

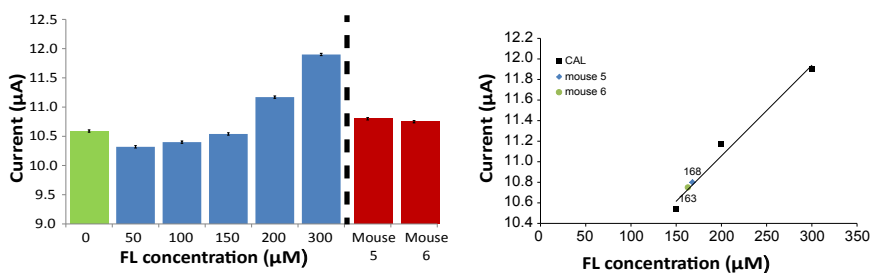


Figure 4.19: CYP2C9 current response to flurbiprofen (FL) in mouse serum. Left: P450 peak current (green – negative control; blue - current increase due to controlled drug addition to the negative control; red – measurement of unknown drug concentrations from two different animals) Right drug calibration curve and extraction of the unknown drug concentrations by interpolation.

of unknown concentrations.

### 4.8 Chapter summary

The current state-of-the-art on P450 biosensors provided an ever increasing characterization of the electrochemistry of P450. However, there is little previous research characterizing the P450 biosensors as a diagnostic instrument. The results presented in this chapter represent a first attempt to characterize P450-mediated electrochemical drug detection in scenarios more close to the reality.

The P450 biosensors presented in this thesis are made on screen printed electrodes nanostructured with carbon nanotubes and functionalized with P450 microsomes. MWCNT add the third spatial dimension to the electrodes; therefore, given the same electrode area, a CNT nanostructuration can generate more current and host a bigger number of enzymes.

The use of multi-walled carbon nanotubes proved essential in enhancing sensor sensitivity and detection limit, enabling the detection of many of these drugs in their therapeutic range and in complex solutions like human serum.

The Faradic contribution of each microsomal protein can be estimated by Gaussian decomposition of the reduction current. To unequivocally highlight the drug contributions to the Faradic current it is necessary to normalize the voltammogram data with a baseline which excludes all the current generated in absence of substrate. Results showed that increasing drug concentrations seem to affect the reduction current only in the region comprised between +100 and -400mV.

Evidence of simultaneous drug metabolism by the same cytochrome has been shown for the first time with electrochemical measurements. Gaussian decomposition has been proposed as a method to infer the contribution of multiple drugs on the total catalytic current.

The measurement of temperature and pH, and the univocal identification of a set of compounds towards combined array responses have been proposed as solutions to improve the P450 biosensor accuracy.

A preliminary result on the point-of-care applicability of the biosensor in sensing unknown drug concentrations has been showed by measuring serum samples coming from mice treated with three different drugs.



## 5 ATP biosensors

Adenosine-5-triphosphate (ATP) is a multifunctional purine nucleotide used by cells as an energy source for many metabolic reactions. In addition, ATP affects different biological processes like neurotransmission, muscle contraction and vascular tone [63]. Moreover, extracellular ATP, together with ADP and adenosine, plays a critical role in the physiological regulation of inflammation. For this reason, ATP monitoring becomes of particular interest in chronic pathologies as it might allow a timely and efficient evaluation of ongoing inflammation.

This chapter will describe the role of ATP in the inflammation and will present the characterization of an ATP biosensor based on carbon nanotubes, glucose oxidase and hexokinase.

### 5.1 Purinergic signaling during inflammation

The *danger theory* of immune system proposes that the defense apparatus of organisms is principally occupied with detecting “danger”, defined as anything that cause tissue damage or molecular stress [110]. Danger signals may have exogenous or endogenous nature. Exogenous molecules are typically microorganism products, as LPS, or antigens, and are known under the name of *pathogen-associated molecular pattern molecules* or PAMPs. Endogenous danger signals can be produced by activated immune cells, or can derive from stressed or damaged host cells. Molecules of this type are known under the name of *damage-associated molecular pattern molecules, or DAMPs*. Chronic inflammation associated with autoimmunity, chronic viral infection and cancer are also mediated by persistent release and function of these molecules [135]. An endogenous molecule is classified as a DAMP if meets five conditions [27]:

1. High intracellular concentrations.
2. Negligible extracellular concentrations.
3. Release following injury, infection or other inflammatory stimuli.

4. Activation of selective and specific cellular receptors over a wide range of concentrations.
5. Quick degradation following their release.

ATP meets all these prerequisites. Healthy cells contain high ATP concentrations, but infections, ischemia, shear stress or necrosis can cause cell rupture and massive ATP release into the extracellular matrix. Moreover, apoptotic cells can release ATP in a controlled fashion, and endothelial cells or activated immune cells secrete ATP during the inflammation. The effect of ATP in the modulation of the immune response is concentration dependent, cell dependent and changes during the various stages of inflammation [27].

During the acute inflammation response, ATP functions as a pro-inflammatory and immunostimulatory mediator. Extracellular concentrations may raise rapidly following tissue damage, marking the damaged site, and contributing to promote the inflammation and the initiation of primary immune responses, such as the production of cytokines<sup>1</sup> and the recruitment of leukocytes. In the second stage of inflammation, the extent of the response is fine-tuned by endogenous immunoregulatory substances. In this phase ATP, together with its byproduct Adenosine (Ado) are involved in a feedback system aimed to prevent over-activation of the immune system and the onset of uncontrolled chronic inflammation. Finally, in the last stage of inflammation, the immune response is down-regulated, allowing damaged tissues to be regenerated and cellular homeostasis to be preserved. High concentrations of extracellular Ado resulted to be an important immunosuppressive and tissue-healing factor.

It is in the second phase of inflammation that ATP monitoring becomes particularly interesting for the follow up and the optimization of the therapeutic regime in chronic pathologies. In fact, pharmacologic studies in a laboratory and drugs that increase extracellular ATP and ADP conversion to adenosine have shown therapeutic effect in patients with chronic inflammatory disease or ischemia [53]. Examples of drugs and compounds that affect the ATP levels and whose efficacy can be monitored through ATP detection include Methotrexate and Sulfasalazine, employed in rheumatoid arthritis and inflammatory bowel disease [53].

An issue concerning ATP detection is that the molecule has a short half-life and it is quickly converted into adenosine [53]; moreover its release is localized in the zone of inflammation. For these reasons, ATP monitoring in personalized therapy implies biosensing in the interstitial fluid and placement of the biosensor in close proximity of the inflamed site. ATP monitoring may therefore find an application in a long-term implantable biosensor for the follow-up of chronic autoimmune pathologies.

---

<sup>1</sup>Cytokines (Greek "cyto-", cell; and "-kinos", movement) are any of a number of substances that are secreted by specific cells of the immune system which carry signals locally between cells, and thus have an effect on other cells. They are a category of signaling molecules that are used extensively in cellular communication. They are proteins, peptides, or glycoproteins. A difference with hormones is that cytokines are involved only in the short range cellular communication and do not have global effects.



### 5.2 ATP detection: state-of-the-art

ATP is routinely measured with spectrophotometry [21], liquid chromatography [87], fluorescence [55], chemiluminescence [1], and bioluminescence [117].

Electrochemical detection of ATP has a wide range of applicability in physiological studies, especially in those directed towards *in vivo* applications, due to the possibility to integrate the sensor and the inexpensive cost of its realization with volume production.

ATP is not an electroactive compound, thus its electrochemical detection must be accomplished with enzymes or enzyme combinations that following ATP consumption will yield a measurable product. This section will review the main approaches presented in literature.

#### 5.2.1 H<sup>+</sup> ATPase

ATPases are membrane bound ion transporters that couple ion movement through a membrane with the synthesis or hydrolysis of ATP. Different forms of membrane-associated ATPases have evolved over time to meet specific demands of cells. Among these, F-ATPases are the prime enzymes involved in ATP synthesis. These membrane proteins can synthesize ATP using an existing H<sup>+</sup> gradient, or can reverse the existing gradient by hydrolyzing ATP. An H<sup>+</sup>ATPase biosensor has been described in the work of Bucking et Al. [28]. The group integrated the enzymes in liposomes fused, in a second step, to a gold electrode functionalized with a phospholipid SAM, to create an artificial phospholipid bilayer. By measuring the proton concentration at the electrode interface the group managed to sense ATP concentrations between 2.5 and 60mM.

#### 5.2.2 Choline Kinase

Choline is an electroactive substrate whose concentration can be monitored potentiometrically; choline kinase is an ATP-dependent enzyme. In presence of ATP the enzyme consumes choline producing the electrode-insensitive choline phosphate, decreasing the choline concentration at the electrode interface and thus altering the potential recorded by the electrode in a way proportional to the ATP concentration. The method was first described by Katsu and Yamanaka [86]. The group managed to detect ATP concentrations up to 10 $\mu$ M using a choline sensitive membrane electrode. Drawbacks of this approach are in the sensor construction based on a membrane electrode, and therefore not suitable for miniaturization and integration in a multi-parameter sensor platform, and in the fact that choline kinase must be added to the sample solution in a second moment. This kind of sensor is therefore not suitable for implantation.

### 5.2.3 Apyrase

Apyrase catalyzes the hydrolysis of ATP and ADP in  $H_2PO_4$  and  $H^+$ . In a recent work [116], Migita et al. entrapped apyrase on the surface of a field effector transistor (ISFET) and successfully detected ATP concentrations ranging from 200 to  $1000\mu M$  by sensing variations in the gate voltage due to the protons created during the enzymatic catalysis. The method, suitable for *in situ* analysis is however extremely sensitive to pH variations in the local environment and cannot distinguish between ATP and ADP.

### 5.2.4 Glycerol kinase / glycerol oxidase

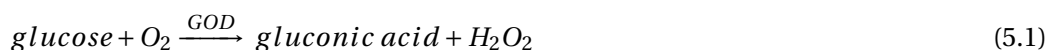
Biosensors based on Glycerol kinase (GK) and glycerol oxidase (GO) sense ATP towards a two-step enzymatic reaction. In the first phase the GK, in presence of ATP, converts glycerol in glycerol-3-phosphate (G3P). In the second phase, the GO converts G3P in glycerone phosphate and  $H_2O_2$ , which is sensed by the electrode by chronoamperometry. Worth of note is the work [102]. The group coated a Pt microelectrode with an ultrathin biolayer containing GK and GO, obtaining linear response over ATP concentrations ranging from 200nM to  $50\mu M$ . The sensor was used *in vivo* to demonstrate ATP release from spinal neurons during locomotor activity. Few years later, the sensor described by Llaudet et al. became the first commercial electrochemical ATP biosensor, the Sarissaprobe©.

## 5.3 ATP detection with nanobiosensors: experimental results

The ATP biosensors described in this chapter are based on the co-immobilization of glucose oxidase (GOD) and hexokinase (HEX). As for P450 detection, ATP biosensors were realized with an eye for practical applications, considering screen printed three-electrode cells for their low cost of realization, and employing multi-walled carbon nanotubes (MWCNT) to enhance the electrochemical response. Data in the next sections, successfully published in [37], will present the characterization of this nanobiosensor.

### 5.3.1 Detection principle

The glucose oxidase / hexokinase ATP biosensor was described for the first time in the work of Scheller and Pfeiffer [141]. Both GOD and HEX are sensitive for the substrate glucose, but with a different catalytic mechanism:



### 5.3. ATP detection with nanobiosensors: experimental results

In absence of ATP, glucose is totally converted in gluconic acid and H<sub>2</sub>O<sub>2</sub> by the glucose oxidase. The current detected is generated by the discharge of the hydrogen peroxide at the electrode surface, according to the following mechanism:



If only glucose is present, the electrochemical response of the biosensor becomes proportional to the glucose concentration in the media; in presence of ATP, the hexokinase can initiate the catalysis of glucose, and competes with the glucose oxidase for the substrate. In this situation, the quantity of hydrogen peroxide decreases and the electrochemical signal is reduced. The discharge of hydrogen peroxide is detected by *chronoamperometry*. In chronoamperometry the electrode is polarized at a fixed potential and the current is recorded in function of time [19]. The applied potential typically corresponds to the oxidation or reduction potential of the analyte. The *Cottrell equation* describes the current flow through the electrochemical cell

$$i(t) = nFAC\sqrt{\frac{D}{\pi t}} \quad (5.4)$$

Where  $n$  is the number of electrons involved in the discharge process,  $F$  the Faraday constant,  $A$  the electrode area,  $C$  the concentration of the electroactive specimen at the electrode interface and  $D$  its diffusion coefficient. The equation clearly shows that current intensity is proportional to the analyte concentration. Hydrogen peroxide is easily detected in chronoamperometry by applying a constant potential of +650mV vs Ag/AgCl.

#### 5.3.2 Sensors fabrication

Gold screen printed electrodes (model DRP 250AT) and multiwalled carbon nanotubes powder (MWCNT-diameter 10nm, lengths 1–2 $\mu$ M, COOH content 5%), were purchased from Dropsens. Glucose oxidase from *Aspergillus Niger*; hexokinase type 3 from Baker Yeast and D-(+) glucose were obtained from Sigma. ATP was bought from Aldrich. GOD and HEX were diluted to the stock concentration of 30mg/ml in PBS buffer pH7.4. Glucose was diluted in PBS to the concentration of 1M and kept at 4°C overnight before the first use, in order to allow the mutarotation of the molecules in solution.

The electrodes were made of a gold working electrode, a platinum counter electrode and a silver reference electrode. The working electrode area was 12.56mm<sup>2</sup>, while the total area of the cell, 22mm<sup>2</sup>. CNT nanostructuring was obtained by drop cast of 30 $\mu$ g of CNT solutions on the working electrode until complete evaporation of the solvent. Glucose oxidase and hexokinase were then mixed in a 1:1 ratio to obtain a solution with 15mg/ml of each protein. 20 $\mu$ l of the solution were then drop cast onto the working electrode, and let dry at 4°C overnight.

The electrochemical response of the electrodes was investigated by chronoamperometry under aerobic conditions and in presence of mild solution stirring (100rpm). Chronoamperometries

were acquired at the potential of +650mV versus Ag/AgCl, using a Versastat 3 Potentiostat (Princeton Applied Technologies). The electrode was dipped in 25ml of PBS 1×, MgCl 5mM pH 7.4. Mg<sup>2+</sup> ions are necessary for the catalysis mediated by the hexokinase. The optimum concentration of the ion was previously described by in [42]. Glucose and ATP samples were then injected in the solution during the chronoamperometry.

### 5.3.3 ATP measurement and CNT nanostructuration

As previously said, ATP detection with the GOD/HEX method is indirect: the current signal of the hydrogen peroxide generated by the glucose oxidase decreases when ATP is present in the sample, as the activated hexokinase competes for the substrate glucose and generates a non-electrolytic compound. In order to detect ATP, we initially measured the output current for glucose. Once the current was stabilized, we recorded the current variation in presence of increasing ATP concentrations, from 200μM to 1mM. After each ATP injection the signal decreased slightly to a new steady state value, as shown in Figure 5.1.

As for P450 biosensors, MWCNT nanostructuration enhanced the output current. Figure 5.2 compares the ATP response on bare and electrodes enriched with drop cast MWCNT. The addition of carbon nanotubes resulted in a 4× increase in sensitivity.

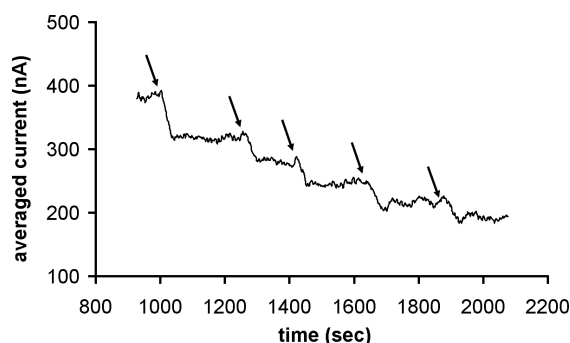


Figure 5.1: Current response following ATP injections. Arrows mark injection time. Every injection corresponds to a 200μM increase in the ATP concentration.

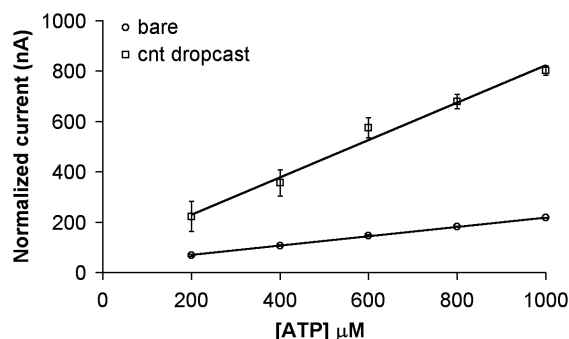


Figure 5.2: Current response in ATP biosensors with and without drop cast CNT. Error bars represent instrument noise.

#### 5.3.4 Effects of multiple enzyme immobilization

Figure 5.3 compares the current response of a glucose biosensor and an ATP biosensor with the same CNT nanostructuration. While the glucose sensor was prepared by drop casting  $18\mu\text{l}$  of a solution containing  $15\text{mg/ml}$  of GOD, the ATP biosensor presents a double protein concentration:  $15\text{mg/ml}$  of GOD plus  $15\text{mg/ml}$  of HEX for the same drop volume. The sensors were tested with 2 injections of  $12.5\mu\text{l}$  of glucose  $1\text{M}$ . In presence of hexokinase, the output current decreased to 2.7%, suggesting that the presence of a second protein is lowering the biosensor performance. Same results were obtained when the total protein concentration for the ATP biosensor was maintained at  $15\text{mg/ml}$ , thus excluding the possibility of an excessive protein amount. A possible explanation is that protein adsorption onto the electrode surface could have created protein interactions that can limit the enzyme efficiency.

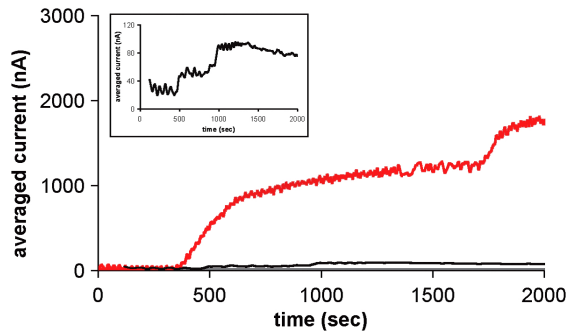


Figure 5.3: Comparison of the glucose current response between single and double enzyme immobilization in nanostructured electrodes. Red line: GOD sensor; Black line and inset, GOD+HEX sensor.

#### 5.3.5 Biosensor response in physiological glucose concentrations

In order to test the ATP biosensor in closer physiological conditions, the measurements were repeated in solutions with glucose concentrations ranging from  $1\text{mM}$  to  $3\text{mM}$ , values typically found in rat interstitium [14]. Figure 5.4 shows the ATP response for a single biosensor tested at different glucose concentrations. For each response, we calculated the sensitivity according to the equation

$$S = \frac{1}{A} \frac{d(i_{ss} - i_{gl})}{dC} \quad (5.5)$$

where  $S$  is the sensitivity,  $A$  is the working electrode area,  $i_{ss}$  is the steady state current reached after each ATP injection,  $i_{gl}$  is the steady state current reached after the glucose injection and  $C$  is the ATP concentration.

We obtained a sensitivity of  $26.8\text{pA}/\mu\text{M} \cdot \text{mm}^2$  for glucose  $1\text{mM}$ ,  $23.9\text{pA}/\mu\text{M} \cdot \text{mm}^2$  for glucose  $2\text{mM}$ , and  $12.5\text{pA}/\mu\text{M} \cdot \text{mm}^2$  for glucose  $3\text{mM}$ . The sensitivity reduction in presence of glucose  $3\text{mM}$  is caused by the saturation of the sensor to the substrate: given identical

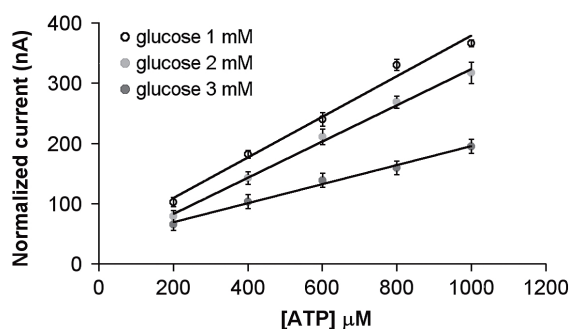


Figure 5.4: Calibration curves for the ATP response from 0 to 1mM at different glucose concentrations. Error bars represent instrument noise.

ATP concentrations, increased glucose availability reduces the extent current decrease operated by hexokinase, leading to an absence of the response/concentration proportionality. A similar effect was already observed with the GOD/HEX sensor developed by Soldatkin et Al. [154]. This behavior was also confirmed in another experiment in which we repeated two consecutive glucose/ATP injection cycles (Figure 5.5). During the second cycle, the biosensor became insensitive to glucose, as we did not record a relevant increase in the current. ATP sensitivity decreased from  $23.1 \text{ pA}/\mu\text{M} \cdot \text{mm}^2$  in the first cycle to  $12.9 \text{ pA}/\mu\text{M} \cdot \text{mm}^2$  in the second: a result comparable with the values shown before. Nevertheless, it is not possible to exclude that for this experiment the total ATP concentration could have affected the biosensor response in the second cycle: high ATP levels could have saturated the Hexokinase, leading to a decrease in sensitivity.

Therefore, it is necessary to constantly monitor the glucose level in an independent manner, for example by coupling a sensor which constantly follows the glucose oscillations. An additional advantage in the employment of an independent glucose sensor is to make the ATP biosensor not subjected to the interference of the molecules oxidized at +650mV, like catechols or ascorbic acid: in the GOD/HEX biosensor, the ATP detection is done on a subtractive basis, detecting a current decrease due to the hydrogen peroxide deprivation caused by the activation of the hexokinase. Contaminants oxidized at +650mV will only affect the initial baseline current which is monitored with another sensor.

It has been shown that tumor interstitium has glucose concentrations in the range of few hundred of  $\mu\text{M}/l$  [34] and accumulates ATP at high concentrations [128]. Our sensor, which resulted sensitive to micro-molar amounts of ATP, and operates with better efficiency with glucose concentrations below 1mM, is therefore able to detect pathological concentrations of ATP, and can ideally find an application as a tool to personalize the anticancer therapy. For example, it is known that ATP hydrolysis favors the tumor growth causing release of the metalloprotease MMP9 [66], which facilitates tumor invasion, and expression of indoleamine oxygenase [106], an immunosuppressive compound. In the perspective of a therapy which inhibits the ATP degradation, the sensor could be used to monitor the stability of ATP in the tumor microenvironment, and therefore validate the efficacy of the treatment.

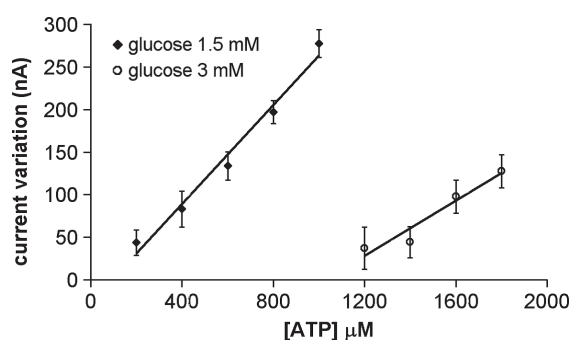


Figure 5.5: Effect of two different glucose concentrations on the ATP detection during the same experiment.

## 5.4 Chapter summary

ATP is a Damage Associated Molecular Pattern molecule involved in the regulation of the inflammatory response. ATP monitoring becomes interesting to evaluate in situ the efficacy of drugs that increase ATP conversion to adenosine.

The chapter presented an ATP biosensor based on MWCNT, glucose oxidase and hexokinase. The sensor is sensitive to the hydrogen peroxide produced by the GOD. In presence of ATP, GOD and HEX compete for the substrate glucose decreasing the current signal with strength proportional to the ATP concentration.

The sensor was able to detect ATP concentrations of hundreds of micromoles. Concentrations detectable with our sensor have been found the interstitium of solid tumors [128]. As putative application, the sensor can be used to monitor the ATP levels during therapeutic intervention.





## 6 Design and test of an implantable sensor platform

The realization of a biosensor array is often necessary in personalized therapy, where multiple parameters must be controlled at the same time. Additional challenges are arising in the case of implantable sensors, since the dimensions must be kept at minimum, and materials should be biocompatible. As already stated in the introduction, mature analytical devices must also face the challenges of signal processing, data transmission, powering and end-user interface: electronics and biosensor components must be integrated together. This need for system integration forces the interaction and the application of design constraints from every actor involved in the device realization. As an example, the sensor platform must be capable to host the electronic equipment, while the sensing techniques employed must be simple enough to be coordinated with a low-power consumption circuitry, and grant at the same time sufficient precision to enable reliable measurements.

In this chapter will be discussed design, fabrication, functionalization and test of a sensor platform hosting an electrochemical cell with five independent working microelectrodes, a temperature sensor and a pH sensor. The presence of multiple electrodes permits us to monitor multiple parameters, such as different drugs, ATP and glucose with a single device, while the presence of pH and temperature sensors ensure precise identification and measurement of the drugs. Indeed, in chapter 5 it was shown how a drug electrochemical signature is dependent on solution pH and how the catalytic current is influenced by temperature.

The implantable array, which measures 2.2x15mm, is designed to be integrated with a CMOS chip for on-board generation of voltage ramps [61], and a multilayer coil for remote powering by inductive link [125]. The three parts together constitute the building blocks of a fully implantable device. The results presented in this chapter have been published in [35]

### 6.1 Platform design and microfabrication

#### 6.1.1 Material choices

Choice of materials and fabrication techniques were done considering biocompatibility, simplicity of fabrication and precision as of primary importance. The sensor platform has been realized with 3 materials: a silicon substrate, a platinum metallization and an alumina ( $Al_2O_3$ ) passivation.

- Silicon has been chosen over glass as carrier substrate for its better thermal conductivity, in order to improve the dissipation of heat generated by the integrated circuit.
- Platinum has been selected for three distinctive advantages:
  1. **Biocompatibility and resistance to corrosion:** platinum has been widely used in medical devices since 1970 [43].
  2. **Pseudo-reference electrode behavior.** The implementation of standard reference electrode systems, such as Ag/AgCl or saturated calomelane may be problematic in miniaturized devices, as they require a compartment of liquid electrolyte which can be subject to leaking, consequently harming the host, and which makes its implementation difficult. Platinum has an established behavior as *pseudo reference electrode* [25]: its potential varies in a predictable manner according with the solutions conditions. Pseudo reference electrodes can be calibrated by including in the solution a redox compound with well-defined potentials, like ferrocene. Observed potentials are then adjusted to the known potential of the redox couple. In an implantable device these calibrations may be done with a sample of body fluids at different pH and temperatures, which are then monitored by the device itself with additional sensors.
  3. **Temperature dependence.** Pt resistance changes proportionally to temperature. This feature makes platinum an excellent material for the fabrication of resistive thermal devices (RTD) [38].
- Aluminum Oxide ( $Al_2O_3$ ) is an insulating material already used in biomedical coatings for its biocompatibility [156].

Thanks to the reduced number of materials, only two masks resulted necessary for the whole microfabrication process, enabling the production of a significant number of samples in few days.

#### 6.1.2 Process flow

The microfabrication was carried out at the Centre of Micro-Nano Technology of EPFL (CMI) using standard photolithography procedures. In brief:

## 6.1. Platform design and microfabrication

- Silicon wafers with 500nm of native oxide were chosen as substrate. The presence of native oxide enhanced the passivation adhesion.
- Metallization was realized by evaporation of 10 nm of Ti, followed by 100 nm of Pt. Ti layer has been included to promote Pt adhesion on silicon.
- Passivation was made by *atomic layer deposition* (ALD) of 10 nm of  $Al_2O_3$ ). ALD enables the controlled growth of thin, uniform and pinhole free passivations [91]. Such procedure conferred improved resistance to chemical etchants: we were able to clean our sensor array up to 45 minutes in piranha solution ( $H_2SO_4/H_2O_2$ 3:1) without noticing any visible degrading of the passivation. Moreover, the limited thickness of the passivation facilitates diffusion of analytes at the micro electrode interface.
- Passivation openings were made by dry etching, by exposing the wafer to 90° of *Argon Ion Milling* (AIM). AIM has been chosen for its ability to produce precise anisotropic etching. We assumed that the elimination of the etch undercut produced by isotropic methods could improve the robustness of the passivation when the platform is subjected to chemical cleaning or highly reactive electrochemical procedures.

The whole microfabrication process relies on only two photolithography masks, and can be described in 10 points, resumed by the Table 6.1 at the end of the chapter.

### 6.1.3 General design choices

Biosensors, pH and temperature sensors and slot for circuit integration have been placed in a row. Although the size of the final assembled prototype is still too big, this solution enables the realization of a sensor platform of cylindrical shape and limited volume, which can be implanted by injection<sup>1</sup>. To facilitate handling and electrochemical characterization with commercial potentiostats, the implantable part has been designed as part of a bigger platform, which hosts pads compatible with commercial connectors. Figure 6.1 shows one of the devices employed for the in-vitro characterization, while Figure 6.2 presents a detail of the implantable part and the single sensor components: the biosensor array, the pH sensor and the temperature sensor, whose description and characterization is presented in the next sections.

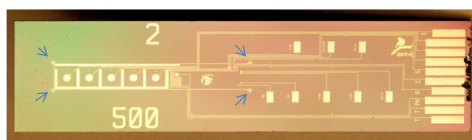


Figure 6.1: Photograph of the microfabricated platform for the in-vitro characterization. Arrows indicate the dicing crosses used to obtain the implantable sensor.

<sup>1</sup>To be injected, the final diameter of packaged implant should not exceed 2.5-2.6mm, as the inner diameter of the biggest needle is 2.692mm. Source: Sigma-Aldrich

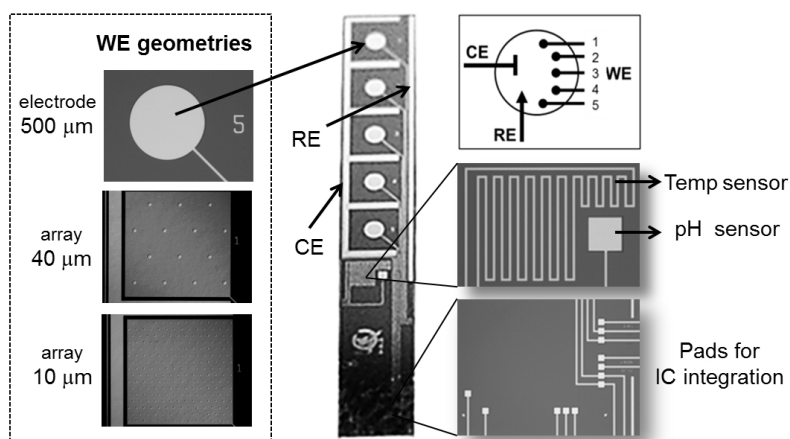


Figure 6.2: Implantable platform – detail. Left, different WE geometries; centre, whole platform ( $500\mu M$  model); right, temperature and pH sensors, pads for IC integration and schematics of the electrochemical cell.

## 6.2 The biosensor array

### 6.2.1 Design

The biosensor block has been designed as an electrochemical cell including 5 independent working electrodes (WE) and common counter (CE) and reference (RE) electrode. This solution simplifies the interconnections with the sensing circuitry, optimizing at the same time the available space. The counter electrode has been realized with an inter-digitated geometry. This design choice granted that each WE is equally surrounded on three sides by the CE and from one side by the RE. Inter-digitation allows the creation of a uniform electric field around each single working electrode and maximizes the local CE area.

The working electrodes were fabricated in the micrometer scale. The diffusion of electroactive substances towards microelectrodes (ME) differs from macroelectrodes, where only planar diffusion perpendicular to the surface occurs. When a current is flowing at microelectrodes, hemispherical diffusion layers are formed within seconds. Due to the radial component of diffusion, more electroactive particles per surface area reach the electrode within a time unit. Sigmoidal cyclic voltammograms instead of peak-shaped ones are obtained, even at scan rates of tens of mV/sec, because of a steady-state mass flux to the electrode surface [20]. In addition, the current density increases and, as a result, an improved signal-to-noise ratio is obtained [172]. The drawback in using ME is the low current produced. Microelectrode arrays (MEA) provide an attractive alternative to because they can yield responses of magnitude similar to macroelectrodes, but with a considerable lower capacitive background [44]. Maximum current density is reached when each electrode in the array acts as an individual microelectrode, a situation achieved when individual diffusion layers do not overlap [44]. For this reason, electrode dimensions and intra-electrode spacing become critical parameters in the optimization

of the MEA response. According to the work of Saito [140], individual diffusion zones for a single microelectrode are approximated to a distance of 6 times the electrode radius. Intra electrode spacing should be therefore at least 12 times the radius of a single electrode. The best properties of MEAs can be assumed for (i) smaller microelectrodes, (ii) situations when the number of electrodes in the microelectrode array is increased because the signal to noise (S/N) ratio increases and (iii) when the distance between electrodes is large [20].

In order to explore the best configuration for our biosensor, the working electrodes were realized in three different geometries: a round electrode (diameter  $500\mu\text{m}$ , area  $196'250\mu\text{m}^2$ ), and two microelectrode arrays (diameter  $10\mu\text{m}$ , 208 electrodes, spacing  $100\mu\text{m}$ , area  $16'328\mu\text{m}^2$ ; diameter  $40\mu\text{m}$ , 14 electrodes, spacing  $400\mu\text{m}$  area  $17'584\mu\text{m}^2$ ), named *Electrode 500*, *Array 10* and *Array 40*. Openings and spacing of the microelectrode array were chosen considering the results presented by Berdoque et Al,[20], which describe a screening of multiple geometries and configurations.

### 6.2.2 Characterization of bare electrodes

Since the platform has common reference and counter electrodes, working electrodes were initially characterized by cyclic voltammetry with potassium ferrocyanide 10mM to test if their response was dependent by their position in the array. Figure 6.3 shows the results for the electrode 500 geometry. As can be seen, voltammograms are well overlaid, with the exception of the topmost electrode (electrode 1 - blue) which yields a slight lower peak current, but whose contribute is negligible (100nA of difference). This result proves that proposed design grants reproducible results among the different working electrodes.

In a second experiment we studied the voltammogram profiles and the scan rate dependence of various geometries. Figure 6.4 shows a comparison between the different designs. As can be seen, both Array 10 and Array 40 present a microelectrode behavior, with reduced capacitive background and a steady state current, while the Electrode 500 behave as a conventional macroelectrode, showing the typical peak profile. All the three geometries shown current/scan rate dependence, however, in proportion, current increase for the Array 10 is more contained compared to the other two geometries. At the same scan rate the Array 10 produced a higher steady state current respect to the Array 40. Since the two geometries have very similar area, this result suggest that the improved signal can be attributed mostly to the electrode design. It is however important to say that other factors may have affected the voltammogram profile of the two microelectrode array as well as the current dependency with respect to the scan rate. Not surprisingly, the Electrode 500, which is the largest, also produced the highest current.

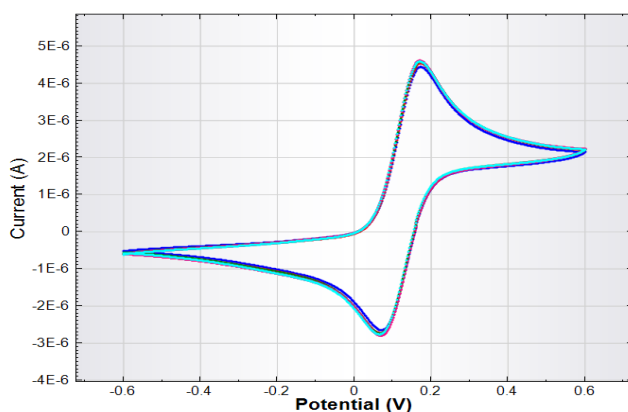


Figure 6.3: Cyclic voltammetry scans of the different working electrodes of the sensing platform. Blue: electrode 1 (topmost); red, electrode 2; green, electrode 3; cyan, electrode 4; purple, electrode 5 (bottommost).

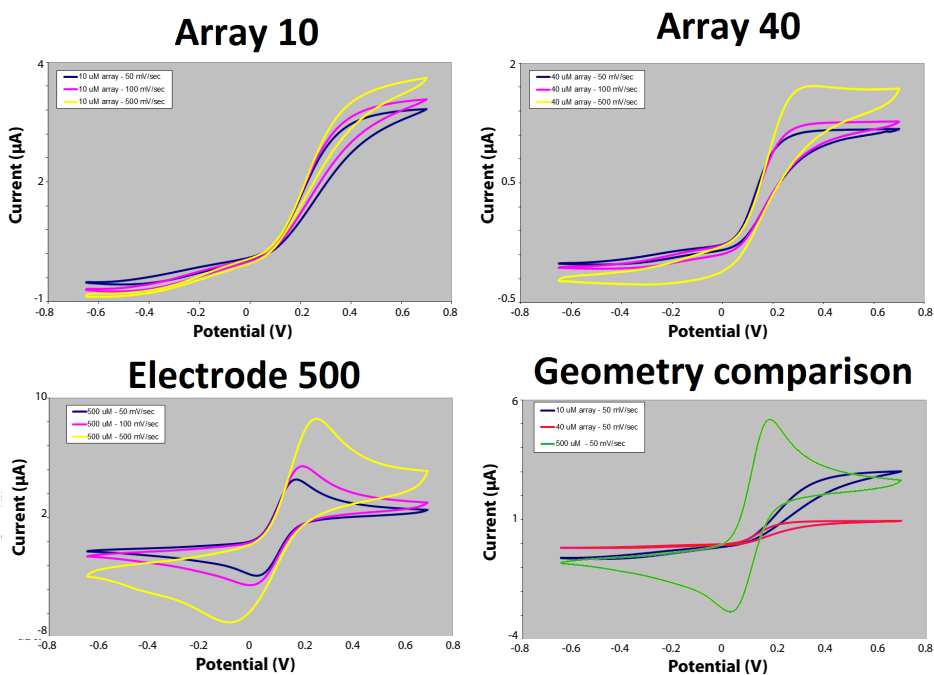


Figure 6.4: Cyclic voltammetry of potassium ferrocyanide 10mM for the three WE geometries at different scan rates. Blue: scan rate 10mV/sec; pink, scan rate 100mV/sec; yellow, scan rate 500mV/sec. Bottom-right, comparison of the CV response at 50mV. Blue, Array 10; red, Array 40, green, Electrode 500.

In a third experiment we compared the electrodes sensitivity towards repeated injections of hydrogen peroxide 10mM measured by chronoamperometry at +650mV. Figure 6.5 reports the results for each WE design, and a comparison with a commercial platinum screen printed electrode. The Array 10 provided the highest sensitivity, but also a larger variability in the results; the Array 40, of equivalent area, showed only the 55% of sensitivity of the Array 10,

but improved reproducibility. The Electrode 500 showed the lowest sensitivity, but values are comparable with the commercial electrode (diameter 1.6mm, area 1'538'600 $\mu\text{m}^2$ ), while standard deviation is remarkably lower.

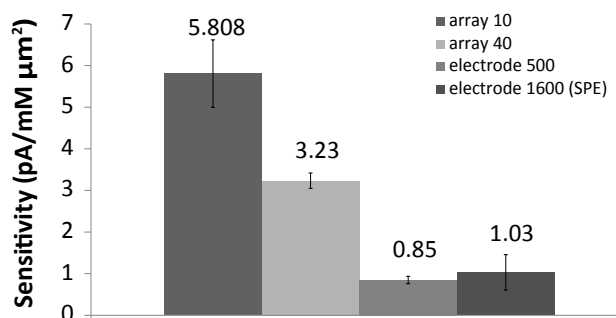


Figure 6.5: Sensitivities of different WE geometries to  $\text{H}_2\text{O}_2$ . Before measurement, the sensors were first dipped in a 1x PBS solution pH7.4, and conditioned for 1200" at +900mV. Values obtained averaging 5 results. Error bars: standard deviation. Image from [35].

### 6.2.3 Microelectrodes nanostructuring

A drawback of employing ME and MEA is the difficulty to precisely functionalize each single microelectrode. An additional complication is due to the presence of multiple biosensors on the same platform: proteins must be precisely immobilized on the right electrode in order to avoid the risk of contamination and the generation of misleading signals. Micro-spotting is a technique commonly employed for the electrode functionalization, but presents several limitations: spot size is fixed therefore electrodes smaller or bigger than the spotting diameter, as well as non-round geometries, cannot be precisely covered; spotting resolution is limited by the machine precision, and finally the instruments are expensive. An alternative technique is the electrode functionalization by chitosan (CHT) electrodeposition. Chitosan is a natural polysaccharide obtained from the deacetylation of chitin which finds large employ in enzymes' immobilization for its biocompatibility, antibacterial properties and affinity to proteins [95], and in the solubilization of carbon nanotubes [103]. The amino group in chitosan has a dissociation constant ( $pK_a$ ) of  $\sim 6.5$ , which leads to a protonation in acidic to neutral solution. When the solution pH exceeds the chitosan  $pK_a$  chitosan becomes insoluble and coagulates to a hydrogel. The polarization of an electrode creates a localized region of high pH that can exceed chitosan's solubility limit, allowing CHT polymerization and entrapment of any other compound present in the original solution with high spatial selectivity, regardless the electrode shape, dimensions or inter-electrode distance. An additional advantage of CHT electrodeposition is that the degree of deposition can be precisely controlled varying the deposition time; therefore this technique enables reproducible functionalizations when the same solution is used. Finally, carbon nanotubes, enzymes and chitosan can be mixed together and deposited in a single step.

### Electrodeposition procedure

Chitosan solution 0.7% w/v was made by dissolving CHT flakes (medium molecular weight – Aldrich) in a solution of acetic acid 2% pH 3 and stirred until complete dissolution. Final pH was then set to 5. MWCNT (diameter 10nm, lengths 1-2 $\mu$ m, COOH content 5% - Dropsens) were added to the solution at the concentration of 1mg/ml. The dispersion was sonicated again until homogenization. Glucose oxidase (GOx) 5mg/ml (Sigma) was added to the mix just before the electrodeposition. To prevent hydrogen evolution at the electrode surface,  $H_2O_2$  20mM was added to the preparations before the electrodeposition [183]. The coating was performed applying a constant potential of + 1.5V for 300, 600 or 1200 seconds to a specific working electrode, followed by a rinsing in water to remove the solution excess.

### Electrodeposition results

As expected the electrodeposition was localized only in proximity of the electrode openings. Figure 6.6 shows the nanostructuration on the 10 $\mu$ m geometry for different electrodeposition times: 300, 600 and 1200" respectively on electrodes 2, 3 and 4 of the same array. Longer times led to more defined films: due to the material accumulation, the nanostructuration radius after 1200" resulted to be almost the double of the one obtained after 300". Radius increase was noticed only for the array 10 geometry, and only between 600" and 1200". This is probably due to the small size of the microelectrodes: after 600" the electrodeposited chitosan/CNT composite probably filled the electrode opening and expanded outside. Figure 6.7 presents the  $H_2O_2$  response for different depositions on the Array 10. Sensitivities decrease, due to the chitosan insulating effect. The inclusion of conductive MWCNT permitted us to recover part of the current response, but doesn't replicate the bare electrode results. No appreciable differences were found between 300" and 600", while a time of 1200" led to a decrease in the performance. A possible explanation is that longer deposition times may have led to thicker and therefore more insulating films, although other factors may have contributed to this effect, since the performance decrease do not seem proportional to the deposition times considered.

The inclusion of glucose oxidase enabled the preparation of a biosensor towards a single step electrodeposition. figure 6.8 shows the response of the Electrode 500 to repeated injections of glucose 2mM. We obtained a sensitivity of 0.09 pA/mM $\cdot\mu$ m<sup>2</sup>. It is important to say that glucose detection was achieved only employing the 500 $\mu$ m geometry, regardless the electrodeposition time. We attribute this effect to the electrode area: the microelectrode arrays have a surface almost ten times smaller than the 500 $\mu$ m geometry, therefore with the current protocol, the amount of immobilized enzyme resulted probably too low to yield appreciable  $H_2O_2$  production, and suggesting that smaller electrode geometries may require the electrodeposition of more concentrated enzyme solutions.



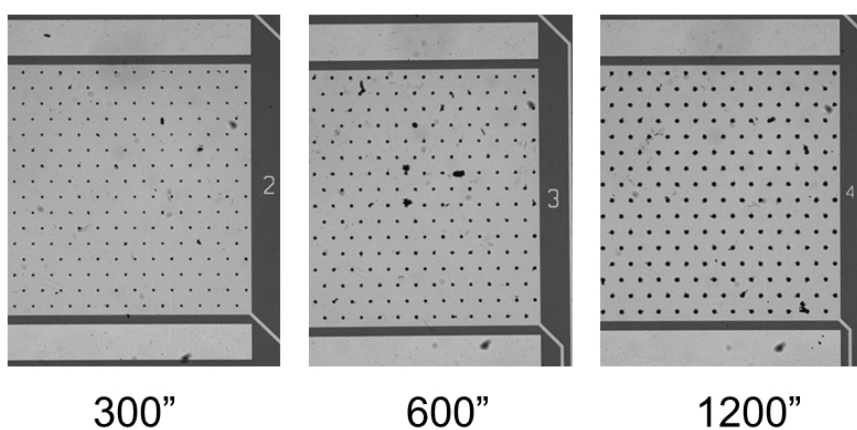


Figure 6.6: Selective nanostructuring of the  $10\mu\text{m}$  array with different electrodeposition times. Polymerization occurs only above the microelectrodes. Longer times lead to larger films. Image from [35].

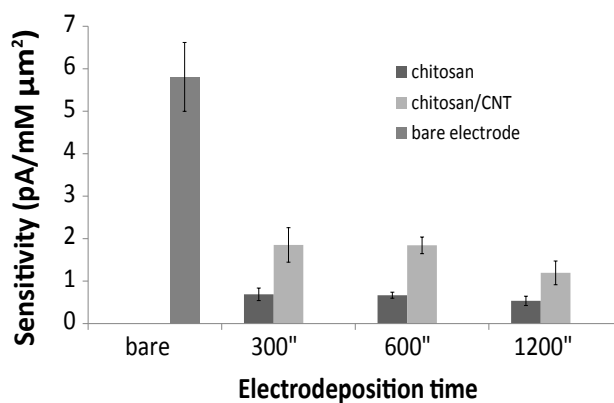


Figure 6.7:  $\text{H}_2\text{O}_2$  response on the  $10\mu\text{m}$  array for different kinds and times of electrodeposition. Values obtained averaging 5 measurements. Error bars, standard deviation. Image from [35].

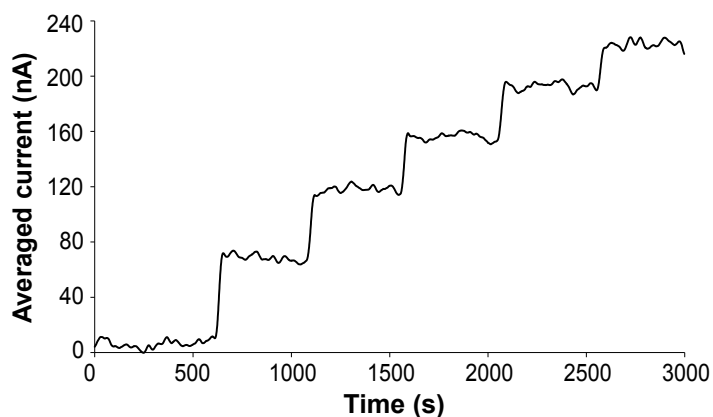


Figure 6.8: Glucose response of the  $500\mu\text{m}$  electrode after 600" electrodeposition of the CHT/CNT/GOx dispersion. Each step corresponds to a 2mM glucose injection. Image from [35].

### 6.3 The pH sensor

The pH sensor, in Figure 6.9, consists of a  $250\mu m^2$  square electrode coated with an electrodeposited film of iridium oxide (IrOx). IrOx is one of the most promising materials for thin-layer pH electrodes, as it confers advantages as wide pH response range, fast response time, high pH sensitivity, low potential drift, and low sensitivity to redox pair interference [108].

Iridium oxide films can be prepared by several methods. Examples include sputtering [90], thermal decomposition of an iridium salt [6], thermal oxidation of an Iridium-carbon film [166], and anodic electrodeposition [178]. While other methods require complex procedures such as high-temperature treatment, electrochemical activation, or expensive iridium targets, the anodic electrodeposition of iridium oxide films (AIROF), become one of the election techniques for the functionalization of planar electrodes because its relative simplicity and manufacturability in large-scale applications.

pH detection with IrOx films is based on the reversible redox reduction of the Ir/IrO<sub>2</sub> couple, according to the relation described in [76]:



Differences in pH affect the stoichiometry of the equation and change the equilibrium potential of the Ir/IrO<sub>2</sub> couple. By monitoring the open circuit potential between the IrOx electrode and the reference electrode it is therefore possible to sense the solution pH.

Our pH sensor was realized by electrodeposition of a solution iridium oxide onto a micro-electrode of  $250\mu m^2$ . The IrOx solution was prepared according to the methods described in [60]. Briefly, 150mg of iridium tetrachloride, 1ml of H<sub>2</sub>O<sub>2</sub> (30% v/v) and 500mg of oxalic acid dehydrate were dissolved in 100ml of milliQ water; once the solution was homogenized, pH was set to 10.5 by adding small aliquots of anhydrous potassium carbonate. The solution was then stored at room temperature for two days to allow stabilization. A color shift from yellow to light-violet indicated it could be used for a successful deposition. Anodic deposition was performed by applying a current density of  $0.15mA/cm^2$  for 80'. After deposition electrodes were rinsed in distilled water and stabilized in PBS pH7.4 for two days before being calibrated. The electrode was then dipped in PBS solutions at different pH and the open circuit potential was used to build a calibration curve. Figure 6.10 shows our best measurement in the pH range 5-8. In the considered range, the potential decreases linearly with increasing pH. The sensor provided a sensitivity of  $0.7\mu V/pH\ unit \cdot \mu m^2$ . This result proves that our pH sensor is able to detect pH variations in the physiological range.

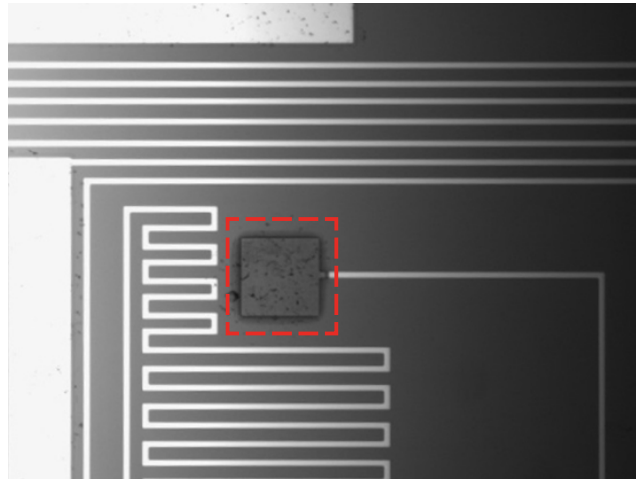


Figure 6.9: Photograph of the pH sensor coated with iridium oxide (red insert).

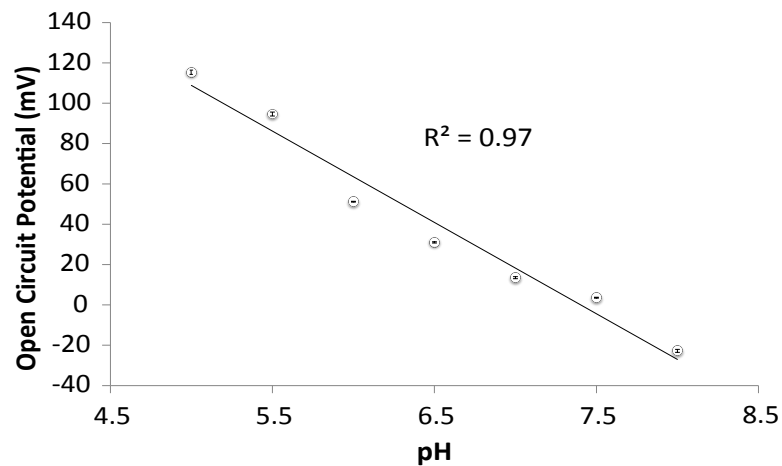


Figure 6.10: Open circuit potential of the IrOx coated electrode to different solutions pH. Error bars, instrument noise. Image from [35].

## 6.4 The temperature sensor

The most popular temperature sensors used today are the Thermocouple, the Resistive Temperature Device (RTD), thermistors, and Integrated Silicon Based Sensors [18]. A thermocouple consists of two dissimilar metals in contact, which produces a voltage when heated; the size of the voltage is dependent on the difference of temperature of the junction to other parts of the circuit. A RTD is a metal conductor which exhibit changes in resistance when the temperature changes; thermistors function similarly to RTD but employ ceramic or polymers instead than metals and finally Silicon based sensor rely on integrated circuit design. Each of these sensor technologies cater to specific temperature ranges and environmental conditions. While the thermocouple is most appropriate for higher temperature sensing, the RTD is best suited for

## Chapter 6. Design and test of an implantable sensor platform

lower temperatures were good linearity is desirable; the thermistor is typically used for applications with smaller temperature ranges, and offers greater accuracy than the thermocouple or the RTD, and finally the silicon based sensor ensures high stability over time [18].

Our sensor consists in a Platinum RTD of 0.02x16mm length (Figure 6.11). Among other metals employed in RTDs such as Cu and Ni, Pt presents linear behavior in the physiological temperature range, biocompatibility, and the highest metal resistivity [18]. The choice of platinum RTD also enabled the micro fabrication of the temperature sensor without additional process-flow steps. An additional advantage of using RTD, instead of temperature sensors integrated in the sensing circuitry is that the metal it is not affected by the circuit heating.

The sensor was tested by dipping the platform in solutions with temperatures ranging from 25 to 40°C. The result is presented in Figure 6.12. Resistance increased linearly with temperature. Our device provided a resistance of 2.2k $\Omega$  and a sensitivity of 6.8 $\Omega$ /°C. Although the sensor succeeded to measure temperature variations in a linear fashion in the physiological range, we found that the power demand was still too high for the sensing circuitry to integrate. After simulation, we established that best results are obtained increasing the resistance to 100k $\Omega$ . RTDs of 0.04x160mm can achieve this result. Further prototypes will be implemented with this solution.

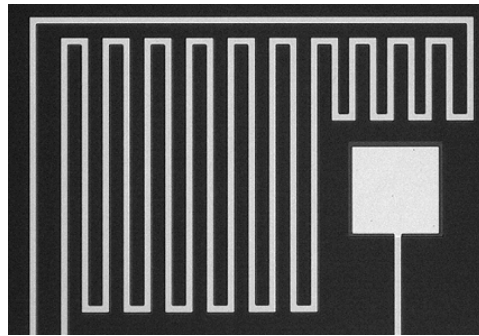


Figure 6.11: Photograph of the temperature sensor.

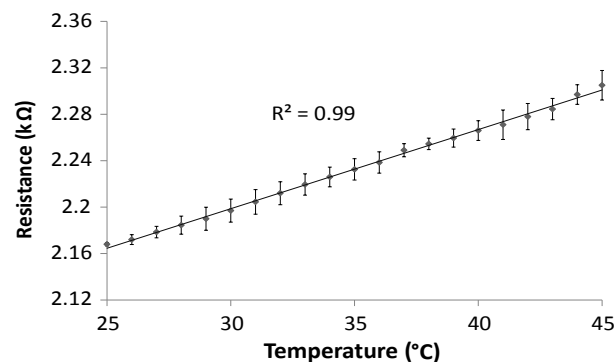



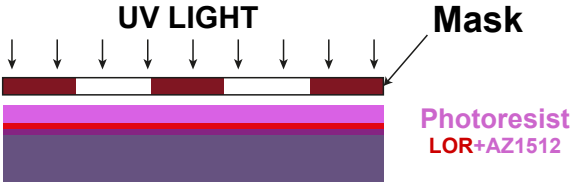
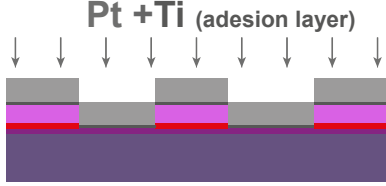
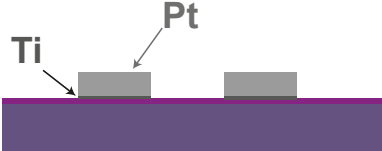
Figure 6.12: Resistance values of the Pt RTD at different solution temperatures. Resistance increases linearly with temperature. Error bars, average of 3 measurements. Image from [35].

### 6.5 Chapter summary

The sensor array was microfabricated considering biocompatibility, performance, robustness and simplicity of fabrication, as leading criteria for the design and the materials choice. Among tested geometries, the Array 10 showed the highest response respect to  $H_2O_2$ , but resulted too small to immobilize sufficient enzyme amounts to permit glucose detection. Electrodeposition proved useful in patterning with CNTs complex geometries and conferred better resolution and uniformity respect to the drop cast. Inclusion of enzymes and CNTs in chitosan granted fast and simple preparation of biosensors in a single step electrodeposition. The use of chitosan reduced the sensors' sensitivity, but the inclusion of CNTs allows recovering part of the original response. The proposed solutions for pH and temperature sensors showed linear response in windows including the physiological range.

These results together suggest that our sensor array can be exploited for the monitoring of multiple parameters. Future work will focus on the improvement of the nanostructuration to enable drugs and ATP detection.

**Chapter 6. Design and test of an implantable sensor platform**

Step	Process description	Cross-section after process
01	<p><b>Wafer dehydration</b> Improvement of photoresist adhesion to the substrate</p> <p><b>Substrate:</b> <i>Si test wafer + SiO<sub>2</sub> 500 nm</i></p>	
02	<p><b>Photolithography – metal mask</b> Coating/exposure/development of a lift off resist (LOR) and a positive photoresist to create the metal pattern</p> <p><b>Materials :</b> <i>LOR + AZ1512 HS</i></p> <p><b>Thickness:</b> <i>400 nm + 1.6 μm</i></p>	
03	<p><b>Metal evaporation</b> e-beam evaporation of a thin layer of Ti and a thick layer of Pt to create the metal patterns. Ti is used to promote Pt adhesion the substrate.</p> <p><b>Materials:</b> <i>Ti 10 nm (stick layer)</i> <i>Pt 100 nm</i></p>	
04	<p><b>Lift off</b> Removal of unwanted metal by dissolution of the lift off resist in a chemical bath.</p>	

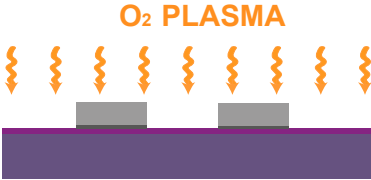
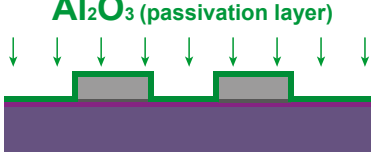
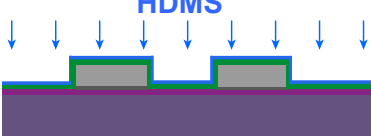
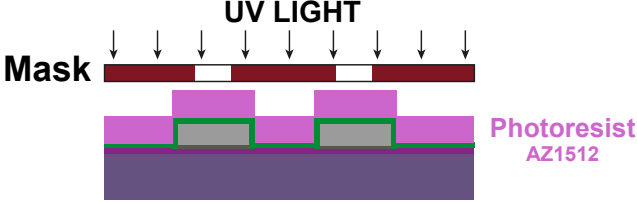
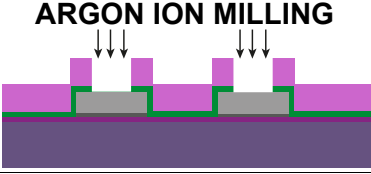
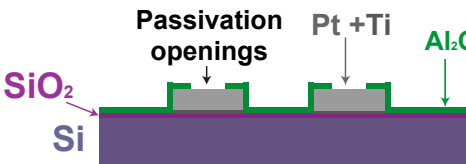
05	<p><b>Oxygen plasma</b></p> <p>Further removal of unwanted metal and photoresist by oxygen plasma and</p> <p>Surface activation before the atomic layer deposition</p> <p><b>Procedure</b>  <math>O_2</math> flow: 400 ml/min  Power: 500 W  Variable time</p>	
06	<p><b>Atomic layer deposition (passivation)</b></p> <p>Application of an insulating layer of <math>Al_2O_3</math> to passivate the chip</p> <p><b>Material:</b>  <math>Al_2O_3</math> – 10 nm</p>	
07	<p><b>HDMS Priming</b></p> <p>Wafer dehydration and vapour deposition of hexadimethylsilazane to improve photoresist adhesion</p>	
08	<p><b>Photolithography - opening mask</b></p> <p><b>Material :</b>  AZ1512 HS</p> <p><b>Thickness:</b>  400 nm + 1.6 <math>\mu</math>m</p>	
09	<p><b>Passivation etch</b></p> <p>Argon Ion Milling  90''</p>	
10	<p><b>Strip resist</b></p>	

Table 6.1: Process flow of the microfabricated sensor platform.





# 7 System packaging and biocompatibility

When discussing implantable biosensors, *biocompatibility* and *biostability* aspects are crucial. Material, size and shape of the implant must be well tolerated by the host, in order to avoid important adverse effects; sensor electronics must be protected by the corrosive action of body fluids and finally strategies to prevent the confinement of the implant by fibrosis must be adopted in order to preserve the sensor functionality.

Biocompatibility and biostability can be promoted by an effective packaging and are assessed by *in-vitro* and *in-vivo* tests. In the first part of this chapter, the immune response to an implant, the strategies to solve specific biocompatibility and biostability issues and the controversies about the biocompatibility of carbon nanotubes will be reviewed. The last part of the chapter will present data on assembly, packaging and short term *in-vitro* and *in-vivo* biocompatibility evaluation of the implantable sensor platform.

## 7.1 Background and state of the art

### 7.1.1 The foreign body reaction

The innate response of the host to the introduction of exogenous material is called the *foreign body reaction* (FBR). A detailed description of this reaction can be found in [133, 173], below a summary is given.

Immediately after insertion, an implant spontaneously acquires a layer of host proteins. Composition, concentration and conformation of this protein layer are dependent on the foreign material and the implantation site. As consequence of the insertion, a fibrin clot is formed to close the lesion, while an oedema is formed close to the wound. Neutrophils and macrophages present at the injured site start to clean up the damaged area and release molecules to promote further infiltration of leukocytes at the injured site. In this phase, the host experiences a period of acute inflammation, with the injured site swelled, warm and painful. Persistent inflammatory stimuli lead to chronic inflammation. This stage is

characterized by the presence of monocytes, macrophages, lymphocytes and plasma cells at the implant site, and a proliferation of blood vessels and connective tissue to heal the affected area. The macrophages will clean up the wound site, and attempt to digest the foreign material by forming a cellular cluster called *foreign body giant cell*. When using biocompatible materials, the chronic inflammation should typically last no longer than 2-3 weeks. In the final stage of the FBR, the body attempts to quarantine the external object: monocytes, macrophages and foreign body giant cells adhere at the implant interface and a fibrous tissue will form, surrounding these white blood cells, and confining the implant from the host. Outside, a highly vascularised granulation tissue is formed.

### 7.1.2 Biocompatibility: definition and test procedures

Biocompatibility has been defined as “the ability of a material to perform with an appropriate host response in a specific application” [173]. An appropriate host reaction includes no local tissue damage due to cytotoxicity, limited FBR and no short or long term adverse body effects. Also, this definition points out that there doesn't exist an absolute status of biocompatibility. The site and duration of the implant, as well as type of material-body contact are important parameters, which makes biocompatibility a contextual concept. Even more, the same material can induce an adverse or a favourable biological response according to its particular employ [3].

Experiments to test biocompatibility are carried out both *in vitro* and *in vivo*, in order to test the local and systemic effect of the material. The ISO 10993 standard<sup>1</sup>, issued and constantly updated by the International Organization for Standardization (ISO), is a well-known standard for evaluation of biocompatibility prior to clinical testing of a device. Various tests are essential for each material/device before medical use. The three most basic evaluations are cytotoxicity, sensitization, and irritation testing. The presence of toxic, leachable substances is investigated, causing adverse effects on biosystems. Based upon the final goal of an implant (implant duration, location in the body, and type of tissue contact) various additional categories of tests have to be performed, such as genotoxicity, hemocompatibility, carcinogenicity tests, etc. Obviously, a medical glove for short time contact with the skin will need much less testing compared to a heart assisting device which will be implanted in the body for over 10 years.

### 7.1.3 Factors affecting implant biocompatibility and design solutions

A device which isn't properly designed will have a disturbed functionality during or after the foreign body reaction, according to different factors:

- **Grafting factors:** depending on the implant surface morphology and properties, the FBR might be mild or strongly pronounced, resulting in a smooth integration in the local

---

<sup>1</sup>ISO 10993 *Biological compatibility of medical devices. Part 5. Tests for cytotoxicity: in vitro methods*, december 1992

tissue or in the presence of a thick fibrous encapsulation or even a chronic infection.

- **Implant fabrication factors:** proper implant design should prevent adverse effects such as corrosion caused by biological fluids penetrating into the device, or release of toxic implant material in the organism.
- **Sensor bio-fouling factors:** due to accumulation of biological material on the sensor surface, the sensor performance might be impaired.

### Grafting factors

The formation of a thick fibrous encapsulation during the FBR should be avoided in case the implant is carrying biosensors, since in most of the cases this barrier will result in a wrong or a delayed sensor read-out. Additionally, biofilm formation at the implant surface should be prevented at all means. Biofilm formation is the accumulation of bacteria at the implant surface, and is a cause of chronic infection. Due to the slimy substance used by the bacteria to encapsulate, the removal of the bacterial colonies by antibiotics is almost impossible, and explantation of the implant is often the only solution to overcome the infection.

Grafting solutions aim to improve cell adhesion, promote vascularization and reduce inflammatory stimuli. A first strategy consists in the use of engineered surfaces: morphology, porosity and mechanical properties of the implant package can influence cell signaling, organization, proliferation and migration [139]. In this respect, it has been demonstrated that porous coatings of polyvinyl alcohol can promote higher vascular density, tissue in-growth and faster response to analytes compared to smooth surfaces [145]. After this initial work, several groups have started to employ nanostructured shells for implantable sensors, using material like titanium [130] or silicon [48].

Other approaches to promote blood vessel formation and reduce fibrosis, are based on hydrogels [131, 132, 181], and coatings containing growth factors [169] or poly-L-lactic acid [93]. In order to reduce the inflammation and biofilm risk upon implantation, the use of drug-releasing coatings can be also considered, such as hydrogel shells loaded with Dexamethasone, a strong anti-inflammatory agent [57, 74].

### Implant fabrication factors

Active implants might consist of microchips, a battery, and other components which are partially made of non-biocompatible materials. Contact of biofluids with the electronics should be avoided by all means, as they will corrode the device and might promote leaking of toxic compounds into the body. This makes the presence of a *bi-directional diffusion barrier* essential to preserve contamination of body and implant from the respective components.

Biocompatible materials are imperative for the fabrication of the diffusion barrier and for the packaging of the total device [126, 45]. The most conventional device package consists

of a Titanium box, equipped with feed-throughs for sensors, such as a pacemaker. Titanium is biocompatible and the box is sufficiently thick to prevent all diffusion; however, package size and the rigidity are not ideal with respect to the resulting FBR, and remote powering transmission by inductive link is not feasible due to the shielding effect of the metal (although electronics within thin Ti packages can be still remotely powered by ultrasounds [88],[111]).

In order to reduce implant size, ceramic or polymer thin films can be used. They have the advantage to be compatible with wafer-level processing and to conform to any shape. Thin films can be divided in organic or inorganic. Organic compounds for packaging include epoxies, silicones, polyimides, polyurethanes and parylene-C. Attention should be paid in using these materials for long-term implants, since they are not totally immune from moisture penetration. Parylene-C is very promising due to its excellent biocompatibility and step coverage, and its high moisture resistance [51], but has the limit of being heat-sensitive. The use of high-temperature sterilization techniques is therefore not possible for devices containing parylene-C. Polyimide is another attractive and flexible substrate for implantable electrodes [124], but due to some remaining moisture permeability, additional measures should be taken to protect the implant for moisture penetration in case of long term implantation.

Among inorganic films, silicon nitride is the most employed for moisture protection [73]. Metal films can be also used for hermetic packaging, when deposited onto another polymeric film which provides electrical isolation. Iridium oxide, Titanium, Titanium nitride, Tantalum and Tantalum nitride can be biocompatible if proper deposition conditions are respected [94]. Noble metals like platinum and gold present high resistance to corrosion and biocompatibility, and despite their cost, represent excellent candidates for the microfabrication and the connection of the subcomponents of an implantable device. An example is the fabrication of a Utah Electrode Array [158].

### **Biofouling factors**

Biofouling is the accumulation of biological material on the device surface. In contrast to biofilms, which consist of bacteria, this biologic material is not causing an infection. The aggregation of cells, macromolecules and small molecules on the biosensor membrane has been extensively reported as detrimental for the sensor function [96, 97, 119, 151]. Biofouling often prevents diffusion of the analyte or adherence of the analyte on the sensor surface. Most of the strategies to reduce biofouling rely on the use of dedicated membranes. An extensive review about this topic can be found in [174]. Below we will briefly describe two techniques for reducing biofouling: hydrogel overlays and nafion coatings.

Hydrogel overlays, present an hydrophilic interface which can favour diffusion of water-soluble analytes. Diffusion rate is controlled by changing the crosslinking density of the gel. A drawback of this approach is their poor adhesion to the substrate, and a poor mechanical stability during the implantation procedure. Common materials for hydrogels are the poly(hydroxymethyl methacrylate) and the poly(ethylene glycol).

Nafion is a commercial polymer that gained a lot of popularity as coating for glucose sensors. It is characterized by chemical inertness and both hydrophobic and hydrophilic properties. An additional reason of its extensive use, is its easy application by dip-coating.

### 7.1.4 Biocompatibility of carbon nanotubes

Despite their fundamental role in enhancing a biosensor performance, a real implementation of carbon nanotubes in biomedical devices relies on the outcome of studies concerning their toxicity. CNT toxicity may arise from their dual nature of nanoparticle and nanofiber: from one side the large surface area / mass ratio of a CNT increases the probability of interaction with a cell, and confers a great capacity of adsorption, transport and uptake of toxic substances in the body, from the other side the carbon nanotube length may induce foreign body reactions, since longer fibres ( $>17\mu m$ ) are difficult to phagocytise [152].

Up to date, information related to CNT safety are contradictory, and present results sustaining both toxicity and inertness of these nanomaterials. Good reviews of experiments concerning the safety of carbon nanotubes is given in [152, 77]. The picture emerging from literature is that CNT toxicity is dependent on many factors including purity, aggregation status, dimensions, coating or functionalization, cell type and bioassay technique.

In general, experiments confirmed that:

- Unrefined CNT, due to the presence of transition metal catalysts and other impurities derived by their synthesis, are cytotoxic.
- Pristine CNT cause minimal *in vitro* and *in vivo* toxicity, but only when they accumulate in cells at high concentrations.
- The aggregation of CNTs in fibers is critical in determining their toxicity. Efficient dispersions techniques, such as covalent binding or electrostatic adsorption of peptides, acids, amines and polymers, seems to prevent their aggregation and didn't show significant toxicity effects.
- CNT immobilized to a substrate or embedded in a nanocomposite are not toxic, although the degradation of the matrix can produce particles that cause dose-dependent adverse effects on cells.

According to these findings, in the perspective of an implantable biosensor, the use of short, functionalized CNTs immobilized in a nanocomposite may represent a safe implementation. However, it is important to say that up to date, due to the novelty of this material, there are no exhaustive studies concerning the long-term effects of carbon nanotubes in living organisms or the impact of these substances on the environment.

### 7.2 System packaging and biocompatibility: results

As pointed previously, the development of an appropriate packaging is essential for promoting smooth wound healing, minimizing the extent of the foreign body reaction and granting prolonged sensor functionality. This section presents data on assembly, packaging and short term in-vitro and in-vivo biocompatibility evaluation of the implantable sensor platform. Platform assembly, packaging and in-vitro biocompatibility tests have been done in collaboration with Imec, Belgium; in-vivo biocompatibility tests are the result of a collaboration with the Istituto di Ricerca in Biomedicina of Bellinzona, Switzerland. The device was realized integrating 3 building blocks: the multi-electrode platform described in the previous chapters and in [35], an inductive coil [125], and an integrated circuit [61]. To promote biostability and biocompatibility, a double protection for electrodes and electronic components was employed: enzymes and CNTs were entrapped in a chitosan (CHT) matrix and then sealed behind a porous polycarbonate membrane.

If biocompatibility, antibacterial properties and affinity to proteins make chitosan a good matrix for enzymes immobilization [95], the inclusion of MWCNT enhances the biosensor electrical properties [35] and improves chitosan's elastic and tensile strength by conferring more resistance [146, 167]. On the other hand, polycarbonate membranes are commonly employed as microdialysis filters in commercial biosensors [163] and can be used to prevent that the particles originated by the degrading of the CHT/CNT nanocomposite diffuse in the body. Corrosion of electronic components and leaking of potentially hazardous substances in the body was prevented with a conformal coating of Parylene C, an inert and biocompatible polymer with widespread industrial use. An outer package of medical grade silicone was then employed to create a soft shell suitable for implantation. A schematic cross-section of the prototype is shown in Figure 7.1.

The efficacy of the parylene C barrier, as well as the toxicity of carbon nanotubes, have been assessed with a 7-day in-vitro cytotoxicity elution test conform to the ISO-10993-1 standards. The integrity of the CHT/CNT matrix and the efficacy of the polycarbonate membrane in preventing CNT leaking were tested exposing the materials to solutions of different nature and pH at 37°C for one week. The final packaged device was then implanted in mice for 7 and 30 days to evaluate the inflammatory response.

## 7.2. System packaging and biocompatibility: results

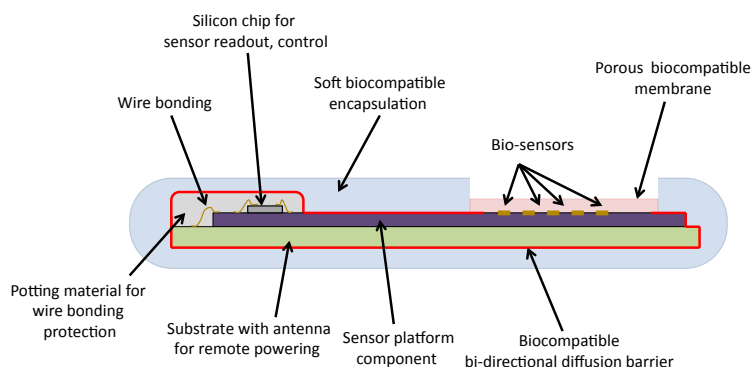


Figure 7.1: A schematics cross-section of the implantable device.

### 7.2.1 Matrix corrosion test

#### Methods

CHT/CNT dispersion was prepared according to [37]. Drops of  $10\mu\text{l}$  were cast onto a 12 well plate and dried under laminar flow. Half of the samples were protected with a polycarbonate membrane (Cyclopore track etched membrane, cut off 100nm, Whatman) and sealed with fast curing medical grade silicone (Med2-4220, Nusil). All samples were covered with 1ml solutions of milliQ water, PBS 1x pH 4, or Mouse Embryonic Fibroblasts (MEF) growth media, and put in a cell incubator at  $37^\circ\text{C}$  5%  $\text{CO}_2$  for 7 days. The 8<sup>th</sup> day the solutions were removed and the samples rinsed twice with DI water before being dried in air under laminar flow. The CHT/CNT matrix integrity and the dispersion of CNT aggregates on the well plate surface were then inspected with an optical microscope.

#### Results

To assess if the CHT/CNT matrix represent a good strategy for enzyme immobilization in implantable sensors, we tested its resistance to corrosion in different solutions: PBS 1x pH 4, distilled water and MEF medium. Figure 7.2 shows the results obtained after 7 days of incubation at  $37^\circ\text{C}$  (5%  $\text{CO}_2$ ). Data shows that at acidic pH the matrix is dissolved. CHT/CNT aggregates are spread on the well surface and tend to accumulate at the well edge. Immersion in distilled water showed discrete matrix corrosion: while the bulk structure was maintained, particles are evident on the well surface and close to the edge. The cell culture medium resulted to be the least aggressive: few particles are visible on the surface and we didn't find significant deposit amounts at the well edge. The impurities visible on the sample are due to the medium components, as shown in the control. The extent of matrix corrosion is due to the different pH of solutions: chitosan has a pKa of  $\approx 6.5$ . When the solution pH is lower than chitosan's pKa, the ammino-groups of chitosan are protonated and the compound becomes water soluble. Differences in corrosion between water and MEF medium are attributed to the

## Chapter 7. System packaging and biocompatibility

buffer properties of the latter: cell substrates are optimized to maintain a physiological pH during the incubation.

In a second experiment we evaluated if the presence of a polycarbonate membrane is sufficient to prevent significant CNT leaking in the body. Figure 7.3 shows the results obtained in PBS 1x pH 4. After 7 days of incubation, the matrix drop is still evident, but a darker area in its proximity denotes the presence of severe corrosion (A). Optical microscope images of the silicone seal edge (B) and of the well edge (C) clearly show that CNTs and chitosan in solution are able to leak from the membrane. Despite the fact that drop cast multi-walled carbon nanotubes form a highly entangled structure and their length exceed 10 to 20 times the pore size of the polycarbonate membrane (100 nm), their diameter is 10 times smaller. We conclude that diffusion can be retarded but not prevented with a membrane cut off bigger than the CNT diameter. Alternative solutions to contain the CNT leaking can rely on the direct growing of CNTs on the electrode substrate [155] or on the crosslinking of the matrix to improve the resistance to corrosion. In this respect, crosslinking with genipin, already employed in tissue engineering [39, 115], represents a biocompatible alternative to the most common glutaraldehyde.

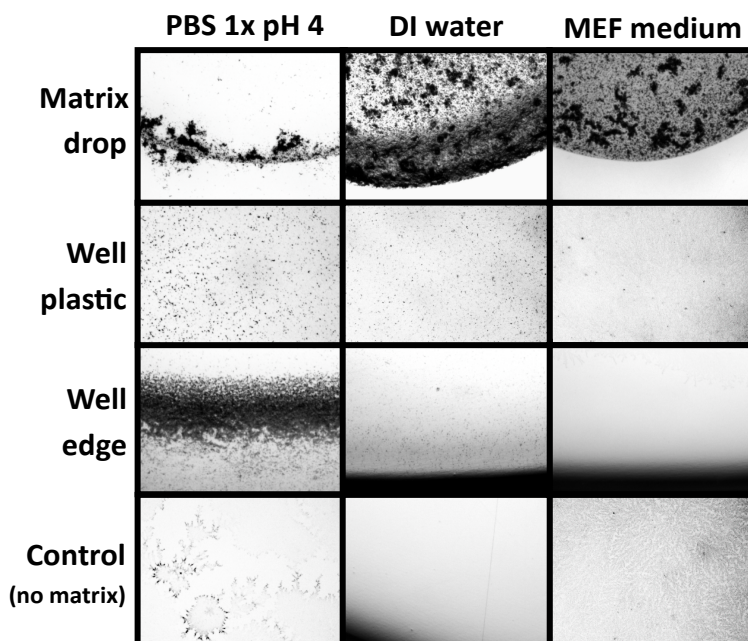


Figure 7.2: Corrosion test of the chitosan/CNT matrix. Optical microscope images in different parts of the well. The black spots represent chunks of CHT/CNT attached to the surface.



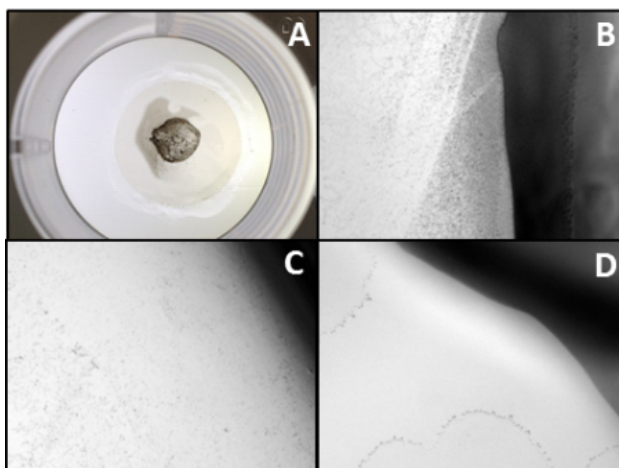


Figure 7.3: Evaluation of chitosan/CNT matrix leaking from a polycarbonate membrane. A) picture of the well showing the matrix drop and the membrane. B) edge of silicone seal; C) well edge; D) edge of the silicone seal on the sample without the matrix.

### 7.2.2 *In vitro* cytotoxicity test

#### Methods

Cytotoxicity was assessed with elution tests according to the ISO 10993-1 guidelines. Each experiment was conducted in triplicate and included a positive control to assure reproducibility and reliability of results. The elution test steps include preparation of contaminated media, cell culture, assessment of viability, and toxicity evaluation by Calcein staining.

- **Preparation of contaminated medium:** The growth medium was obtained adding to a Dulbecco Modified Eagle Medium, Fetal Calf Serum (10% v/v); L-glutamine 200mM (1% v/v); Glutamax (2% v/v); non-essential aminoacids (1% v/v), Penicillin/Streptavidin (1% v/v). All the reagents were purchased from Gibco. Test materials were placed in cell culture dishes, sterilized with ethanol 70% and dried under laminar flow. MEF medium was added according to the ratio  $1\text{ ml}/6\text{ cm}^2$  of material. The samples were put in a cell incubator at  $37^\circ\text{C}$ , 5%  $\text{CO}_2$  for 7 days. A negative control of MEF medium was also included to account for the aging of nutrients in solution. The contaminated medium and the control were then collected, stored at  $4^\circ\text{C}$  and used within 3 days.
- **Cell culture:** Mouse Embryonic Fibroblasts (MEF) were extracted in Imec, Belgium, seeded in 12-well plates at the concentration of  $1.2 \times 10^4$  cells/ml and grown for 3 days. The 3<sup>th</sup> day, the growth medium was collected and replaced with the contaminated terrain and the control. Cells were grown for 4 additional days before being inspected for viability and toxicity.
- **Assessment of Viability:** The specimens were rejected when the viability of healthy control cells resulted less than 75% [45]. Control wells were incubated 30' with  $1\mu\text{g/ml}$

of DAPI and PI fluorescent dyes (Invitrogen) to highlight respectively total cell nuclei and dead cells. For each well, three DAPI and PI counts in different spots were performed. Cell viability was then calculated according to the equation  $viability = \frac{viable\ cells}{total\ cells} 100\%$ , where viable cells is the total number of DAPI counts minus PI counts and total cells is total number of DAPI counts.

- **Toxicity evaluation:** Cells were incubated 30' with  $1\mu g/ml$  of Calcein AM (Invitrogen). The fluorescence in each sample was immediately measured with a commercial scanner (Tecan infinite M1000, excitation  $\lambda$  485nm, emission 525nm). Total fluorescence count for each well was obtained averaging 225 readings evenly distributed in a 15x15 round shape along the well area. Since Calcein AM stains only living cells, cytotoxicity was evaluated comparing the fluorescence intensity of the contaminated samples with the control. Intensity decrease of more than 20% from the control was considered cytotoxic. Additionally, cells were inspected for morphologic abnormalities at the fluorescence microscope. Samples presenting a majority of abnormal cells respect to the control were considered cytotoxic.

### Results

The building blocks of the implantable sensor are partially made from non-biocompatible or potentially toxic materials. For example, the receiving coil presents a copper metallization, notably cytotoxic [100], while materials of the integrated circuit and of the auxiliary electric components, realized by external companies, are not totally disclosed, and have to be considered as potentially harmful. A conformal coating of  $3\mu m$  parylene C was employed to prevent corrosion of the electrical parts and toxic metals leaking in the host. Parylene efficacy was evaluated by elution tests on the receiving coil substrate. When immersed in a fluid, the copper contained in the coil diffuses in the solution, producing severe cytotoxicity even at very small concentrations.

Figure 7.4A presents the average fluorescence of Calcein-AM stained cells. After 4 days of incubation with the contaminated medium, cells grown in presence of the terrain eluted with the unprotected coil yielded severe cytotoxicity, as demonstrated by very low fluorescence; on the other hand, the parylene C coating proved effective in preventing severe cytotoxicity, as the fluorescence intensity resulted the 88% of control. It is worth mentioning that while variations up to 20% from the control are not considered cytotoxic by the USP guidelines, such variability could be unacceptable in long term implants [45]. In this respect, the protection of the parylene C may be enhanced improving its substrate adhesion and its thickness.

In a second experiment we evaluated the cytotoxicity of the CHT/CNT matrix (Figure 7.4B). After 7 days of elution and four days of incubation with healthy cells, no significant differences with the control cells have been observed, proving that in the considered period the CNT leaking is not cytotoxic. A possible explanation is that CNT toxicity depends on many factors like length, functionalization or aggregation, the tight wrapping of chitosan to the nanotubes,

## 7.2. System packaging and biocompatibility: results

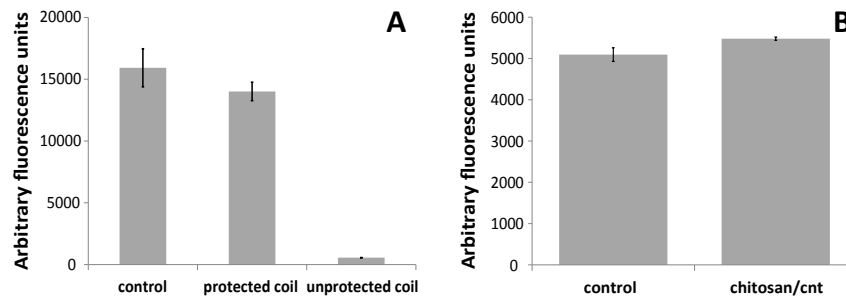


Figure 7.4: Evaluation of materials cytotoxicity by calcein staining – average fluorescence values. A) effectiveness of the parylene C coating on the inductive coil B) evaluation of chitosan/CNT cytotoxicity. Error bars, standard deviation ( $1\sigma$ ).

which is also responsible for their dispersion in aqueous solutions, can shield the nanoparticle and its reactive groups, reducing the inherent toxicity and preventing their aggregation.

As additional cytotoxicity control we performed a morphological analysis of cells. Figure 7.5 shows that cells from the protected coil (B) and from the CHT/CNT matrix (C) are similar in shape and distribution to the control (A). No living cells were found on the sample with fluid eluted from the unprotected coil (D, bright field image). The giant cells shown in the pictures are due to the initial cell density, which after 7 days resulted too low to give a confluent coverage and the typical tight and elongated shape of fibroblasts.

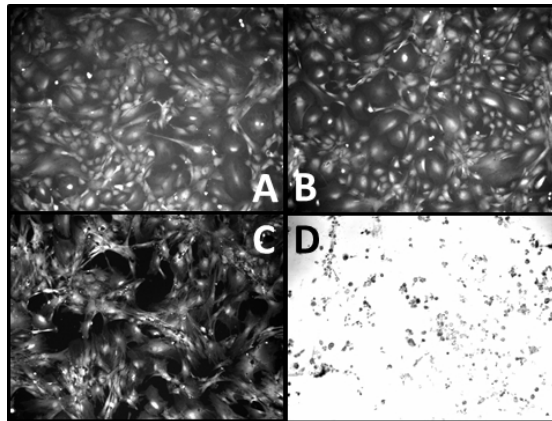


Figure 7.5: Morphology of MEF grown in different contaminated media. Optical microscope images. A) control; B) receiving coil and parylene C coating; C) CHT/CNT matrix; D) unprotected coil, bright field image.

### 7.2.3 Assembly and packaging of the implantable device

The sensor building blocks were glued together using a USP class VI biocompatible glue (Loctite 3211). Components interconnection was realized with Al wire bonding and protected with glob top. To further improve parylene C adhesion and moisture penetration, the assembled platform was treated with the silane A-174 (Merk) according to the procedure described in [71],

## Chapter 7. System packaging and biocompatibility

and coated by chemical vapor deposition of  $16\mu\text{m}$  of parylene C (Speciality Coating Systems).

The outer silicon shell was realized by placing the implant into a plexiglass mold realized by micromachining, and injecting biocompatible medical-grade silicone (Med 6033, Nusil). To increase the host comfort, the outer shell was made 1mm thick and with rounded corners. In a design variant, two “wings” of 3x3mm placed along the main body have been included to prevent the sensor to capsize after implantation, since misalignment between the receiving coil and the external wearable device can compromise the remote powering of the sensor array.  $0.1\mu\text{l}$  of CHT/CNT suspension was then manually drop cast on the electrodes and dried in air. A polycarbonate membrane was placed above the electrodes and sealed to the external shell using fast curing medical grade silicone. Without considering the external wings, the packaged device measures 20 x 4.2 x 3mm. The assembly schematics and the final result is shown in Figure 7.6.

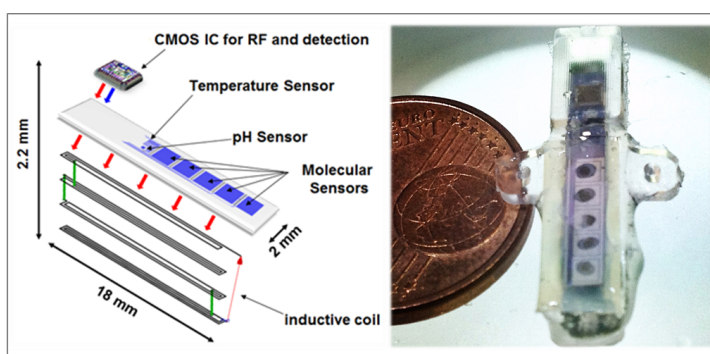


Figure 7.6: Assembly and packaging of the device.

### 7.2.4 *In vivo* biocompatibility

#### Methods

Microchips were cleaned and disinfected with Gigasept instru AF (Schuelke), placed in cell culture dishes, sterilized with ethanol 70% and dried under laminar flow. An Air Pouch (AP) was created by subcutaneous injection of sterile air in the back of male C57BL/6 mice at day 1 (5mL) and 3 (3mL); this procedure creates a cavity of 1.5cm diameter and 0.5cm height. At day 6, mice were anesthetized with isoflurane 4%, shaved and locally sterilized with Betadine Solution; microchips were implanted and the cavity sutured with Vicryl 6.0 (Provet AG). As a control of local inflammation bacterial lipopolysaccharide (LPS) ( $50\mu\text{g}/\text{mouse}$ ) (LabForce AG) was injected daily into the cavity for 4 days or 2 weeks for short term and long term biocompatibility, respectively. As negative control we generated air pouches in the absence of any surgical procedure. After 7 or 30 days, microchips were removed. The cavity was rinsed with 0.5mL of PBS (Gibco) and the liquid collected and centrifuged at 7000rpm for 10 min at  $4^\circ\text{C}$ . We then determined the concentration of ATP in the supernatant with ATP detection kit (ATP Determination Kit, Invitrogen). For polymorphonuclear neutrophils detection, the

## 7.2. System packaging and biocompatibility: results

---

pellet was resuspended in 0. mL RPMI 10% fetal bovine serum (FBS) (Gibco) and analyzed at flow cytometer (FACS Canto, Becton Dickinson) with antibodies specific for CD11b and Gr1, respectively labeled with allophycocyanin (APC) and fluorescein isothiocyanate (FITC) (both from BioLegend).

### Results

Potential sources of inflammation in implantable devices can be attributed to the implant materials, shape and size [7]. In order to investigate which elements are critical in eliciting an inflammatory response, we fabricated devices of different nature and shape to subcutaneously implant in mice. To account for inter-individual variability, each model was tested in eight different animals. Half of the mice carried the implant for 7 days, the other half for 30 days. At the end of the period, the implant site was washed with PBS, and levels of ATP and neutrophils in the elution liquid were compared to follow the local inflammatory response. While ATP release is a consequence of cellular necrosis and it is therefore a measure of the local cell death, neutrophils are recruited to the inflammation site by chemical signaling. Variations in neutrophil percentage at the implant site are therefore informative of the status of tissue inflammation [137].

Figure 7.7 presents neutrophils and ATP variation in the liquid collected from the implant site after 7 and 30 days. Sensors packaged with a soft shell presenting or not presenting external wings (W), were compared with dummy package replicas entirely made in biocompatible silicone. Bacterial lipopolysaccharide (LPS) was administered to a separate group of mice in order to induce an inflammatory response not dependent by an artificial implant, while mice with air pouch only served as negative control. After 7 days, we measured high levels of ATP and neutrophils, but after 30 days both values seem to decrease, suggesting that the organism became tolerant to the implants. Data from neutrophils suggests that the insert complexity (presence of wings and/or sensors) tends to increase the short-term and long-term inflammatory response. Considering average values, after 30 days, residual neutrophils in mice treated with winged inserts were 2-3 folds higher than their counterparts, while the presence of the sensor platform induced slightly higher inflammatory responses. ATP measurements in mice bearing the implant were affected by large statistical variability. A possible explanation is that upon removal we found that several implants were displaced from their original location. This may have led to internal tissue damage due to mechanical friction and therefore insurgence of cellular damage and ATP release in some individuals [23]. Unfortunately, this large variation in the ATP measurements makes difficult to establish a clear relationship between implant complexity and extent of local cell death.

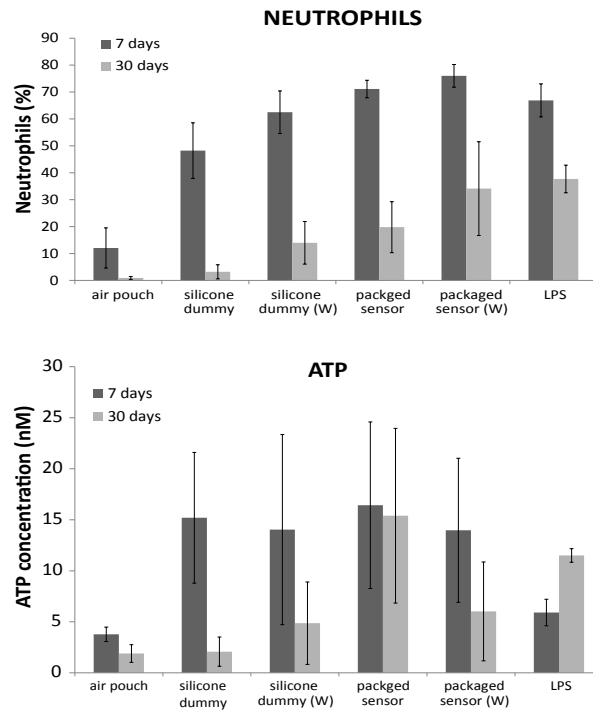


Figure 7.7: *In vivo* biocompatibility results after 7 and 30 days. Top: percent of neutrophils infiltration in the implant cavity; bottom ATP concentration. Error bars, standard deviation ( $1\sigma$ ).

Values from LPS injection further suggest how after 30 days the host seems to accept the insert. Although LPS-induced ATP and neutrophils were detected in lower amounts compared to the values obtained from implants, ATP concentration in animals treated with LPS almost doubled after 30 days. The pyrogenic effect of LPS is also evident with respect to the neutrophils infiltration: in one month, LPS-treated mice presented the highest percentage of neutrophils and the slightest time-dependent reduction among the animals considered. Percentage variations of neutrophils and ATP are summarized in Table 7.1.

Table 7.1: Percent variation of neutrophils and ATP after 30 days.

Percent variation of neutrophils and ATP after 30 days						
	Air pouch	Silicone dummy	Silicone dummy (W)	Packaged sensor	Packaged sensor (w)	LPS
<i>Neutrophilis</i>	-92.4	-93.3	-77.6	-72.2	-55.1	-43.6
<i>ATP</i>	-49.8	-86.3	-65.3	-6.3	-56.9	+94.6

From the neutrophils measurements it appears that the package shape has a role in determining the inflammatory response, as the presence of wings tends to increase the immune reaction. Although the introduction of stitching wings may be necessary to hold the insert in place and correctly aligned with the external powering coil, their presence can exert an uncomfortable localized pressure on some parts of the tissue, and angles where tissue stress

might promote localized immune responses [113]. The presence of the electronic platform further increased the inflammation response.

However, it is important to say that more than strong conclusions, these are trends suggested by the average values obtained. *In vivo* experiments tend to have large variability, and due to the reduced number of animals used, the overlap of error bars indicates that results are not statistically different. A larger number of experiments, and additional investigation techniques are advised for a more precise evaluation of the *in vivo* biocompatibility.

The removal of copper components from the sensor electronics, together with thicker parylene coatings may further reduce the inflammation caused by the biosensor platform. Employing bigger animals may also help decreasing the inflammation, since the size of our device is too big for a mouse. Implant size can also be further reduced: in this respect, the bulkiest component of our platform is the inductive coil, which with a thickness of 2mm, contributes to almost 4/5 of the total platform volume. Our group is currently developing a single layer coil on silicon, which will reduce the platform thickness to 1 – 1.5mm.

### 7.3 Chapter summary

This chapter presented data on assembly, packaging, *in vitro* and *in vivo* biocompatibility evaluation of the implantable platform described in this thesis.

Biocompatibility is a concept of primary importance, which should be considered starting from the implant design, and including all aspects of its fabrication, until the follow up of the implantation. A device can be considered fully biocompatible not only if it safe for the host, but also if it is capable to preserve its functionality in time. In this respect, the development of an appropriate packaging is essential for promoting smooth wound healing, minimizing the extent of the foreign body reaction and granting prolonged sensor functionality.

*In vitro* experiments on primary fibroblasts proved that coatings of  $3\mu\text{M}$  of parylene C are effective in preventing copper leaking and cytotoxicity for at least seven days; similar test on a chitosan/ MWCNT matrix showed that release of chitosan/MWCNT complexes in the growth terrain are not cytotoxic in the short term. This last result is in agreement with recent studies demonstrating that the employ of short, functionalized CNT immobilized in a nanocomposite may be implemented with a certain degree of safety. Although, in last analysis, the fate of nanotubes in implantable devices is still largely dependent by studies concerning their long-term toxicity. *In vivo* tests of the packaged sensor array demonstrated that the foreign body reaction significantly decreased after 30 days, suggesting normal recovery of the host. Package shape is suspected to have a role in inducing the inflammatory response, suggesting that future implants must possess smoother geometries.





## 8 Conclusions and future developments

The objective of this thesis was the development of a fully implantable biosensor for personalized therapy applications. The thesis presented innovative research on the electrochemical detection of common marketed drugs, drug cocktails, glucose and ATP with biosensors based on cytochromes P450 and different oxidases. The presence of carbon nanotubes provided increased sensitivity and detection limit, enabling the detection of several drugs in their therapeutic range in undiluted human serum.

The assembled system has been packaged with an inner moisture barrier in parylene C, to prevent circuit corrosion and toxic metals leaking, and an external biocompatible silicone shell to improve the host tolerance and reduce the local inflammation. The efficacy of the parylene barrier, as well as the toxicity of carbon nanotubes, has been assessed with *in vitro* cytotoxicity tests conform to the ISO-109931 standards. The final packaged device was then implanted in mice to assess its biocompatibility. Comparison between 7 and 30 days in *in vivo* implantations showed significant reduction of the inflammatory response in time, suggesting normal host recovery.

The results achieved are promising, even if the ambition of realizing a fully operational implantable device in human subjects requires additional research.

For example, stability of enzymes for at least several months must be a priority in a long-term fully implantable device: experiments are needed to understand for how long biosensors retain their activity when they immobilized to a substrate or when are in prolonged contact with a biological fluid. In this respect, a simple drop cast of protein and nanostructures may be not sufficient, and strategies to promote enzymes immobilization and protection, such as entrapment in a matrix or confinement behind a protective membrane should be investigated and optimized. The entrapment in chitosan of enzymes and CNT represents a good starting point for additional research. Additionally, to compensate the inevitable loss and denaturation of proteins in time, the implementation of an “enzyme reservoir” in the implantable sensor should be considered [64].

## Chapter 8. Conclusions and future developments

---

Optimization of the drug detection with cytochromes P450 requires more basic research regarding this protein electrochemistry: for example, it is known that prolonged electrochemical activation of P450 and poor enzyme immobilization can transform the P450 proteins in P420, an inactive form of the enzyme that is still capable to generate an electrochemical signal [127]; while recent work demonstrated that coupling efficiency of the P450 is very low, and that the electron transfer between electrode and cytochrome is preferentially accomplished via the P450 reductase as intermediary protein [49]. As additional complication, even in absence of a specific substrate, the P450 active site can shunt and produce electro-reactive specimens that can generate misleading signals [49]. The development of engineered CYP enzymes may solve these issues and help to produce more stable sensors.

Additional research is also necessary in case of multiple drug detection with the same P450 isoform. Even if the experiments presented here provided the proof-of-principle of the method, to fully demonstrate the atypical P450 kinetics in electrochemical systems, it will be important to design experiments with compounds whose interaction and kinetics is well documented in literature, regardless their effective employ in medical treatments.

P450 biosensors need to be realized and tested on the electrodes of the microfabricated platform. In this respect we found that commercial microsomes are not sufficiently concentrated to produce visible signals on the microelectrodes. To overcome this problem, many biosensor research groups produce their own cytochromes. So far, for time and cost reasons we avoided this strategy.

Biosensor detection limits must be pushed even further: the sensors described in this thesis are capable to detect micromolar concentrations of analytes, which are acceptable to detect many of the drugs considered in this thesis in their therapeutic range. However, many prescriptions possess a therapeutic window in the nanomolar range. The situation is similar for the ATP detection: the detection limit achieved in this thesis restricts the application of the biosensor to specific cases, and the follow up of chronic inflammation with ATP monitoring requires nanomolar detection limits. The implementation of more sensitive electrochemical techniques, such as square wave or differential pulse voltammetry can be considered to reduce the capacitive background and highlight the faradic contributions. However, this will also require the design of more complex integrated circuits to implement in the implantable sensor platform, and the control of a bigger number of parameters.

The final implantable device has been so far realized, assembled and tested for short-term biocompatibility, and even if the receiving coil and the sensing circuit have been individually characterized, fully automatic *in vitro* and *in vivo* measurements of the system remain to be tested.

With respect to the biostability of the implant, the long term endurance of the device must be tested with corrosion tests aimed to check if the electrical connections can endure long term implantation, while long lasting protective membranes must be developed and implemented in order to prevent the electrodes biofouling. Additionally, the package must promote an

---

adequate vascularization around the implant, as the formation of fibrotic tissue can block the diffusion of the analytes and definitively compromise the biosensors functionality. Additional research has still to be done to ensure long term biocompatibility: for example, implant dimensions can be further reduced, in order to increase the host tolerance, and histopathologic analysis should be implemented in the next future to evaluate the implant fibrosis of the new prototypes. Also, according to the ISO10993 standards, many additional experiments such as multiple cytotoxicity tests, as well as different hemocompatibility, irritation, sensitization and systemic toxicity analysis are requested before the final device is declared safe for implantation. The development of a proper packaging and its complete biocompatibility assessment is a complex matter that alone requires years of dedicated research.

As this thesis demonstrated, a mature diagnostic device is an *integrated system* which requires multidisciplinary work and competences, and where each choice in the development of a single aspect should be done considering the impact it has on the whole. However, despite the additional work there is still to do, the realization of a fully operational prototype may be not so far<sup>1</sup>.

---

<sup>1</sup><http://www.youtube.com/watch?v=DBa41wej-NE>



# A List of abbreviations

- **ADO** - Adenosine
- **AIROF** - Anodic iridium oxide film
- **ALD** - Atomic layer deposition
- **ATP** - Adenosine triphosphate
- **BARE** - Bare electrode
- **BZ** - Benzphetamine
- **CE** - Counter electrode
- **CHT** - Chitosan
- **CMOS** - Complementary metal oxide semiconductor
- **CNT** - Carbon nanotubes
- **CP** - Cyclophosphamide
- **CPR** - Cytochrome P450 reductase
- **CV** - Cyclic voltammetry
- **CYP** - Cytochrome P450
- **DAMP** - Damage associated molecular pattern
- **DNA** - Deoxyribonucleic Acid
- **DMEM** - Dulbecco modified Eagle medium
- **DX** - Dextromethorphan
- **EM** - Erythromycin

## Appendix A. List of abbreviations

---

- **ET** - Electron transfer
- **FBR** - Foreign body reaction
- **FLU** - Flurbiprofen
- **GOD** - Glucose oxidase
- **HEX** - Hexokinase
- **IBU** - Ibuprofen
- **IC** - Integrated circuit
- **LOD** - Limit of detection
- **LOEL** - Lowest observable effect level
- **LOR** - Lift off resist
- **LPS** - Lipopolysaccharide
- **ME** - Micro electrode
- **MEA** - Micro electrode array
- **MEC** - Minimum effective concentration
- **MEF** - Mouse embryonic fibroblasts
- **mRNA** - Messenger RNA
- **MTC** - Minimum toxic concentration
- **MWCNT** - Multi walled carbon nanotubes
- **NADPH** - Nicotinamide adenine dinucleotide phosphate
- **NAP** - Naproxen
- **NMR** - Nuclear magnetic resonance
- **NOEL** - No observable effect level
- **OTC** - Over the counter
- **P450** - Cytochrome P450
- **PAMP** - Pathogen associated molecular pattern
- **PBS** - Phosphate buffered saline solution
- **PFV** - Protein film voltammetry

- 
- **PK** - Pharmacokinetics
  - **RE** - Reference electrode
  - **RNA** - Ribonucleic Acid
  - **RTD** - Resistive thermal device
  - **SAM** - Self assembled monolayer
  - **SWCNT** - Single walled carbon nanotubes
  - **TDM** - Therapeutic drug monitoring
  - **WE** - Working electrode





## Bibliography

- [1] Determination of atp via the photochemical generation of hydrogen peroxide using flow injection luminol chemiluminescence detection. *Analytical and bioanalytical chemistry*, 377(1):189–194, 2003.
- [2] Standard Amino Acid. Lehninger principles of biochemistry. 2004.
- [3] James M Anderson and John J Langone. Issues and perspectives on the biocompatibility and immunotoxicity evaluation of implanted controlled release systems. *Journal of controlled release*, 57(2):107–113, 1999.
- [4] Sara Ghoreishizadeh Jacopo Olivo Maaik Op de Beeck Benjamin Gorissen Fabio Grassi Giovanni De Micheli Sandro Carrara Andrea Cavallini, Tanja Rezzonico. A subcutaneous biochip for remote monitoring of human metabolism: development, packaging, and biocompatibility assessment. *IEEE sensors journal*, 2013.
- [5] John H Ansede and Dhiren R Thakker. High-throughput screening for stability and inhibitory activity of compounds toward cytochrome p450-mediated metabolism. *Journal of pharmaceutical sciences*, 93(2):239–255, 2004.
- [6] S Ardizzzone, A Carugati, and S Trasatti. Properties of thermally prepared iridium dioxide electrodes. *Journal of Electroanalytical Chemistry*, 126(1-3):287–292, 1981.
- [7] St Arens, U Schlegel, G Printzen, WJ Ziegler, SM Perren, and M Hansis. Influence of materials for fixation implants on local infection an experimental study of steel versus titanium dcp in rabbits. *Journal of Bone & Joint Surgery, British Volume*, 78(4):647–651, 1996.
- [8] Fraser A Armstrong, Hendrik A Heering, and Judy Hirst. Reaction of complex metallo-proteins studied by protein-film voltammetry. *Chem. Soc. Rev.*, 26(3):169–179, 1997.
- [9] Fraser A Armstrong, H Allen O Hill, and Nicholas J Walton. Direct electrochemistry of redox proteins. *Accounts of Chemical Research*, 21(11):407–413, 1988.
- [10] Peter R Ashton, George R Brown, Neil S Isaacs, Daniele Giuffrida, Franz H Kohnke, John P Mathias, Alexandra MZ Slawin, Diane R Smith, J Fraser Stoddart, and David J

## Bibliography

---

- Williams. Molecular lego. 1. substrate-directed synthesis via stereoregular diels-alder oligomerizations. *Journal of the American Chemical Society*, 114(16):6330–6353, 1992.
- [11] Mara G Aspinall and Richard GP450-Based Nano-Bio-Sensors for Personalized Medicine Hamermesh. Realizing the promise of personalized medicine. *Harvard business review*, 85(10):108–, 2007.
- [12] Prashanth Asuri, Shyam Sundhar Bale, Ravindra C Pangule, Dhiral A Shah, Ravi S Kane, and Jonathan S Dordick. Structure, function, and stability of enzymes covalently attached to single-walled carbon nanotubes. *Langmuir*, 23(24):12318–12321, 2007.
- [13] William M Atkins. Non-michaelis-menten kinetics in cytochrome p450-catalyzed reactions. *Annu. Rev. Pharmacol. Toxicol.*, 45:291–310, 2005.
- [14] B Aussedat, M Dupire-Angel, R Gifford, JC Klein, GS Wilson, and G Reach. Interstitial glucose concentration and glycemia: implications for continuous subcutaneous glucose monitoring. *American Journal of Physiology-Endocrinology And Metabolism*, 278(4):E716–E728, 2000.
- [15] KL Austin, LE Mather, CR Philpot, and PJ McDonald. Intersubject and dose - related variability after intravenous administration of erythromycin. *British journal of clinical pharmacology*, 10(3):273–279, 1980.
- [16] Charles M Bagley, Frieda W Bostick, and Vincent T DeVita. Clinical pharmacology of cyclophosphamide. *Cancer Research*, 33(2):226–233, 1973.
- [17] Camilla Baj-Rossi, Giovanni De Micheli, and Sandro Carrara. P450-based nano-biosensors for personalized medicine. *Invited book chapter in A. Serra (Ed)" Biosensors for Health, Environment and Biosecurity", ISBN, pages 978–953, 2010.*
- [18] Bonnie Baker. Temperature sensing technologies. *AN679, Microchip Technology Inc, pages –, 1998.*
- [19] Allen J Bard and Larry R Faulkner. *Electrochemical methods: fundamentals and applications*, volume 2. Wiley New York, 1980.
- [20] Alfonso Berduque, Yvonne H Lanyon, Valerio Beni, Grégoire Herzog, Yvonne E Watson, Kenneth Rodgers, Frank Stam, John Alderman, and Damien WM Arrigan. Voltammetric characterisation of silicon-based microelectrode arrays and their application to mercury-free stripping voltammetry of copper ions. *Talanta*, 71(3):1022–1030, 2007.
- [21] Hans Ulrich Bergmeyer. *Principles of enzymatic analysis*. Verlag Chemie., 1978.
- [22] Nikitas Bistolas, Ulla Wollenberger, Christiane Jung, and Frieder W Scheller. Cytochrome p450 biosensors - a review. *Biosensors and Bioelectronics*, 20(12):2408–2423, 2005.
- [23] P Bodin and G Burnstock. Increased release of atp from endothelial cells during acute inflammation. *Inflammation research*, 47(8):351–354, 1998.

- [24] Cristina Boero, Sandro Carrara, Giovanna Del Vecchio, Laura Calzà, and Giovanni De Micheli. Highly sensitive carbon nanotube-based sensing for lactate and glucose monitoring in cell culture. *NanoBioscience, IEEE Transactions on*, 10(1):59–67, 2011.
- [25] Alan M Bond and Peter A Lay. Cyclic voltammetry at microelectrodes in the absence of added electrolyte using a platinum quasi-reference electrode. *Journal of electroanalytical chemistry and interfacial electrochemistry*, 199(2):285–295, 1986.
- [26] PA Boudreau and SP Perone. Quantitative resolution of overlapped peaks in programmed potential-step voltammetry. *Analytical Chemistry*, 51(7):811–817, 1979.
- [27] MJL Bours, ELR Swennen, F Di Virgilio, BN Cronstein, and PC Dagnelie. Adenosine 5-triphosphate and adenosine as endogenous signaling molecules in immunity and inflammation. *Pharmacology & therapeutics*, 112(2):358–404, 2006.
- [28] Wendelin Bücking, Gerald A Urban, and Thomas Nann. An electrochemical biomimetic atp-sensor. *Sensors and Actuators B: Chemical*, 104(1):111–116, 2005.
- [29] Sandro Carrara, Andrea Cavallini, Victor Erokhin, and Giovanni De Micheli. Multi-panel drugs detection in human serum for personalized therapy. *Biosensors and Bioelectronics*, 26(9):3914–3919, 2011.
- [30] Sandro Carrara, Andrea Cavallini, Abhishek Garg, and Giovanni De Micheli. Dynamical spot queries to improve specificity in p450s based multi-drugs monitoring. In *Complex Medical Engineering, 2009. CME. ICME International Conference on*, pages 1–6. IEEE, 2009.
- [31] Sandro Carrara, Sara Ghoreishizadeh, Jacopo Olivo, Irene Taurino, Camilla Baj-Rossi, Andrea Cavallini, Maaïke Op de Beeck, Catherine Dehollain, Wayne Bursleson, and Francis Gabriel Moussy. Fully integrated biochip platforms for advanced healthcare. *Sensors*, 12(8):11013–11060, 2012.
- [32] Sandro Carrara, Victoria V Shumyantseva, Alexander I Archakov, and Bruno Samorì. Screen-printed electrodes based on carbon nanotubes and cytochrome p450scc for highly sensitive cholesterol biosensors. *Biosensors and Bioelectronics*, 24(1):148–150, 2008.
- [33] Sandro Carrara, Michele Daniel Torre, Andrea Cavallini, Daniela De Venuto, and Giovanni De Micheli. Multiplexing ph and temperature in a molecular biosensor. In *Biomedical Circuits and Systems Conference (BioCAS), 2010 IEEE*, pages 146–149. IEEE, 2010.
- [34] Joseph J Casciari, Stratis V Sotirchos, and Robert M Sutherland. Glucose diffusivity in multicellular tumor spheroids. *Cancer research*, 48(14):3905–3909, 1988.
- [35] Andrea Cavallini, Camilla Baj-Rossi, Sara Ghoreishizadeh, Giovanni De Micheli, and Sandro Carrara. Design, fabrication, and test of a sensor array for perspective biosensing

## Bibliography

---

- in chronic pathologies. In *Biomedical Circuits and Systems Conference (BioCAS), 2012 IEEE*, pages 124–127. IEEE, 2012.
- [36] Andrea Cavallini, Sandro Carrara, Giovanni De Micheli, and V Erokhin. P450-mediated electrochemical sensing of drugs in human plasma for personalized therapy. In *Ph. D. Research in Microelectronics and Electronics (PRIME), 2010 Conference on*, pages 1–4. IEEE, 2010.
- [37] Andrea Cavallini, Giovanni De Micheli, and Sandro Carrara. Comparison of three methods of biocompatible multi-walled carbon nanotubes confinement for the development of implantable amperometric adenosine-5-triphosphate biosensors. *Sensor Letters*, 9(5):1838–1844, 2011.
- [38] PRN Childs, JR Greenwood, and CA Long. Review of temperature measurement. *Review of scientific instruments*, 71(8):2959–2978, 2000.
- [39] Valeria Chiono, Ettore Pulieri, Giovanni Vozzi, Gianluca Ciardelli, Arti Ahluwalia, and Paolo Giusti. Genipin-crosslinked chitosan/gelatin blends for biomedical applications. *Journal of Materials Science: Materials in Medicine*, 19(2):889–898, 2008.
- [40] Alison Chou, Till Böcking, Nagindar K Singh, and J Justin Gooding. Demonstration of the importance of oxygenated species at the ends of carbon nanotubes for their favourable electrochemical properties. *Chemical communications*, (7):842–844, 2005.
- [41] T Andrew Clayton, John C Lindon, Olivier Cloarec, Henrik Antti, Claude Charuel, Gilles Hanton, Jean-Pierre Provost, Jean-Loïc Le Net, David Baker, and Rosalind J Walley. Pharmaco-metabonomic phenotyping and personalized drug treatment. *Nature*, 440(7087):1073–1077, 2006.
- [42] Dario Compagnone and George G Guilbault. Glucose oxidase/hexokinase electrode for the determination of atp. *Analytica chimica acta*, 340(1):109–113, 1997.
- [43] Alison Cowley and Brian Woodward. A healthy future: platinum in medical applications. *Platinum Metals Review*, 55(2):98–107, 2011.
- [44] Trevor J Davies and Richard G Compton. The cyclic and linear sweep voltammetry of regular and random arrays of microdisc electrodes: Theory. *Journal of Electroanalytical Chemistry*, 585(1):63–82, 2005.
- [45] Maaïke Op de Beeck, Karen Qian, Paolo Fiorini, Karl Malachowski, and Chris Van Hoof. Design and characterization of a biocompatible packaging concept for implantable electronic devices. *Journal of microelectronics and electronic packaging*, 9(1):43–50, 2012.
- [46] Jose de Leon, Margaret T Susce, and Elaina Murray-Carmichael. The amplichip cyp450 genotyping test. *Molecular diagnosis & therapy*, 10(3):135–151, 2006.

- [47] Paul R Ortiz de Montellano. *Cytochrome P450: structure, mechanism, and biochemistry*. Springer, 2004.
- [48] Tejal A Desai, Derek J Hansford, Lara Leoni, Matthias Essenpreis, and Mauro Ferrari. Nanoporous anti-fouling silicon membranes for biosensor applications. *Biosensors and Bioelectronics*, 15(9):453–462, 2000.
- [49] Vikash R Dodhia, Carlo Sassone, Andrea Fantuzzi, Giovanna Di Nardo, Sheila J Sadeghi, and Gianfranco Gilardi. Modulating the coupling efficiency of human cytochrome p450 cyp3a4 at electrode surfaces through protein engineering. *Electrochemistry Communications*, 10(11):1744–1747, 2008.
- [50] Tina H Duedahl, Jesper Dirks, Kamilla B Petersen, Janne Romsing, Niels-Erik Larsen, and Jorgen B Dahl. Intravenous dextromethorphan to human volunteers: relationship between pharmacokinetics and anti-hyperalgesic effect. *Pain*, 113(3):360–368, 2005.
- [51] Eric Dy, Rita Vos, Jens Rip, Antonio La Manna, and Maaikje Op de Beeck. Biocompatibility assessment of advanced wafer-level based chip encapsulation. In *Electronic System-Integration Technology Conference (ESTC), 2010 3rd*, pages 1–4. IEEE, 2010.
- [52] M Eichelbaum, A Somogyi, GE Von Unruh, and HJ Dengler. Simultaneous determination of the intravenous and oral pharmacokinetic parameters of d, l-verapamil using stable isotope-labelled verapamil. *European Journal of Clinical Pharmacology*, 19(2):133–137, 1981.
- [53] Holger K Eltzschig, Michail V Sitkovsky, and Simon C Robson. Purinergic signaling during inflammation. *New England Journal of Medicine*, 367(24):2322–2333, 2012.
- [54] Carmelita Estavillo, Zhongqing Lu, Ingela Jansson, John B Schenkman, and James F Rusling. Epoxidation of styrene by human cytochrome p450 1a2 by thin film electrolysis and peroxide activation compared to solution reactions. *Biophysical chemistry*, 104(1):291–296, 2003.
- [55] Gregory P Foy and GE Pacey. Determination of atp using chelation-enhanced fluorescence. *Talanta*, 43(2):225–232, 1996.
- [56] Jane E Frew and H Allen O Hill. Direct and indirect electron transfer between electrodes and redox proteins. *European Journal of Biochemistry*, 172(2):261–269, 1988.
- [57] Izabela Galeska, Tae-Kyoung Kim, Siddhesh D Patil, Upkar Bhardwaj, Debjit Chattopadhyay, Fotios Papadimitrakopoulos, and Diane J Burgess. Controlled release of dexamethasone from plga microspheres embedded within polyacid-containing pva hydrogels. *The AAPS journal*, 7(1):E231–E240, 2005.
- [58] Aleksandra Galetin, Stephen E Clarke, and J Brian Houston. Multisite kinetic analysis of interactions between prototypical cyp3a4 subgroup substrates: midazolam, testosterone, and nifedipine. *Drug metabolism and disposition*, 31(9):1108–1116, 2003.

## Bibliography

---

- [59] Sean C Gay, Arthur G Roberts, and James R Halpert. Structural features of cytochromes p450 and ligands that affect drug metabolism as revealed by x-ray crystallography and nmr. *Future medicinal chemistry*, 2(9):1451–1468, 2010.
- [60] Igor A Ges, Borislav L Ivanov, David K Schaffer, Eduardo A Lima, Andreas A Werdich, and Franz J Baudenbacher. Thin-film iridium microelectrode for microfluidic-based microsystems. *Biosensors and Bioelectronics*, 21(2):248–256, 2005.
- [61] S Sara Ghoreishizadeh, Sandro Carrara, and Giovanni De Micheli. Circuit design for human metabolites biochip. In *Biomedical Circuits and Systems Conference (BioCAS), 2011 IEEE*, pages 460–463. IEEE, 2011.
- [62] Joyce A Goldstein and Sonia MF de Morais. Biochemistry and molecular biology of the human cyp2c subfamily. *Pharmacogenetics and Genomics*, 4(6):285–300, 1994.
- [63] John L Gordon. Extracellular atp: effects, sources and fate. *Biochemical Journal*, 233(2):309–, 1986.
- [64] David A Gough, Lucas S Kumosa, Timothy L Routh, Joe T Lin, and Joseph Y Lucisano. Function of an implanted tissue glucose sensor for more than 1 year in animals. *Science Translational Medicine*, 2(42):42ra53–42ra53, 2010.
- [65] Annette S Gross. Best practice in therapeutic drug monitoring. *British journal of clinical pharmacology*, 46(2):95–99, 1998.
- [66] Ben J Gu and James S Wiley. Rapid atp-induced release of matrix metalloproteinase 9 is mediated by the p2x7 receptor. *Blood*, 107(12):4946–4953, 2006.
- [67] F Peter Guengerich. *Human cytochrome P450 enzymes*, pages 377–530. Springer, 2005.
- [68] F Peter Guengerich. Cytochrome p450 and chemical toxicology. *Chemical research in toxicology*, 21(1):70–83, 2007.
- [69] John Michael Hammersley, David Christopher Handscomb, and George Weiss. Monte carlo methods. *Physics Today*, 18:55–, 1965.
- [70] Frank Hannemann, Andreas Bichet, Kerstin M Ewen, and Rita Bernhardt. Cytochrome p450 systems - biological variations of electron transport chains. *Biochimica et Biophysica Acta (BBA)-General Subjects*, 1770(3):330–344, 2007.
- [71] Christina Hassler, Rene P von Metzen, Patrick Ruther, and Thomas Stieglitz. Characterization of parylene c as an encapsulation material for implanted neural prostheses. *Journal of Biomedical Materials Research Part B: Applied Biomaterials*, 93(1):266–274, 2010.
- [72] You-ai He, Zongshu Luo, Paul A Klekotka, Vicki L Burnett, and James R Halpert. Structural determinants of cytochrome p450 2b1 specificity: evidence for five substrate recognition sites. *Biochemistry*, 33(14):4419–4424, 1994.

- [73] Jamille F Hetke, Jennifer L Lund, Khalil Najafi, Kensall D Wise, and David J Anderson. Silicon ribbon cables for chronically implantable microelectrode arrays. *Biomedical Engineering, IEEE Transactions on*, 41(4):314–321, 1994.
- [74] T Hickey, D Kreutzer, DJ Burgess, and F Moussy. In vivo evaluation of a dexamethasone/plga microsphere system designed to suppress the inflammatory tissue response to implantable medical devices. *Journal of biomedical materials research*, 61(2):180–187, 2002.
- [75] Christoph Hiemke. Clinical utility of drug measurement and pharmacokinetics - therapeutic drug monitoring in psychiatry. *European journal of clinical pharmacology*, 64(2):159–166, 2008.
- [76] James P Hoare. On the mixed potentials observed in the iridium-oxygen acid system. *Journal of The Electrochemical Society*, 111(8):988–992, 1964.
- [77] MA Hussain, MA Kabir, and AK Sood. On the cytotoxicity of carbon nanotubes. *Current science*, 96(5):664–673, 2009.
- [78] J Matthew Hutzler and Timothy S Tracy. Atypical kinetic profiles in drug metabolism reactions. *Drug metabolism and disposition*, 30(4):355–362, 2002.
- [79] A Ignaszak, N Hendricks, T Waryo, E Songa, N Jahed, R Ngece, A Al-Ahmed, B Kgarebe, P Baker, and EI Iwuoha. Novel therapeutic biosensor for indinavir - a protease inhibitor antiretroviral drug. *Journal of pharmaceutical and biomedical analysis*, 49(2):498–501, 2009.
- [80] Magnus Ingelman-Sundberg. Pharmacogenetics of cytochrome p450 and its applications in drug therapy: the past, present and future. *Trends in pharmacological sciences*, 25(4):193–200, 2004.
- [81] KK Jain. Applications of biochip and microarray systems in pharmacogenomics. *Pharmacogenomics*, 1(3):289–307, 2000.
- [82] Zhengwen Jiang, Nadine Dragin, Lucia F Jorge-Nebert, Martha V Martin, F Peter Guengerich, Eleni Aklillu, Magnus Ingelman-Sundberg, George J Hammons, Beverly D Lyn-Cook, and Fred F Kadlubar. Search for an association between the human cyp1a2 genotype and cyp1a2 metabolic phenotype. *Pharmacogenetics and genomics*, 16(5):359–367, 2006.
- [83] DL Johnson, BC Lewis, DJ Elliot, JO Miners, and LL Martin. Electrochemical characterisation of the human cytochrome p450 cyp2c9. *Biochemical pharmacology*, 69(10):1533–1541, 2005.
- [84] Shiba Joseph, James F Rusling, Yuri M Lvov, Thomas Friedberg, and Uwe Fuhr. An amperometric biosensor with human cyp3a4 as a novel drug screening tool. *Biochemical pharmacology*, 65(11):1817–1826, 2003.

## Bibliography

---

- [85] FD Juma, HJ Rogers, and JR Trounce. Pharmacokinetics of cyclophosphamide and alkylating activity in man after intravenous and oral administration. *British journal of clinical pharmacology*, 8(3):209–217, 1979.
- [86] Takashi Katsu and Koji Yamanaka. Potentiometric method for the determination of adenosine-5-triphosphate. *Analytica chimica acta*, 276(2):373–376, 1993.
- [87] Yoko Kawamoto, Kazumasa Shinozuka, Masaru Kunitomo, and Jun Haginaka. Determination of atp and its metabolites released from rat caudal artery by isocratic ion-pair reversed-phase high-performance liquid chromatography. *Analytical biochemistry*, 262(1):33–38, 1998.
- [88] Hideyuki Kawanabe, Tamotsu Katane, Hideo Saotome, Osami Saito, and Kazuhito Kobayashi. Power and information transmission to implanted medical device using ultrasonic. *Japanese Journal of Applied Physics*, 40:3865, 2001.
- [89] Kathryn E Kenworthy, Stephen E Clarke, Julie Andrews, and J Brian Houston. Multisite kinetic models for cyp3a4: simultaneous activation and inhibition of diazepam and testosterone metabolism. *Drug metabolism and disposition*, 29(12):1644–1651, 2001.
- [90] JD Klein, SL Clauson, and SF Cogan. Morphology and charge capacity of sputtered iridium oxide films. *Journal of Vacuum Science & Technology A: Vacuum, Surfaces, and Films*, 7(5):3043–3047, 1989.
- [91] Mato Knez, Kornelius Nielsch, and Lauri Niinistö. Synthesis and surface engineering of complex nanostructures by atomic layer deposition. *Advanced Materials*, 19(21):3425–3438, 2007.
- [92] KR Korzekwa, N Krishnamachary, M Shou, A Ogai, RA Parise, AE Rettie, FJ Gonzalez, and TS Tracy. Evaluation of atypical cytochrome p450 kinetics with two-substrate models: evidence that multiple substrates can simultaneously bind to cytochrome p450 active sites. *Biochemistry*, 37(12):4137–4147, 1998.
- [93] HE Koschwanez, FY Yap, B Klitzman, and WM Reichert. In vitro and in vivo characterization of porous poly-l-lactic acid coatings for subcutaneously implanted glucose sensors. *Journal of Biomedical Materials Research Part A*, 87(3):792–807, 2008.
- [94] Geoffrey Kotzar, Mark Freas, Phillip Abel, Aaron Fleischman, Shuvo Roy, Christian Zorman, James M Moran, and Jeff Melzak. Evaluation of mems materials of construction for implantable medical devices. *Biomaterials*, 23(13):2737–2750, 2002.
- [95] Barbara Krajewska. Application of chitin-and chitosan-based materials for enzyme immobilizations: a review. *Enzyme and microbial technology*, 35(2):126–139, 2004.
- [96] M Kyrolainen, P Rigsby, S Eddy, and P Vadgama. Bio-haemocompatibility: implications and outcomes for sensors? *Acta Anaesthesiologica Scandinavica*, 39(s104):55–60, 1995.



- [97] Nathalie Labat-Allietta and Daniel R Thavenot. Influence of calcium on glucose biosensor response and on hydrogen peroxide detection. *Biosensors and Bioelectronics*, 13(1):19–29, 1998.
- [98] Craig R Lee, John A Pieper, Reginald F Frye, Alan L Hinderliter, Joyce A Blaisdell, and Joyce A Goldstein. Differences in flurbiprofen pharmacokinetics between cyp2c9\* 1/\* 1, \* 1/\* 2, and \* 1/\* 3 genotypes. *European journal of clinical pharmacology*, 58(12):791–794, 2003.
- [99] Chenghong Lei, Ulla Wollenberger, Christiane Jung, and Frieder W Scheller. Clay-bridged electron transfer between cytochrome p450 cam and electrode. *Biochemical and biophysical research communications*, 268(3):740–744, 2000.
- [100] María Eugenia Letelier, Ana María Lepe, Mario Faúndez, Julia Salazar, Rigoberto Marín, Paula Aracena, and Hernán Speisky. Possible mechanisms underlying copper-induced damage in biological membranes leading to cellular toxicity. *Chemico-biological interactions*, 151(2):71–82, 2005.
- [101] Jun Li, Alan Cassell, Lance Delzeit, Jie Han, and M Meyyappan. Novel three-dimensional electrodes: electrochemical properties of carbon nanotube ensembles. *The Journal of Physical Chemistry B*, 106(36):9299–9305, 2002.
- [102] Enrique Llaudet, Sonja Hatz, Magali Droniou, and Nicholas Dale. Microelectrode biosensor for real-time measurement of atp in biological tissue. *Analytical chemistry*, 77(10):3267–3273, 2005.
- [103] Xiliang Luo, Aoife Morrin, Anthony J Killard, and Malcolm R Smyth. Application of nanoparticles in electrochemical sensors and biosensors. *Electroanalysis*, 18(4):319–326, 2006.
- [104] Yuri Lvov, Katsuhiko Ariga, Izumi Ichinose, and Toyoki Kunitake. Assembly of multicomponent protein films by means of electrostatic layer-by-layer adsorption. *Journal of the American Chemical Society*, 117(22):6117–6123, 1995.
- [105] MICHAEL EDWARD LYONS. Carbon nanotube based modified electrode biosensors. part 1. electrochemical studies of the flavin group redox kinetics at swcnt/glucose oxidase composite modified electrodes. pages –, 2008.
- [106] Frédéric Marteau, Nathalie Suarez Gonzalez, David Communi, Michel Goldman, Jean-Marie Boeynaems, and Didier Communi. Thrombospondin-1 and indoleamine 2, 3-dioxygenase are major targets of extracellular atp in human dendritic cells. *Blood*, 106(12):3860–3866, 2005.
- [107] Carmen Martinez. The effect of the cytochrome p450 cyp2c8 polymorphism on the disposition of (r)-ibuprofen enantiomer in healthy subjects. *British journal of clinical pharmacology*, 59(1):62–68, 2005.

## Bibliography

---

- [108] Sayed AM Marzouk, Stefan Ufer, Richard P Buck, Timothy A Johnson, Larry A Dunlap, and Wayne E Cascio. Electrodeposited iridium oxide ph electrode for measurement of extracellular myocardial acidosis during acute ischemia. *Analytical chemistry*, 70(23):5054–5061, 1998.
- [109] M Mascini and S Tombelli. Biosensors for biomarkers in medical diagnostics. *Biomarkers*, 13(7-8):637–657, 2008.
- [110] Polly Matzinger. The danger model: a renewed sense of self. *Science Signaling*, 296(5566):301–, 2002.
- [111] Francesco Mazzilli, Michela Peisino, Rostand Mitouassiwou, Benjamin Cotté, Prakash Thoppay, Cyril Lafon, Patrick Favre, Eric Meurville, and Catherine Dehollain. In-vitro platform to study ultrasound as source for wireless energy transfer and communication for implanted medical devices. In *Engineering in Medicine and Biology Society (EMBC), 2010 Annual International Conference of the IEEE*, pages 3751–3754. IEEE, 2010.
- [112] Alan D McNaught and Andrew Wilkinson. *Compendium of chemical terminology*, volume 1669. Blackwell Science Oxford, 1997.
- [113] GA Melcher, B Claudi, U Schlegel, SM Perren, G Printzen, and J Munzinger. Influence of type of medullary nail on the development of local infection. an experimental study of solid and slotted nails in rabbits. *Journal of Bone & Joint Surgery, British Volume*, 76(6):955–959, 1994.
- [114] Jose A. Rey Karen Whalen Michelle a. Clark, R.F. *Pharmacology 5th ed.* Lippincott Williams & Wilkins, 2012.
- [115] Yasuhiro Mie, Masiki Ikegami, and Yasuo Komatsu. Gold sputtered electrode surfaces enhance direct electron transfer reactions of human cytochrome p450s. *Electrochemistry Communications*, 12(5):680–683, 2010.
- [116] Satoshi MIGITA, Kazunari OZASA, Tomoya TANAKA, and Tetsuya HARUYAMA. Enzyme-based field-effect transistor for adenosine triphosphate (atp) sensing. *Analytical sciences*, 23(1):45–48, 2007.
- [117] JN Miller, MB Nawawi, and C Burgess. Detection of bacterial atp by reversed flow-injection analysis with luminescence detection. *Analytica chimica acta*, 266(2):339–343, 1992.
- [118] Saraju P Mohanty and Elias Kougiianos. Biosensors: a tutorial review. *Potentials, IEEE*, 25(2):35–40, 2006.
- [119] Francis Moussy and D Jed Harrison. Prevention of the rapid degradation of subcutaneously implanted ag/agcl reference electrodes using polymer coatings. *Analytical chemistry*, 66(5):674–679, 1994.

- [120] Katsunori Nakamura, Imad H Hanna, Hongliang Cai, Yuki Nishimura, Kevin M Williams, and F Peter Guengerich. Coumarin substrates for cytochrome p450 2d6 fluorescence assays. *Analytical biochemistry*, 292(2):280–286, 2001.
- [121] Daniel W Nebert and Elliot S Vesell. Can personalized drug therapy be achieved? a closer look at pharmaco-metabonomics. *Trends in pharmacological sciences*, 27(11):580–, 2006.
- [122] David L Nelson and Michael M Cox. *Lehninger principles of biochemistry*. Wh Freeman, 2010.
- [123] Diana Nicoll, Stephen J McPhee, Michael Pignone, and Chuanyi Lu. *Pocket guide to diagnostic tests*. Lange Medical Books/McGraw-Hill, 2001.
- [124] SA Nikles, DS Pellinen, J Kitagawa, RM Bradley, DR Kipke, and K Najafi. Long term in vitro monitoring of polyimide microprobe electrical properties. In *Engineering in Medicine and Biology Society, 2003. Proceedings of the 25th Annual International Conference of the IEEE*, volume 4, pages 3340–3343. IEEE, 2003.
- [125] Jacopo Olivo, Sandro Carrara, and Giovanni De Micheli. A study of multi-layer spiral inductors for remote powering of implantable sensors. pages –.
- [126] M Op de Beeck, Antonio La Manna, Thibault Buisson, Eric Dy, Dimitrios Velenis, Fabrice Axisa, Philippe Soussan, and Chris Van Hoof. An ic-centric biocompatible chip encapsulation fabrication process. In *Electronic System-Integration Technology Conference (ESTC), 2010 3rd*, pages 1–6. IEEE, 2010.
- [127] Paola Panicco, Yeni Astuti, Andrea Fantuzzi, James R Durrant, and Gianfranco Gilardi. P450 versus p420: Correlation between cyclic voltammetry and visible absorption spectroscopy of the immobilized heme domain of cytochrome p450 bm3. *The Journal of Physical Chemistry B*, 112(44):14063–14068, 2008.
- [128] Patrizia Pellegatti, Lizzia Raffaghello, Giovanna Bianchi, Federica Piccardi, Vito Pistoia, and Francesco Di Virgilio. Increased level of extracellular atp at tumor sites: in vivo imaging with plasma membrane luciferase. *PLoS One*, 3(7):e2599, 2008.
- [129] Junmin Peng, Joshua E Elias, Carson C Thoreen, Larry J Licklider, and Steven P Gygi. Evaluation of multidimensional chromatography coupled with tandem mass spectrometry (lc/lc-ms/ms) for large-scale protein analysis: the yeast proteome. *Journal of proteome research*, 2(1):43–50, 2003.
- [130] Ketul C Popat, Matthew Eltgroth, Thomas J LaTempa, Craig A Grimes, and Tejal A Desai. Decreased *staphylococcus epidermis* adhesion and increased osteoblast functionality on antibiotic-loaded titania nanotubes. *Biomaterials*, 28(32):4880–4888, 2007.

## Bibliography

---

- [131] Chris P Quinn, Chandrashekhar P Pathak, Adam Heller, and Jeffrey A Hubbell. Photocrosslinked copolymers of 2-hydroxyethyl methacrylate, poly (ethylene glycol) tetraacrylate and ethylene dimethacrylate for improving biocompatibility of biosensors. *Biomaterials*, 16(5):389–396, 1995.
- [132] Christopher AP Quinn, Robert E Connor, and Adam Heller. Biocompatible, glucose-permeable hydrogel for *in situ* coating of implantable biosensors. *Biomaterials*, 18(24):1665–1670, 1997.
- [133] Buddy D Ratner, Allan S Hoffman, Frederick J Schoen, and Jack E Lemons. Biomaterials science: an introduction to materials in medicine. *San Diego, California*, pages 162–164, 2004.
- [134] SV Romanenko, AG Stromberg, and TN Pushkareva. Modeling of analytical peaks: Peaks properties and basic peak functions. *Analytica chimica acta*, 580(1):99–106, 2006.
- [135] Anna Rubartelli and Michael T Lotze. Inside, outside, upside down: damage-associated molecular-pattern molecules (damps) and redox. *Trends in immunology*, 28(10):429–436, 2007.
- [136] Richard Runkel, Enrico Forchielli, Gerhard Boost, Melvin Chaplin, Robert Hill, Hilli Sevelius, Geoffrey Thompson, and Eugene Segre. Naproxen-metabolism, excretion and comparative pharmacokinetics. *Scandinavian Journal of Rheumatology*, 2(S2):29–36, 1973.
- [137] GB Ryan and G Majno. Acute inflammation. a review. *The american journal of pathology*, 86(1):183–, 1977.
- [138] Sheila J Sadeghi, Andrea Fantuzzi, and Gianfranco Gilardi. Breakthrough in p450 bioelectrochemistry and future perspectives. *Biochimica et Biophysica Acta (BBA)-Proteins & Proteomics*, 1814(1):237–248, 2011.
- [139] Krishanu Saha, Jacob F Pollock, David V Schaffer, and Kevin E Healy. Designing synthetic materials to control stem cell phenotype. *Current opinion in chemical biology*, 11(4):381–387, 2007.
- [140] Y Saito. A theoretical study on the diffusion current at the stationary electrodes of circular and narrow band types. *Rev. Polarogr*, 15:177–187, 1968.
- [141] F Scheller and D Pfeiffer. Glucose oxidase - hexokinase bienzyme electrode sensor for adenosine triphosphate. *Analytica Chimica Acta*, 117:383–386, 1980.
- [142] Raf JF Schepers, Jonathan M Oyler, Robert E Joseph, Edward J Cone, Eric T Moolchan, and Marilyn A Huestis. Methamphetamine and amphetamine pharmacokinetics in oral fluid and plasma after controlled oral methamphetamine administration to human volunteers. *Clinical chemistry*, 49(1):121–132, 2003.

- [143] Elizabeth Schneider and Douglas S Clark. Cytochrome p450 (cyp) enzymes and the development of cyp biosensors. *Biosensors and Bioelectronics*, pages –, 2012.
- [144] Emily E Scott, You Ai He, Michael R Wester, Mark A White, Christopher C Chin, James R Halpert, Eric F Johnson, and C David Stout. An open conformation of mammalian cytochrome p450 2b4 at 1.6-Å resolution. *Proceedings of the National Academy of Sciences*, 100(23):13196–13201, 2003.
- [145] A Adam Sharkawy, Bruce Klitzman, George A Truskey, and W Monty Reichert. Engineering the tissue which encapsulates subcutaneous implants. ii. plasma–tissue exchange properties. *Journal of biomedical materials research*, 40(4):586–597, 1998.
- [146] Yeong-Tarng Shieh and Yu-Fong Yang. Significant improvements in mechanical property and water stability of chitosan by carbon nanotubes. *European polymer journal*, 42(12):3162–3170, 2006.
- [147] Magang Shou. Kinetic analysis for multiple substrate interaction at the active site of cytochrome p450. *Methods in enzymology*, 357:261–276, 2002.
- [148] Victoria V Shumyantseva, Tatiana V Bulko, and Alexander I Archakov. Electrochemical reduction of cytochrome p450 as an approach to the construction of biosensors and bioreactors. *Journal of inorganic biochemistry*, 99(5):1051–, 2005.
- [149] Victoria V Shumyantseva, Yuri D Ivanov, Nikitas Bistolas, Frieder W Scheller, Alexander I Archakov, and Ulla Wollenberger. Direct electron transfer of cytochrome p450 2b4 at electrodes modified with nonionic detergent and colloidal clay nanoparticles. *Analytical chemistry*, 76(20):6046–6052, 2004.
- [150] VV Shumyantseva, TV Bulko, GP Kuznetsova, NF Samenkova, and AI Archakov. Electrochemistry of cytochromes p450: Analysis of current-voltage characteristics of electrodes with immobilized cytochromes p450 for the screening of substrates and inhibitors. *Biochemistry (Moscow)*, 74(4):438–444, 2009.
- [151] A Silber, N Hampp, and W Schuhmann. Poly (methylene blue)-modified thick-film gold electrodes for the electrocatalytic oxidation of nadh and their application in glucose biosensors. *Biosensors and Bioelectronics*, 11(3):215–223, 1996.
- [152] SK Smart, AI Cassady, GQ Lu, and DJ Martin. The biocompatibility of carbon nanotubes. *Carbon*, 44(6):1034–1047, 2006.
- [153] Anthony Smith, Satya Prakash Datta, G Howard Smith, Peter Nelson Campbell, R Bentley, and HA McKenzie. *Oxford dictionary of biochemistry and molecular biology*. Oxford University Press (OUP), 2000.
- [154] OO Soldatkin, OM Schuvailo, S Marinesco, R Cespuoglio, and AP Soldatkin. Microbiosensor based on glucose oxidase and hexokinase co-immobilised on platinum microelectrode for selective atp detection. *Talanta*, 78(3):1023–1028, 2009.

## Bibliography

---

- [155] Irene Taurino, Sandro Carrara, Mauro Giorcelli, Alberto Tagliaferro, and Giovanni De Micheli. Comparing sensitivities of differently oriented multi-walled carbon nanotubes integrated on silicon wafer for electrochemical biosensors. *Sensors and Actuators B: Chemical*, 160(1):327–333, 2011.
- [156] TV Thamaraiselvi and S Rajeswari. Biological evaluation of bioceramic materials-a review. *Carbon*, 24(31):172–, 2004.
- [157] Jeffrey J Toman and SD Brown. Peak resolution by semiderivative voltammetry. *Analytical Chemistry*, 53(9):1497–1504, 1981.
- [158] M Topper, M Klein, K Buschick, V Glaw, K Orth, O Ehrmann, M Hutter, H Oppermann, K-F Becker, and T Braun. Biocompatible hybrid flip chip microsystem integration for next generation wireless neural interfaces. In *Electronic Components and Technology Conference, 2006. Proceedings. 56th*, pages 4–pp. IEEE, 2006.
- [159] Timothy S Tracy. Atypical enzyme kinetics: their effect on in vitro-in vivo pharmacokinetic predictions and drug interactions. *Current drug metabolism*, 4(5):341–346, 2003.
- [160] Matthew J Traylor, Jessica D Ryan, Eric S Arnon, Jonathan S Dordick, and Douglas S Clark. Rapid and quantitative measurement of metabolic stability without chromatography or mass spectrometry. *Journal of the American Chemical Society*, 133(37):14476–14479, 2011.
- [161] Olga V Trubetskoy, Jasmin R Gibson, and Bryan D Marks. Highly miniaturized formats for in vitro drug metabolism assays using vivid fluorescent substrates and recombinant human cytochrome p450 enzymes. *Journal of biomolecular screening*, 10(1):56–66, 2005.
- [162] Andrew K Udit, Katharine D Hagen, Peter J Goldman, Andrew Star, James M Gillan, Harry B Gray, and Michael G Hill. Spectroscopy and electrochemistry of cytochrome p450 bm3-surfactant film assemblies. *Journal of the American Chemical Society*, 128(31):10320–10325, 2006.
- [163] Francesco Valgimigli, Fausto Lucarelli, Cosimo Scuffi, Sara Morandi, and Iolanda Sposato. Evaluating the clinical accuracy of glucomen-day: a novel microdialysis-based continuous glucose monitor. *Journal of diabetes science and technology*, 4(5):1182–, 2010.
- [164] Christine M Walko and Ogechi Ikediobi. Pharmacogenomic applications in oncology. *Journal of Pharmacy Practice*, 25(4):439–446, 2012.
- [165] Jing-Fang Wang, Cheng-Cheng Zhang, Kuo-Chen Chou, and Dong-Qing Wei. Structure of cytochrome p450s and personalized drug. *Current medicinal chemistry*, 16(2):232–244, 2009.

- [166] Min Wang, Sheng Yao, and Marc Madou. A long-term stable iridium oxide ph electrode. *Sensors and Actuators B: Chemical*, 81(2):313–315, 2002.
- [167] Shao-Feng Wang, Lu Shen, Wei-De Zhang, and Yue-Jin Tong. Preparation and mechanical properties of chitosan/carbon nanotubes composites. *Biomacromolecules*, 6(6):3067–3072, 2005.
- [168] Siqun Wang and Qiong Cheng. Microarray analysis in drug discovery and clinical applications. In *Bioinformatics and Drug Discovery*, pages 49–65. Springer, 2006.
- [169] W Kenneth Ward, Michael D Wood, Heather M Casey, Matthew J Quinn, and Isaac F Federiuk. The effect of local subcutaneous delivery of vascular endothelial growth factor on the function of a chronically implanted amperometric glucose sensor. *Diabetes technology & therapeutics*, 6(2):137–145, 2004.
- [170] Michael P Washburn, Dirk Wolters, and John R Yates. Large-scale analysis of the yeast proteome by multidimensional protein identification technology. *Nature biotechnology*, 19(3):242–247, 2001.
- [171] Danièle Werck-Reichhart and René Feyereisen. Cytochromes p450: a success story. *Genome Biol*, 1(6):3003–1, 2000.
- [172] R Mark Wightman and David O Wipf. Voltammetry at ultramicroelectrodes. *Electroanalytical chemistry*, 15:267–353, 1989.
- [173] David Franklyn Williams. *The Williams dictionary of biomaterials*. Liverpool University Press, 1999.
- [174] Natalie Wisniewski and Monty Reichert. Methods for reducing biosensor membrane biofouling. *Colloids and Surfaces B: Biointerfaces*, 18(3):197–219, 2000.
- [175] J Woodcock. The prospects for personalized medicine in drug development and drug therapy. *Clinical Pharmacology & Therapeutics*, 81(2):164–169, 2007.
- [176] Yunhua Wu and Shengshui Hu. Biosensors based on direct electron transfer in redox proteins. *Microchimica Acta*, 159(1-2):1–17, 2007.
- [177] Julia D Wulffuhle, Kirsten H Edmiston, Lance A Liotta, and Emanuel F Petricoin. Technology insight: pharmacoproteomics for cancer - promises of patient-tailored medicine using protein microarrays. *Nature Clinical Practice Oncology*, 3(5):256–268, 2006.
- [178] Kazusuke Yamanaka. Anodically electrodeposited iridium oxide films(aeirof) from alkaline solutions for electrochromic display devices. *Japanese journal of applied physics*, 28(part 1):632–637, 1989.
- [179] Mingli Yang, Jarod L Kabulski, Lance Wollenberg, Xinqi Chen, Murali Subramanian, Timothy S Tracy, David Lederman, Peter M Gannett, and Nianqiang Wu. Electrocatalytic drug metabolism by cyp2c9 bonded to a self-assembled monolayer-modified electrode. *Drug metabolism and disposition*, 37(4):892–899, 2009.

## Bibliography

---

- [180] Jason K Yano, Michael R Wester, Guillaume A Schoch, Keith J Griffin, C David Stout, and Eric F Johnson. The structure of human microsomal cytochrome p450 3a4 determined by x-ray crystallography to 2.05-Å resolution. *Journal of Biological Chemistry*, 279(37):38091–38094, 2004.
- [181] Bazhang Yu, Chunyan Wang, Young Min Ju, Leigh West, Julie Harmon, Yvonne Moussy, and Francis Moussy. Use of hydrogel coating to improve the performance of implanted glucose sensors. *Biosensors and Bioelectronics*, 23(8):1278–1284, 2008.
- [182] Rae Yuan, Soraya Madani, Xiao-Xiong Wei, Kellie Reynolds, and Shiew-Mei Huang. Evaluation of cytochrome p450 probe substrates commonly used by the pharmaceutical industry to study in vitro drug interactions. *Drug metabolism and disposition*, 30(12):1311–1319, 2002.
- [183] Qingmei Zhou, Qingji Xie, Yingchun Fu, Zhaohong Su, Xue'en Jia, and Shouzhuo Yao. Electrodeposition of carbon nanotubes-chitosan-glucose oxidase biosensing composite films triggered by reduction of p-benzoquinone or h<sub>2</sub>o<sub>2</sub>. *The Journal of Physical Chemistry B*, 111(38):11276–11284, 2007.



## PERSONAL INFORMATION

### Cavallini Andrea

📍 Route de Chavannes 68, 1007 Lausanne (Switzerland)

📞 +41 78 770 3209

✉ [cavallini.andrea@gmail.com](mailto:cavallini.andrea@gmail.com)

## WORK EXPERIENCE

August 2008 – June 2013

### PhD Candidate - EPFL

Giovanni de Micheli, Sandro Carrara  
EPFL IC ISIM LSI1 INF341 (batiment INF) station 14, CH-1015 Lausanne (Switzerland)

**Development of an implantable biosensor for personalized therapy applications**

November 2011 – April 2012

### PhD Internship - IMEC

Maaikje Op de Beeck  
IMEC, Kapeldreef 75 - 3001 Leuven (Belgium)

**Development of a biocompatible packaging for a fully implantable biosensor**

September 2007 – March 2008

### Researcher - Universita' degli studi di Bologna

Luca Benini  
Dipartimento di Elettronica, Informatica e Sistemistica (DEIS) via Risorgimento n°2, 40136 Bologna (Italy)

**Development of an electrochemical functionalization for the capacitive detection of DNA on micro-fabricated arrays**

## EDUCATION AND TRAINING

2004 – 2007

### Biomolecular Biotechnology - Master Degree

110 cum laude

Universita' degli studi di Bologna, Bologna (Italy)

**Final project:** Design, fabrication, functionalization and test of a DNA biochip

**Advisors:** Sandro Carrara, Bruno Samori

2001 – 2004

### Pharmaceutical Biotechnology - Bachelor Degree

110 cum laude

Universita' di Ferrara, Ferrara (Italy)

**Final project:** Development of a tissue-specific HSV-1 vector for anti-angiogenic cancer therapy

**Advisors:** Peggy Marconi, Roberto Manservigi

## LANGUAGES

Italian Mother Tongue

English Proficient – level C1 of the common European framework

French Upper intermediated – level B2 of the common European framework

Spanish Basic – level A2 of the common European framework

## ADDITIONAL INFORMATION

### Awards

Best Poster award at the Nanoeurope Conference - Rapperswil 25,26 november 2009.

Bronze leaf award for the paper "P450-Mediated Electrochemical Sensing of Drugs in Human Plasma for Personalized Therapy" at the PRIME conference - Berlin 18,21 July 2010.

### Publications

S. Carrara, L. Bolomey, C. Boero, [A. Cavallini](#) and E. Meurville et al. **Remote System for Monitoring Animal Models With Single-Metabolite Bio-Nano-Sensors**, in IEEE Sensors Journal, vol. 13, num. 3, p. 1018 - 1024, 2013.

[A. Cavallini](#), C. Baj-Rossi, S. Ghoreishizadeh, G. De Micheli and S. Carrara. **Design, fabrication, and test of a sensor array for perspective biosensing in chronic pathologies**. IEEE Biomedical Circuits and Systems Conference (BioCAS 2012), Hsinchu, Taiwan, 2012.

S. Carrara, [A. Cavallini](#), S. Ghoreishizadeh, J. Olivo and G. De Micheli. **Developing Highly-Integrated Subcutaneous Biochips for Remote Monitoring of Human Metabolism**. IEEE Sensors Conference, Taipei, Taiwan, 2012.

S. Carrara, S. S. Ghoreishizadeh, J. Olivo, I. Taurino and C. Baj-Rossi, [A. Cavallini](#) et al. **Fully Integrated Biochip Platforms for Advanced Healthcare**, in Sensors, vol. 12, num. 8, p. 11013-11060, 2012.

[A. Cavallini](#), G. De Micheli and S. Carrara. **Comparison of Three Methods of Biocompatible Multi-Walled Carbon Nanotubes Confinement for the Development of Implantable Amperometric Adenosine-5'-Triphosphate Biosensors**, in Sensor Letters, vol. 9, num. 5, p. 1838-1844, 2011.

S. Carrara, L. Bolomey, C. Boero, [A. Cavallini](#) and E. Meurville et al. **Single-Metabolite Bio-Nano-Sensors and System for Remote Monitoring in Animal Models**. IEEE Sensors 2011 Conference, Limerick, Ireland, 2011.

S. Carrara, [A. Cavallini](#), V. Erokhin and G. De Micheli. **Multi-panel drugs detection in human serum for personalized therapy**, in Biosensors and Bioelectronics, vol. 26, num. 9, p. 3914-3919, 2011.

S. Carrara, M. D. Torre, [A. Cavallini](#), D. De Venuto and G. De Micheli. **Multiplexing pH and Temperature in a Molecular Biosensor**. IEEE BIOCAS 2010 Conference, Paphos, Cyprus, 2010.

[A. Cavallini](#), S. Carrara, G. De Micheli and V. Erokhin. **P450-mediated electrochemical sensing of drugs in human plasma for personalized therapy**. 6th Conference on Ph.D. Research in Microelectronics and Electronics (PRIME), Berlin, Germany, 2010.

S. Carrara, [A. Cavallini](#), A. Garg and G. De Micheli. **Dynamical Spot Queries to Improve Specificity in P450s based Multi-Drugs Monitoring**. IEEE/ICME International Conference on Complex Medical Engineering, Tempe, Arizona, USA, 2009.

S. Carrara, [A. Cavallini](#), G. De Micheli, J. Olivo and L. Benini et al. **Circuits Design and Nano-Structured Electrodes for Drugs Monitoring in Personalized Therapy**. IEEE Biomedical Circuits and Systems Conference (BioCAS), Baltimore, Maryland, USA, 2008.

### Publications - not related to the PhD project

S. Carrara, [A. Cavallini](#), Y. Leblebici, G. De Micheli and V. Bhalla et al. **Capacitance DNA bio-chips improved by new probe immobilization strategies**, in MicroelectronicsJournal, num. 41, p. 711-717, 2010.

S. Carrara, [A. Cavallini](#), Y. Maruyama, E. Charbon and G. De Micheli. **A new ethylene glycol-silane monolayer for highly-specific DNA detection on Silicon Chips**, in Surface Science Letters, vol. 604, num. 23-24, p. L71-L74, 2010.

S. Carrara, [A. Cavallini](#), Y. Leblebici, G. De Micheli and V. Bhalla et al. **New probe immobilizations by lipote-diethalonamine or ethylene-glycol molecules for capacitance DNA chip**. 3rd IEEE International Workshop on Advances in Sensors and Interfaces (IWASI), Trani, Italy, 2009.

S. Carrara, L. Benini, V. Bhalla, C. Stagni, A. Ferretti, [A. Cavallini](#) et al. **New insights for using self-assembly materials to improve the detection stability in label-free DNA-chip and immuno-sensors**, in Biosensors & Bioelectronics, vol. 24, p. 3425-3429, 2009

